ERDC/GSL TR-05-14

Geotechnical and Structures Laboratory

US Army Corps of Engineers®
Engineer Research and Development Center

Folsom Dam Outlet Works Modification Project; Simplified Three-Dimensional Stress Analysis of Monolith 12

Enrique E. Matheu and Sharon B. Garner

June 2005

ERDC/GSL TR-05-14
June 2005

Folsom Dam Outlet Works Modification Project; Simplified Three-Dimensional Stress Analysis of Monolith 12

Enrique E. Matheu, Sharon B. Garner

Geotechnical and Structures Laboratory
U.S. Army Engineer Research and Development Center
3909 Halls Ferry Road
Vicksburg, MS 39180-6199

Final report

Prepared for U.S. Army Engineer District, Sacramento
Sacramento, CA 95814-2922

ABSTRACT: This report presents a finite-element stress analysis of monolith 12 conducted to assess any potential adverse effects caused by the proposed dimensions of the air vent near the base of the spillway pier wall. A simplified three-dimensional finite-element model was developed to simplify the analysis while preserving the main characteristics of the section. The numerical model included fixed boundary conditions along the base and appropriate boundary conditions along the two lateral planes representative of the vertical contraction joints. The analyses included static (self-weight and hydrostatic) and dynamic (inertial and hydrodynamic) effects. The dynamic effects were accounted for using equivalent lateral loads and following Chopra's simplified procedure for seismic analysis of concrete gravity sections. The results provide an estimate of the stress field around the air manifold opening along the downstream face, and they provide a quantitative basis to evaluate its impact at the proposed location and to complete the design of any necessary reinforcement to be placed around the conduit.

Contents

List of Figures

List of Tables

Conversion Factors, Non-SI to SI Units of Measurements

Non-SI units of measurements used in this report can be converted to SI units as follows:

Multiply	By	To Obtain
cubic feet	0.02831685	cubic meters
feet	0.3048	meters
inches	25.4	millimeters
miles (U.S. statute)	1.609347	kilometers
pounds (force) per square inch	6.894757	kilopascals
pounds (mass) per cubic foot	16.01846	kilograms per cubic meter
square inches	6.4516	square centimeters

Preface

This report describes a research study conducted by the U.S. Army Engineer Research and Development Center (ERDC) consisting of a finite element-based stress analysis of monolith 12 of Folsom Dam, California. This study was sponsored by the U.S. Army Engineer District, Sacramento (SPK).

The research described herein was conducted by Dr. Enrique E. Matheu and Ms. Sharon B. Garner, ERDC, Geotechnical and Structures Laboratory (GSL), Vicksburg, MS. Dr. Matheu prepared this publication under the general supervision of Dr. Joseph P. Koester, Chief, Geotechnical and Earthquake Engineering Branch, GSL; Dr. Robert L. Hall, Chief, Geosciences and Structures Division, GSL; and Dr. David W. Pittman, Director, GSL.

At the time of publication of this report, COL James R. Rowan, EN, was Commander and Executive Director of ERDC, and Dr. James R. Houston was Director.

1 Introduction

Objective

Openings or discontinuities may have a significant impact on the stress field induced by dynamic loads on concrete structures. In the case of concrete dams, the size and position of features such as air vents and conduits may introduce adverse stress concentration effects that need to be properly quantified to assess the resulting stress state. The situation may be aggravated if the openings intersect those regions along the upstream or downstream faces that could exhibit high dynamic stresses caused by seismic loads. In the case of monolith 12 of Folsom Dam, the evaluation of these effects is complicated by the nonuniformity of the section geometry.

The objective of the technical work documented in this report is to estimate the stress demands near the downstream exit of the proposed air vent in monolith 12 when subjected to the Maximum Credible Earthquake (MCE). The U.S. Army Engineer District, Sacramento (SPK), commissioned this work to provide additional information regarding the impact of the proposed air vent design on the resulting dynamic performance of monolith 12. The results and conclusions presented in this report are intended to complement the information provided by other previous and current technical studies.

Scope

A finite-element stress analysis of monolith 12 is proposed to assess any potential adverse effects caused by the proposed dimensions of the air vent near the base of the spillway pier wall. A three-dimensional (3D) finite-element model is developed based on the monolith geometry provided by SPK. Some modifications are introduced in the actual geometry to simplify the analysis while preserving the main characteristics of the section. For example, the dam-foundation contact is idealized as a horizontal plane. The modal characteristics of the numerical model are determined assuming fixed boundary conditions along the base and appropriate boundary conditions along the two lateral vertical planes. The analyses include the effects of the static loads (self-weight and hydrostatic loads), and the dynamic effects (inertial and hydrodynamic loads) are accounted for using equivalent lateral loads in a manner consistent with the methodology already implemented by SPK in previous analyses. The analyses account for the effects of the horizontal component of the input ground motion. The effects of the vertical component are approximated by increasing the computed dynamic

responses. The results provide an estimate of the stress field around the air manifold opening along the downstream face, and they provide a quantitative basis to evaluate its impact at the proposed location and to complete the design of any necessary reinforcement to be placed around the conduit.

Project Characteristics

Folsom Dam is located on the American River, about 20 miles[1] northeast of the city of Sacramento, CA. The reservoir is used for flood control, irrigation, and power-generation purposes. The maximum height of the gravity dam section is 340 ft with a crest length of about 1,400 ft. It consists of 28 monoliths, 50 ft wide each, and its construction was completed in 1956. The monoliths were constructed in 5-ft lifts and are founded in hard granodiorite rock (Hall et al. 1989). Additional project details can be found in Wong et al. (2002).

1 A table of factors for converting non-SI units of measurement to SI units is presented on page vii.

2 Maximum Credible Earthquake

The controlling MCE was defined as an event of magnitude 6.5 at a source-to-site distance of 14 km (URS Corporation 2001). The corresponding peak horizontal ground acceleration value was 0.38 g (84th percentile). The vertical response spectrum was defined based on the horizontal spectrum using a period-dependent scaling relationship (URS Corporation 2003). The resulting 5-percent-damping response spectra for horizontal and vertical motion are shown in Figure 1.

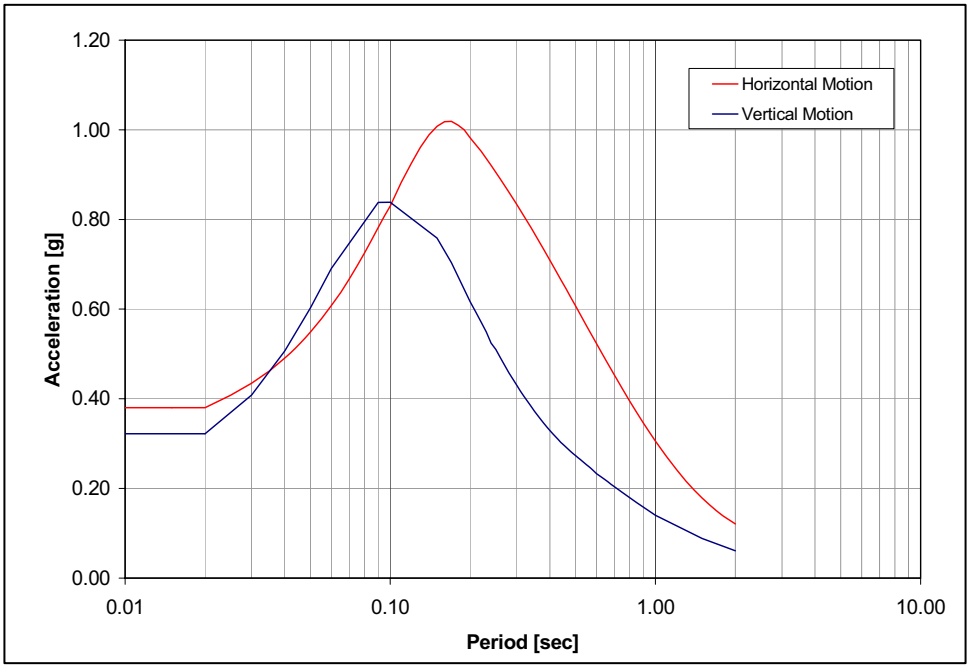

Figure 1. MCE 5-percent-damped horizontal and vertical response spectra

The horizontal spectrum peaks at 0.17 sec, whereas 0.10 sec corresponds to the peak of the vertical spectrum. Considering a practical range of interest that extends between 0.16 and 0.32 sec, it can be seen that the vertical spectral values for this range vary between 70 and 50 percent of the corresponding horizontal spectral ordinates.

3 Simplified Dynamic Analysis

Introduction

This section briefly describes the main steps involved in the application of a dynamic analysis procedure specifically developed by Prof. A. Chopra and co-workers at the University of California at Berkeley for the analysis of concrete gravity sections. Since the late 1960s, Prof. Chopra's research efforts have led to significant developments in the field of earthquake response of concrete dams (Chopra 1967). His initial work, which was mainly concerned with the determination of the hydrodynamic forces on dams, evolved into a comprehensive formulation of the dynamic problem that accounted for dam-reservoir and dam-foundation interaction phenomena. The formulation was based on the substructure concept, with the system constituted by the dam (represented by a finite-element model), the reservoir (represented by a continuum domain with infinite length in the upstream direction), and the foundation (represented by a visco-elastic half-plane). This formulation, which also incorporated energy-absorption effects at the reservoir bottom, constituted the analytical framework for the computer program EAGD-84 (Fenves and Chopra 1984) for two-dimensional (2D) time-history analysis of concrete gravity dams subject to earthquake excitations.

Description of Procedure

In 1978, Chopra introduced a simplified procedure to analyze concrete gravity dams using an equivalent lateral force method (Chopra 1978). A main assumption of this analysis procedure is that the primary dynamic characteristics of the response of the dam-reservoir system can be described by the fundamental mode of vibration of the dam on rigid foundation rock. Even the approximate analysis of the fundamental mode response still represents a complex problem because of the frequency-dependent characteristics of the interaction phenomena. To simplify the analysis, frequency-independent parameters are defined in the formulation so that an equivalent single degree-of-freedom (SDOF) system can be used to represent the fundamental mode response. To facilitate the implementation of the approach, standard values were originally provided for the fundamental vibration period, fundamental mode shape, and other parameters of typical gravity sections. The water impounded in the reservoir is modeled as a

fluid domain of constant depth and infinite length in the upstream direction, and the upstream face of the dam is assumed vertical for the purpose of evaluating the hydrodynamic terms. The procedure takes into account dam-water interaction phenomena by defining the equivalent SDOF system with a natural vibration period and damping ratio that are appropriately modified to consider the hydrodynamic effects. The effects of vertical ground motion were ignored in the original formulation of the simplified procedure, for which the ground excitation (defined in terms of a response spectrum) was assumed to act along the upstream-downstream direction of the model.

The formulation of the simplified analysis procedure was extended to include the absorptive effects of reservoir bottom materials and the effects of dam-foundation rock interaction (Fenves and Chopra 1985a,b) by idealizing the foundation region as a homogeneous, isotropic, viscoelastic half-plane. The procedure was also extended to include the response contribution of the higher vibration modes by using a static correction approach (Fenves and Chopra 1986, 1987). The analysis of gated spillway monoliths was also addressed (Chopra and Tan 1989). The formulation has been recently extended to consider the vertical component of the ground motion (Chopra and Basu 2003a,b).

This approach was originally developed as a 2D analysis procedure in which the seismic response of the dam section is obtained by applying sets of equivalent lateral forces as static loads. The corresponding response can be determined by performing a static analysis. Stresses and other response quantities can be calculated by standard finite-element analysis of the section. In some cases, the monolith under consideration may exhibit geometric irregularities or nonsymmetric characteristics. To conduct a simplified dynamic analysis in these situations, it is necessary to assume that these features do not have a substantial influence on the computation of the equivalent lateral loads. A decoupled approach can be implemented where the equivalent lateral loads are essentially determined using an idealized 2D representation of the monolith. If necessary, the sectional properties may be appropriately modified to account for out-of-plane thickness variations and to achieve a 2D model that captures the global dynamic response characteristics of the actual structure. This 2D model can be used to generate the lateral loads associated with an equivalent unit-thickness slice of the original monolith. Since geometric irregularities or nonsymmetric characteristics may have an important influence on the stress distribution, the stress analysis is then conducted by applying those loads into a 3D model of the original monolith. This general procedure has been successfully employed by SPK engineers in a comprehensive series of earthquake analyses of overflow and nonoverflow monoliths of Folsom Dam.

Horizontal Ground Motion

Equivalent lateral forces

The determination of the equivalent lateral forces is based on a simplified representation of the monolith consisting of a 2D model with a horizontal dam-foundation interface. As mentioned before, the upstream face of the dam is

assumed vertical for computation of the corresponding hydrodynamic pressures. (Actual hydrodynamic pressure distributions are not very sensitive to small departures from this assumption.) The total dynamic response of most structures subjected to base input motion is generally characterized by a very important contribution associated with the fundamental mode of vibration. However, the typical mass distribution of gravity dams (monotonically decreasing with the height of the monolith) tends to increase the relative importance of the contributions of higher vibration modes to the total response. Therefore, the procedure not only addresses the earthquake effects associated with the fundamental vibration mode, but also incorporates a correction for higher mode response.

Considering only the fundamental mode response of the dam, the maximum effects of the horizontal earthquake ground motion are represented by equivalent lateral forces $f_1(y)$ per unit height of the dam:

$$f_1(y) = \frac{\tilde{L}_1}{\tilde{M}_1} \frac{S_a(\tilde{T}_1, \tilde{\xi}_1)}{g} \left[w_s(y)\phi(y) + g\bar{p}_1(y, \tilde{T}_r) \right] \tag{1}$$

where the y-coordinate is measured along the height of the monolith from its base, as indicated in Figure 2, which also shows the fundamental mode shape $\phi(y)$, idealized as only a function of the y-coordinate, and corresponds to the dam supported on rigid foundation rock and empty reservoir. This vibration mode shape is associated with the fundamental period T_1 (first natural period of the dam with rigid foundation and empty reservoir).

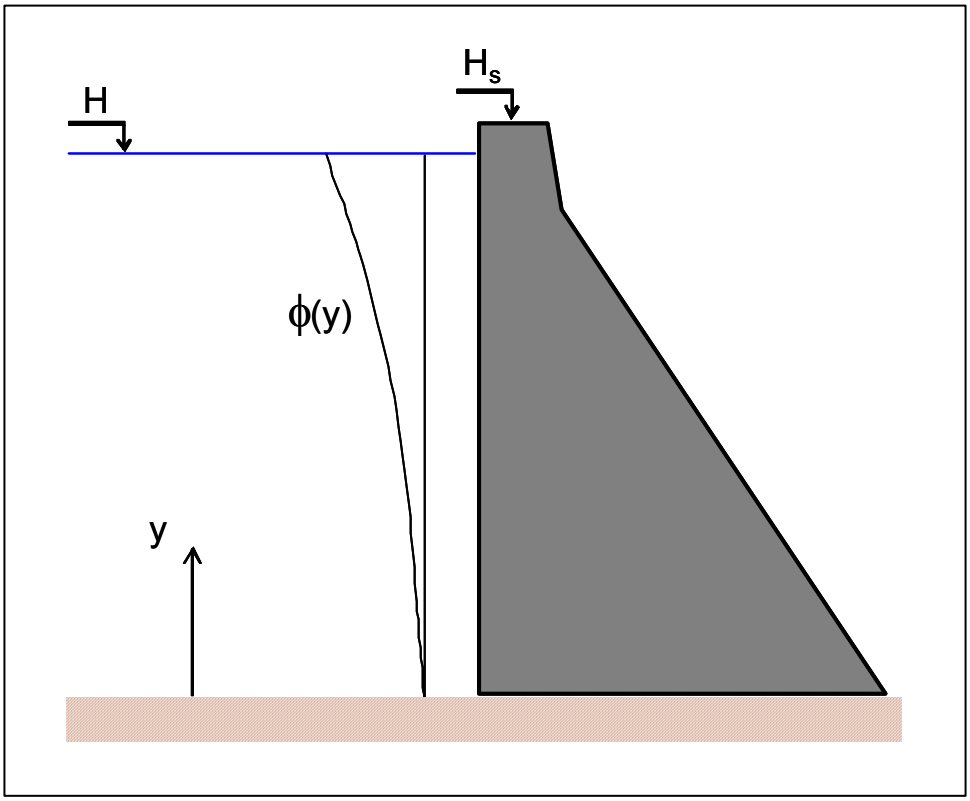

Figure 2. Idealized model for simplified analysis procedure

The parameters $\tilde{L}_1$ and $\tilde{M}_1$ in Equation 1 represent the generalized earthquake force coefficient and generalized mass, respectively, of the equivalent SDOF representing the dam and including hydrodynamic effects. These are given by

$$\tilde{L}_1 = L_1 + \int_0^H \overline{p}_1(y,\tilde{T}_r)\,dy$$

$$\tilde{M}_1 = M_1 + \int_0^H \mathrm{Re}\left[\overline{p}_1(y,\tilde{T}_r)\right]\phi(y)\,dy \tag{2}$$

where L_1 and M_1 are the generalized earthquake force coefficient and generalized mass, respectively, corresponding to the fundamental vibration mode of the dam on rigid foundation and empty reservoir,

$$\tilde{L}_1 = \frac{1}{g}\int_0^{H_s} w_s(y)\phi(y)\,dy$$

$$\tilde{M}_1 = \frac{1}{g}\int_0^{H_s} w_s(y)\phi^2(y)\,dy \tag{3}$$

The function $\overline{p}_1$, which appears in Equations 1 and 2, denotes the hydrodynamic pressure distribution along the upstream face of the dam that corresponds to a harmonic acceleration with frequency $\tilde{\omega}_r = 2\pi/\tilde{T}_r$. The hydrodynamic pressure function, which depends on the vertical ordinate and the frequency, is generally complex valued; details related to its definition are included in Appendix A. The parameter $S_a(\tilde{T}_1,\tilde{\xi}_1)$ denotes the spectral acceleration of the design earthquake corresponding to period $\tilde{T}_1$ and damping $\tilde{\xi}_1$ of the equivalent SDOF system, $w_s(y)$ denotes the unit weight of the model per unit height, and g is the acceleration of gravity.

The parameter $\tilde{T}_r$ denotes the natural vibration period of the equivalent SDOF representing the fundamental mode response of the dam on rigid foundation with impounded water, and its value is affected by dam-water interaction and reservoir bottom absorption phenomena. These effects can be expressed as follows:

$$\tilde{T}_r = R_r T_1 \tag{4}$$

where T_1 is the first natural period of the dam with rigid foundation and empty reservoir and R_r is a period modification factor that depends on the properties of the dam, the depth of the water, and the absorptiveness of the reservoir bottom materials.

The parameter $\tilde{T}_1$ indicates the natural vibration period of the equivalent SDOF representing the fundamental mode response of the dam on flexible foundation rock with impounded reservoir and can be determined by the following expression:

$$\tilde{T}_1 = R_f \tilde{T}_r = R_f R_r T_1 \tag{5}$$

where R_f is a period modification factor that depends on the properties of the dam and the foundation rock.

If ξ_1 indicates the fundamental damping ratio of the dam on rigid foundation with empty reservoir, then the damping ratio of the equivalent SDOF representing the fundamental mode response of the dam on flexible foundation rock with impounded reservoir can be determined by the following expression:

$$\tilde{\xi}_1 = \frac{1}{R_r (R_f)^3} \xi_1 + \xi_r + \xi_f \tag{6}$$

where ξ_r denotes the added damping due to dam-water interaction and reservoir bottom absorption, and ξ_f indicates the added damping due to dam-foundation interaction.

As indicated by Equations 5 and 6, the effects of dam-water interaction and dam-foundation interaction are quantified independently and then combined to determine the dynamic properties of the equivalent SDOF system.

To simplify the implementation of the procedure, the imaginary-valued component of the hydrodynamic pressure is neglected in the determination of the equivalent lateral forces, which can be defined as follows:

$$f_1(y) = \frac{\tilde{L}_1}{\tilde{M}_1} \frac{S_a(\tilde{T}_1, \tilde{\xi}_1)}{g} \left[w_s(y)\phi(y) + gp(y, \tilde{T}_r) \right] \tag{7}$$

where $p(y, \tilde{T}_r) = \mathrm{Re}\left[\overline{p}_1(y, \tilde{T}_r) \right]$. Considering only the real component of the hydrodynamic pressure, the parameters $\tilde{L}_1$ and $\tilde{M}_1$ are now given by

$$\begin{aligned} \tilde{L}_1 &= L_1 + \int_0^H p(y, \tilde{T}_r)\, dy \\ \tilde{M}_1 &= M_1 + \int_0^H p(y, \tilde{T}_r)\phi(y)\, dy \end{aligned} \tag{8}$$

It is convenient to write the equivalent lateral forces associated with the fundamental mode response of the dam in terms of the components associated with inertial effects and with the hydrodynamic pressures as follows:

$$f_1(y) = f_1^i(y) + f_1^h(y) \tag{9}$$

where

$$f_1^i(y) = \frac{\tilde{L}_1}{\tilde{M}_1}\frac{S_a(\tilde{T}_1,\tilde{\xi}_1)}{g}w_s(y)\phi(y)$$

$$f_1^h(y) = \frac{\tilde{L}_1}{\tilde{M}_1}\frac{S_a(\tilde{T}_1,\tilde{\xi}_1)}{g}gp(y,\tilde{T}_r) \tag{10}$$

The formulation incorporates the response contributions of higher vibration modes by means of an additional set of equivalent lateral forces, developed based on the assumption that higher vibration modes essentially respond in a static manner. The equivalent lateral forces associated with higher vibration modes are given by the following expressions:

$$f_{sc}(y) = f_{sc}^i(y) + f_{sc}^h(y) \tag{11}$$

where

$$f_{sc}^i(y) = \frac{a_g}{g}w_s(y)\left[1-\frac{L_1}{M_1}\phi(y)\right]$$

$$f_{sc}^h(y) = \frac{a_g}{g}\left[gp_0(y)-\frac{\hat{B}_1}{M_1}w_s(y)\phi(y)\right] \tag{12}$$

where $p_0(y)$ denotes the hydrodynamic pressure distribution acting on a rigid dam undergoing unit acceleration and neglecting water compressibility. The parameter $\hat{B}_1$ is given by

$$\hat{B}_1 = \int_0^H p_0(y)\phi(y)dy \tag{13}$$

Computation of parameters

The evaluation of the equivalent lateral forces as defined in Equations 10 and 12 requires the determination of the fundamental dynamic characteristics of the dam on rigid foundation with empty reservoir [T_1 and $\phi(y)$]. This can be achieved by the eigenvalue analysis of an appropriate finite-element of the section. In addition, the procedure requires the determination of the parameters R_r R_f, ξ_r, and ξ_f, whose values can be assigned based on a series of standard values tabulated for a range of typical conditions. To avoid the computation of the hydrodynamic pressure functions, nondimensional functions $gp(\hat{y})/\gamma_w H$ and $gp_0(\hat{y})/\gamma_w H$, defined in terms of $\hat{y} = y/H$, are available in tabulated form

for a range of conditions. The associated integral quantities $\tilde{L}_1$ and $\tilde{M}_1$ can be conveniently computed as follows:

$$\tilde{L}_1 = L_1 + A_p \frac{F_{st}}{g}\left(\frac{H}{H_s}\right)^2$$

$$\tilde{M}_1 = \left(R_r\right)^2 M_1 \tag{14}$$

where F_{st} denotes the resultant of the hydrostatic actions on the upstream face of the dam, and

$$A_p = 2\int_0^1 \frac{gp(\hat{y})}{\gamma_w H} d\hat{y} \tag{15}$$

The coefficient A_p is also available in tabulated form for a range of conditions. Similarly, the parameter $\hat{B}_1$ can be computed as

$$\hat{B}_1 = \beta_1 \frac{F_{st}}{g}\left(\frac{H}{H_s}\right)^2 \tag{16}$$

where the coefficient β_1 is given by

$$\beta_1 = 2\int_0^1 \frac{gp_0(\hat{y})}{\gamma_w H}\phi(\hat{y}) d\hat{y} \tag{17}$$

The tabulated values available in the literature were determined for a specific range of conditions (Fenves and Chopra 1986, Chopra and Tan 1989). For example, standard values of the parameters R_r and ξ_r are available for values of the modulus of elasticity of concrete (E_s) that do not exceed $5 \cdot 10^6$ psi. In particular, the standard values of R_r were determined based on an approximate expression for the vibration period of the equivalent SDOF representing the fundamental response of the dam with impounded water. This procedure was found to be not sufficiently reliable for some conditions ($E_s > 4 \cdot 10^6$ psi, $E_s = 4 \cdot 10^6$ psi with $H/H_s \geq 0.80$, and $E_s = 3.5 \cdot 10^6$ psi with $H/H_s \geq 0.85$), and it was necessary to use an alternative approach directly based on the exact fundamental mode response function of the dam-water system to generate the standard values of R_r for those conditions. This example highlights the fact that the analyst must be aware of the limitations regarding the applicability of the standard data available in the literature. In particular, special judgment must be exercised when using the standard values for conditions outside the original parameter ranges, and extra conservatism should be incorporated into the analysis to compensate for the increased uncertainty.

It is important to note that the appropriate determination of R_r influences the definition of the hydrodynamic pressure function as well as the determination of

the coefficients $\tilde{L}_1$ and $\tilde{M}_1$ (Equation 14). The tabulated values of the normalized hydrodynamic pressure function $gp(\hat{y})/\gamma_w H$ and the coefficient A_p are given as a function of the ratio R_w, which clearly depends on R_r as follows:

$$R_w = \frac{T_1^r}{\bar{T}_r} = \frac{1}{R_r}\frac{T_1^r}{T_1} \tag{18}$$

in which $T_1^r = 4H/C_w$ is the fundamental vibration period of the impounded water for rigid reservoir bottom conditions, and C_w is the velocity of pressure waves in water.

Response Combination

Let r_1 and r_{sc} denote the values of a response quantity obtained after performing static analyses of the dam subjected to the sets of equivalent lateral forces $f_1(y)$ and $f_{sc}(y)$, respectively. The response quantities associated with each set of lateral forces represent maximum design values and therefore must be combined appropriately by a statistical method, such as the square root of the sum of the squares. Therefore, the estimate of the dynamic response r_d can be obtained as follows:

$$r_d = \sqrt{(r_1)^2 + (r_{sc})^2} \tag{19}$$

The total response is obtained by considering the static effects,

$$r_{peak} = r_{st} \pm r_d \tag{20}$$

It is necessary to consider the directionality of the seismic excitation and to apply the equivalent lateral forces in both upstream and downstream directions because of the nonsymmetric characteristics of the monolith cross section.

4 Finite-Element Model and Analysis Parameters

Introduction

This section describes the finite-element model developed to represent monolith 12, as well as the definition of the equivalent lateral forces for the simplified dynamic analysis. The main focus of this study is to evaluate the potential impact that the dimensions and location of the proposed air vent might have on the local and global structure integrity of the monolith when subject to the MCE. The implementation of the simplified dynamic analysis procedure requires an appropriate finite-element idealization of the structure, which has a twofold purpose. It is used first to determine the fundamental dynamic characteristics (fundamental period and mode shape) of the monolith and later to perform the corresponding stress analyses. Therefore, the model was developed in such a way it captures the relevant global features of the section influencing the fundamental vibration mode for upstream-downstream motion, and it also provides enough detail about the local conditions near the downstream exit of the air manifold.

Monolith Geometry

Figure 3 shows the main characteristics of the nonoverflow and overflow halves of monolith 12. To facilitate the analysis, the 3D finite-element mesh was based on a simplified version of the actual geometry. The following simplifications were introduced:

a. The base of the model was defined as a horizontal plane at elevation 195.[1] The actual average elevation of the base of the monolith approximately corresponds to el 197 for the upstream 75 percent of the section, while the remaining downstream portion falls steeply toward the spillway.

b. The spillway surface was defined consistently with respect to other models of spillway monoliths developed by SPK (curved surface modeled with segments).

[1] All elevations (el) cited herein are in meters referenced to the National Geodetic Vertical Datum.

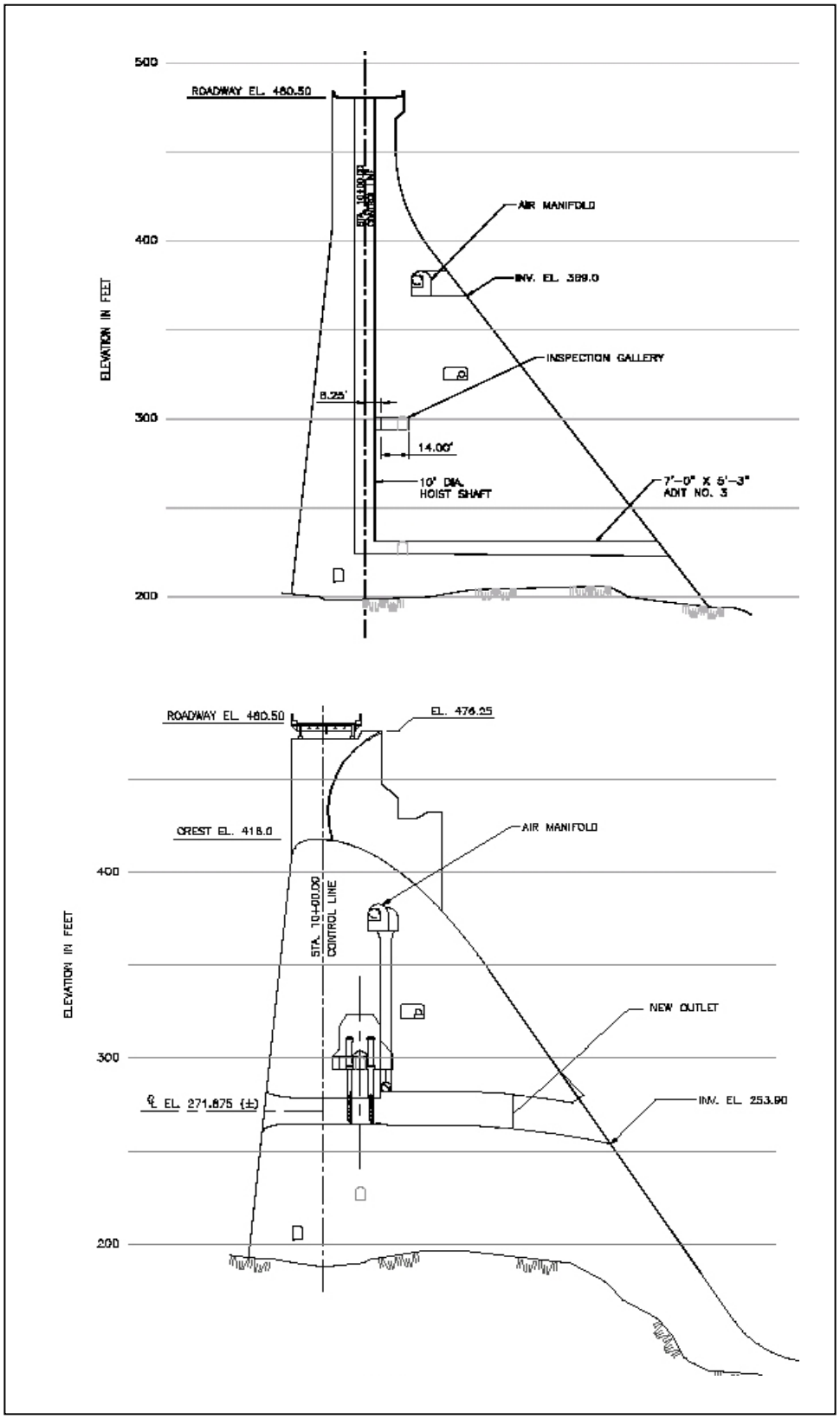

Figure 3. Nonoverflow and overflow sections of monolith 12

c. The pier shape was simplified to three linear segments, similar to previous models.

d. A single rectangular void was used to represent the total volume of the chamber and equipment room, and the inspection gallery connecting the chamber to each side of the monolith was eliminated.

e. The upstream and downstream portions of the conduit were defined continuously with the same size, and the conduit was re-aligned parallel to the lateral monolith faces (conduit skew was eliminated).

f. The vertical airshaft was eliminated.

g. The downstream face of the upper part of the nonoverflow section was defined vertically up from el 451 (top of curved transition).

h. The pipe gallery was defined with a rectangular section and oriented normal to the lateral monolith faces.

i. The side adits coming off adit No. 3 at el 224 (along the transverse direction) were eliminated.

j. Air-manifold turnout was assumed at a right angle, and air-manifold exit (downstream face) was defined with a rectangular section.

k. The tainter gate was not included in the model, but the force resultants associated with hydrostatic and hydrodynamic actions were incorporated as concentrated forces acting on the pier wall at the trunnion location, which was defined 10 ft upstream from the lowest corner of the pier wall.

Finite-Element Model

A finite-element grid representative of the adopted simplified geometry was developed using PATRAN, taking advantage of the CAD information generated by SPK. This finite-element mesh, shown in Figure 4, includes 65,197 nodes and 57,559 solid elements (8-noded and 6-noded elements). The model was assumed fixed at its horizontal base, where the three displacement components were restrained for the base nodes. Two different boundary conditions were considered along the two lateral surfaces of the monolith representing the two extreme conditions of no lateral restraint (no displacement restriction on the lateral surface nodes) and total lateral restraint (no displacements parallel to the dam axis were allowed on the lateral surface nodes).

The material properties adopted for the mass concrete are presented in Table 1. The total height of the model (H_s) is 285.5 ft, and the reservoir water surface was assumed at gross pool elevation (el 466 ft), which represents a height of impounded water (H) of 272 ft with respect to the base. Based on the elevation corresponding to the spillway crest (el 418 ft), the height of the overflow section without the pier (H_{sp}) is 223 ft.

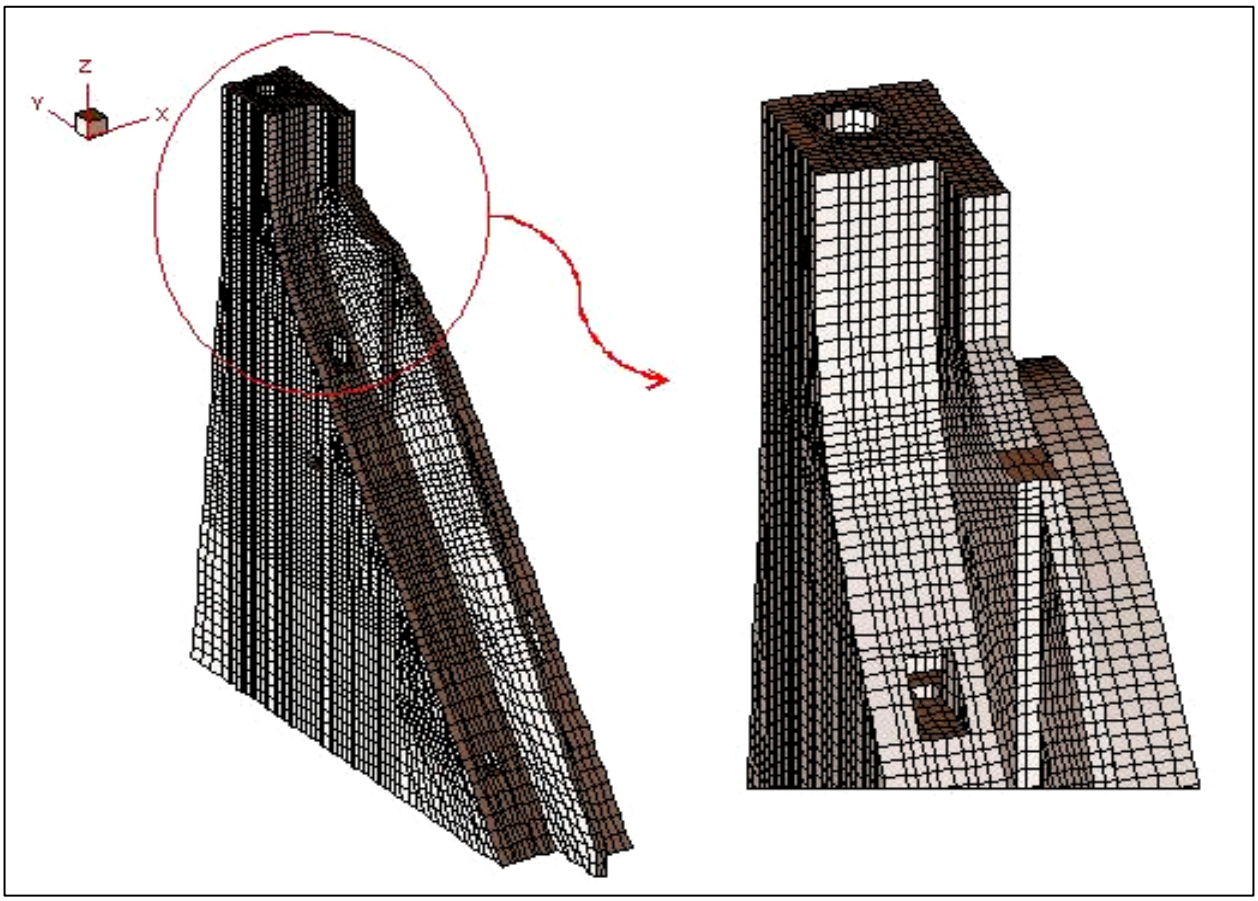

Figure 4. Finite-element model of monolith 12

Effects of uplift pressures or tail-water were not included in the model; therefore, they were not considered for the stress computations presented in this report.

Table 1
Material Parameters for Mass Concrete

Material Property	Value
Unit weight γ_s, pcf	158
Dynamic modulus of elasticity E_s, psi	5.9 10^6
Poisson's ratio ν	0.19

The total volume of the simplified model is virtually identical to that portion of the original 3D model above el 195 ft. The total weight of the model was 226,560 kips, which is about 6 percent lighter than the weight of the entire original 3D model (equal to 240,300 kips, including the volume beneath el 195 ft).

Dynamic Characteristics

The analyses were performed using ABAQUS. An eigenvalue extraction was performed for the model representing the dam on rigid foundation rock with empty reservoir. Two sets of lateral boundary conditions representing limit cases of monolith behavior along the axis of the dam were evaluated. The first case

corresponds to an isolated monolith whose lateral surfaces (contraction joint planes) are totally unrestricted along the dam axis, and the second case represents a monolith whose lateral surfaces are constrained to in-plane motion. Table 2 indicates the relevant natural frequencies for both cases. For the case without lateral restraint, the first mode shape is associated with the fundamental out-of-plane behavior, which is dominated by lateral bending response. The second mode shape is associated with the fundamental in-plane behavior in the form of upstream-downstream bending response. This second mode shape shows no significant torsional components, and the corresponding natural period was determined as 0.156 sec. Of course, the presence of the adjacent monoliths (11 and 13) will induce a significant restraint on out-of-plane displacements. Assuming that the lateral surfaces are restricted to in-plane motion, the first mode shape represents the fundamental in-plane behavior and is associated with a natural vibration period of 0.151 sec. This value is slightly lower than in the previous case because it reflects the effects of the restrained lateral deformations. For the purpose of the simplified analysis, it will be assumed that the fundamental response of the system can be adequately represented by a model with lateral restraint.

Table 2
Natural Frequencies and Periods from Finite-Element Model

Monolith 12 (Unrestricted along X)			Monolith 12 (Restricted along X)		
Mode	Frequency [Hz]	Period [sec]	Mode	Frequency [Hz]	Period [sec]
1	2.394	0.418	1	6.602	0.151
2	6.426	0.156	2	13.890	0.072
3	7.828	0.128	3	14.632	0.068
4	9.488	0.105	4	16.789	0.060
5	13.436	0.074	5	16.989	0.059
6	13.990	0.071	6	19.173	0.052
7	15.896	0.063	7	20.978	0.048
8	16.303	0.061	8	23.322	0.043
9	16.788	0.060	9	24.561	0.041
10	18.259	0.055	10	27.097	0.037

Table 3
Computed and Standard Values for Fundamental Period

Properties	Value
Computed fundamental period T_1, sec	0.151
Standard fundamental period T_1^*, sec (overflow sections, H_s < 300 ft)	0.147
Standard fundamental period T_1^*, sec (nonoverflow sections)	0.165

Monolith 12 is a hybrid monolith in the sense that it consists of overflow and nonoverflow sections. Table 3 shows a comparison between the computed fundamental period and the values obtained using the formulas developed for standard overflow and nonoverflow sections (Fenves and Chopra 1986, Chopra and Tan 1989). The table reveals that the value predicted assuming an overflow section shows a closer agreement than the standard value corresponding to a nonoverflow section.

Figure 5 shows the mode shape corresponding to the first natural frequency computed for the monolith with lateral restraint. This constitutes the fundamental vibration mode for the system response mainly associated with upstream/ downstream motion, and this mode shape is used to develop the inertial and hydrodynamic equivalent loads for the simplified analysis. An average fundamental mode shape can be computed considering the horizontal components of this fundamental vibration mode for all the nodes along the upstream face. The resulting mode shape depends only on the vertical ordinate, and it can be used for the implementation of the simplified stress analysis procedure. This average mode shape is shown in Figure 6, and it is compared with the standard mode shapes for nonoverflow (Fenves and Chopra 1985a) and overflow sections

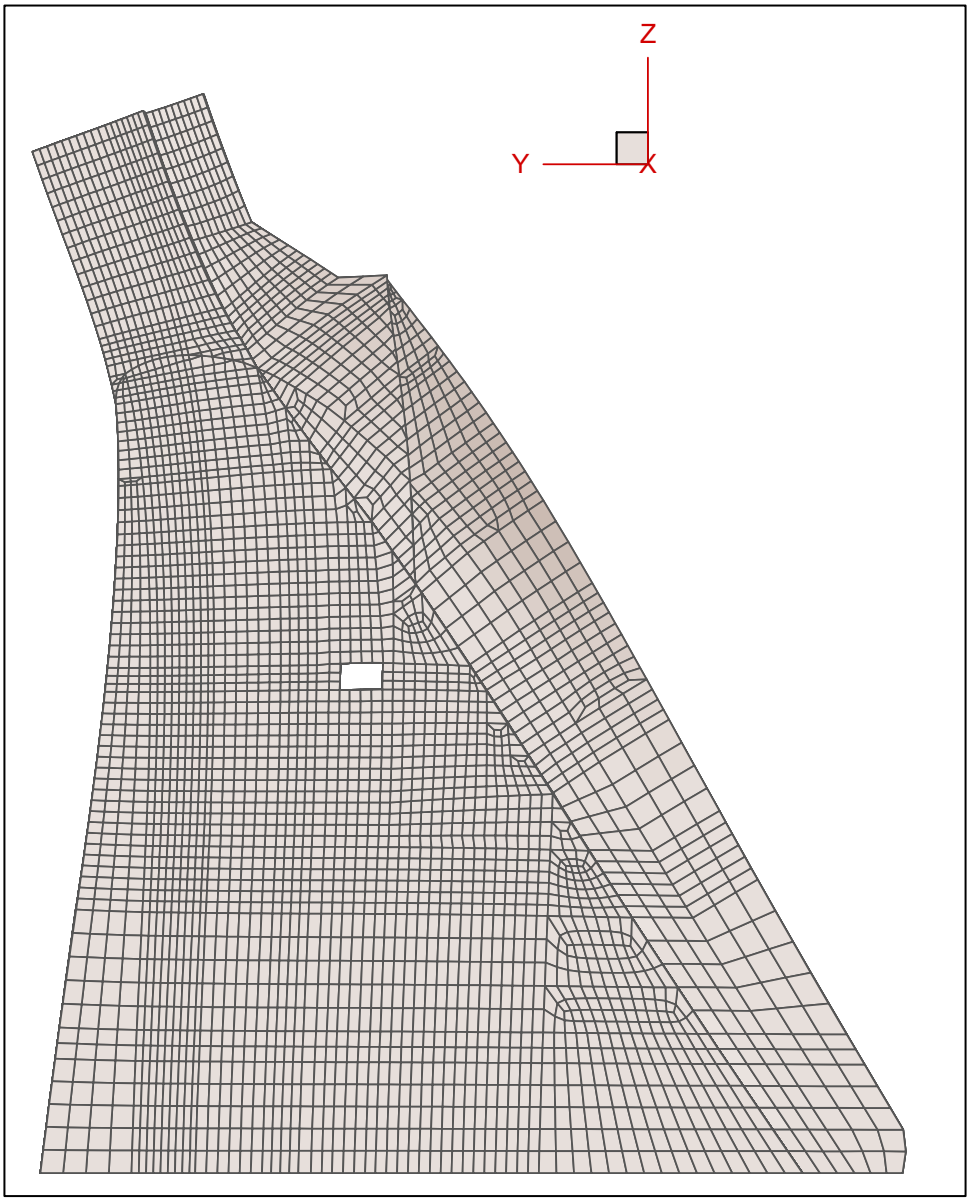

Figure 5. Fundamental mode of vibration for monolith 12 (upstream/ downstream response)

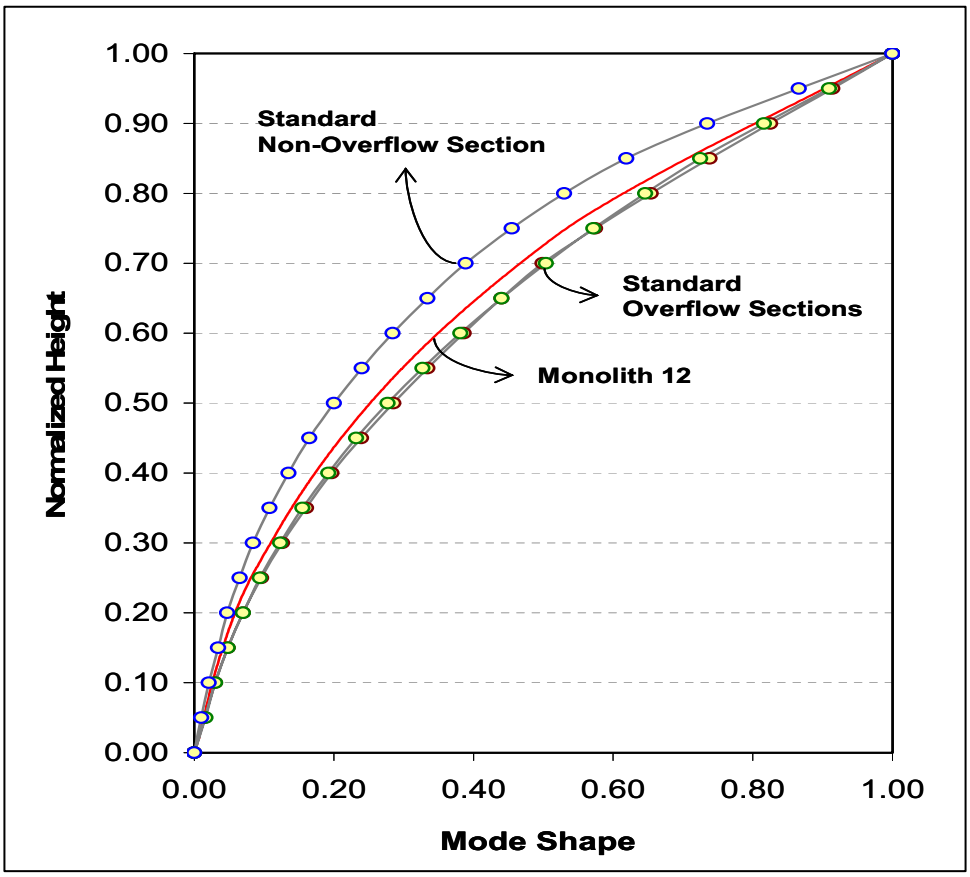

Figure 6. Simplified fundamental mode shape compared with "standard" mode shapes for overflow and nonoverflow sections

(Chopra and Tan 1989). In the case of overflow sections, two standard mode shapes were developed, for lower (H_s <300 ft) and higher ($H_s \geq$ 300 ft) dams. To facilitate the comparison, modal components and coordinates along the vertical axis are normalized. It can be seen that the standard mode shape for shorter overflow sections (H_s <300 ft) shows a relatively closer agreement with the average mode shape developed for monolith 12. It is also interesting to compare the average mode shape developed for monolith 12 with the fundamental mode shape for a typical overflow monolith such as monolith 14. Figure 7 shows these mode shapes for monoliths 12 and 14, along with those for standard overflow sections.

Based on this discussion, it is assumed that the standard data for shorter overflow sections can be used as a baseline for the parameters required in the computation of the equivalent lateral loads. Therefore, it is assumed that, for the purpose of determining the seismic loads, the fundamental in-plane dynamic behavior of monolith 12 is dominated by its overflow characteristics.

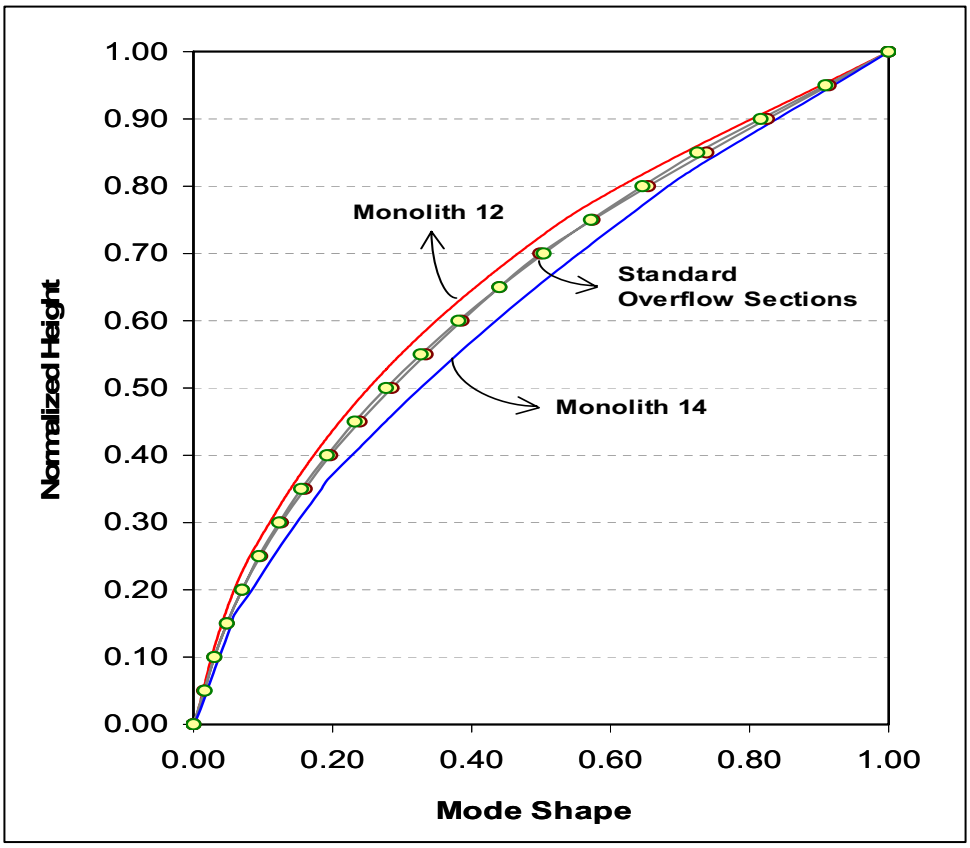

Figure 7. Simplified fundamental mode shapes for monoliths 12 and 14 compared with "standard" mode shapes for overflow sections

Parameters for Simplified Analysis

The depth of impounded water considered for the analyses is $H = 271$ ft; therefore, the ratio between the total height of the upstream face of the dam and the depth of the impounded water is given by $H/H_s = 0.95$. A value of 0.75 is adopted for the wave reflection coefficient, as indicated by previous seismic evaluation studies of Folsom Dam ($\alpha = 0.75$). In addition, a hysteretic damping coefficient of 10 percent is adopted for the foundation rock ($\eta_f = 0.10$). Considering the value of elastic modulus for the foundation rock employed in previous studies ($E_f = 7.9 \cdot 10^6$ psi), the ratio between the foundation rock and dam concrete values is given by $E_f/E_s = 1.34$.

To determine the equivalent lateral loads associated with inertial actions, it is necessary to quantify the mass (or volume) distribution along the height of the section. Figure 8 shows the variation of volume per unit height for monolith 12. This volume distribution can be determined in exact form by considering the finite-element model and taking into account each element's contribution as a function of the elevation. The discrete model was divided in N_b zones, with height Δh_i and centroid elevation y_i. If $N_e^{(i)}$ denotes the number of elements within the i^{th} zone, the zone volume can be obtained by adding the corresponding

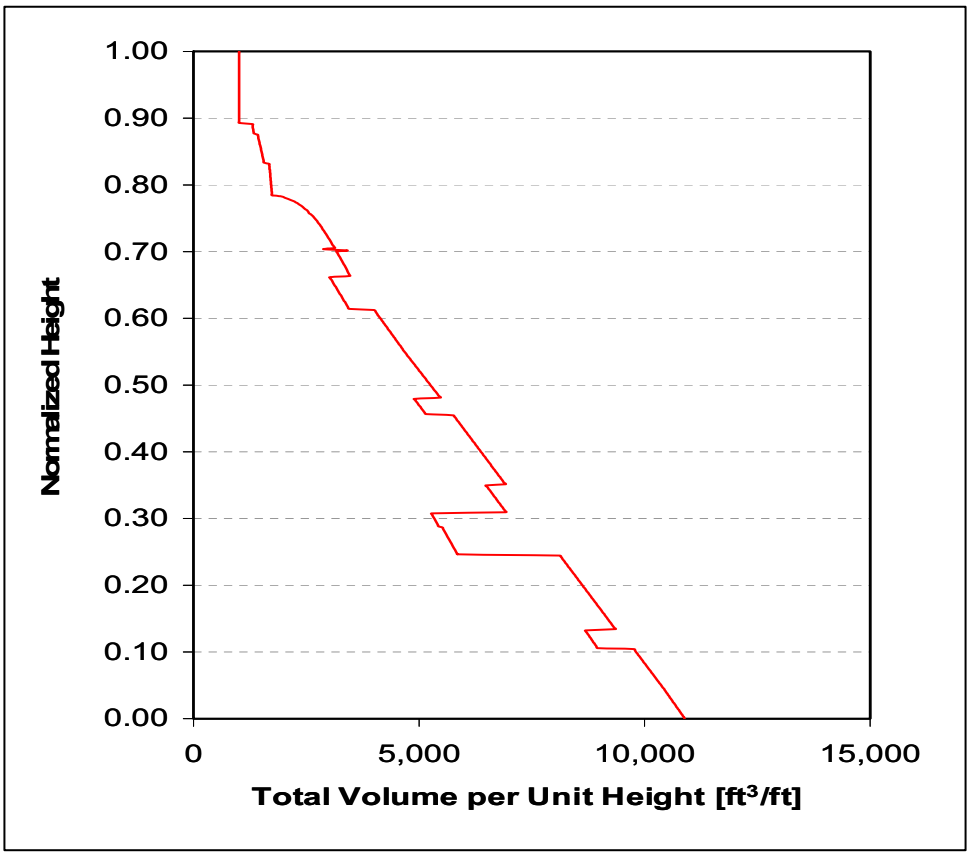

Figure 8. Total volume distribution along the height of monolith 12

element volumes v_j^e. By dividing by Δh_i, the zone volume for unit height can be finally obtained as follows:

$$v(y_i) = \frac{1}{\Delta h_i} \sum_{j=1}^{N_e^{(i)}} v_j^e \tag{21}$$

Based on this volume distribution, the variation of weight along the height for the complete monolith can be obtained by simply multiplying $v(y_i)$ by the concrete unit weight. This procedure generates the distribution of weight per unit height for the complete monolith. To obtain the distribution of weight per unit height $w_s(y_i)$ that corresponds to an equivalent "slice" of the model with unit thickness, it is necessary to divide the previous result by the width of the monolith (50 ft). Figure 9 compares the weight distribution for equivalent sections (unit thickness) of monoliths 12 and 14.

Based on the weight distribution for a section with unit thickness, and considering the simplified fundamental mode shape determined in the previous section, the parameters L_1 and M_1 are calculated as follows:

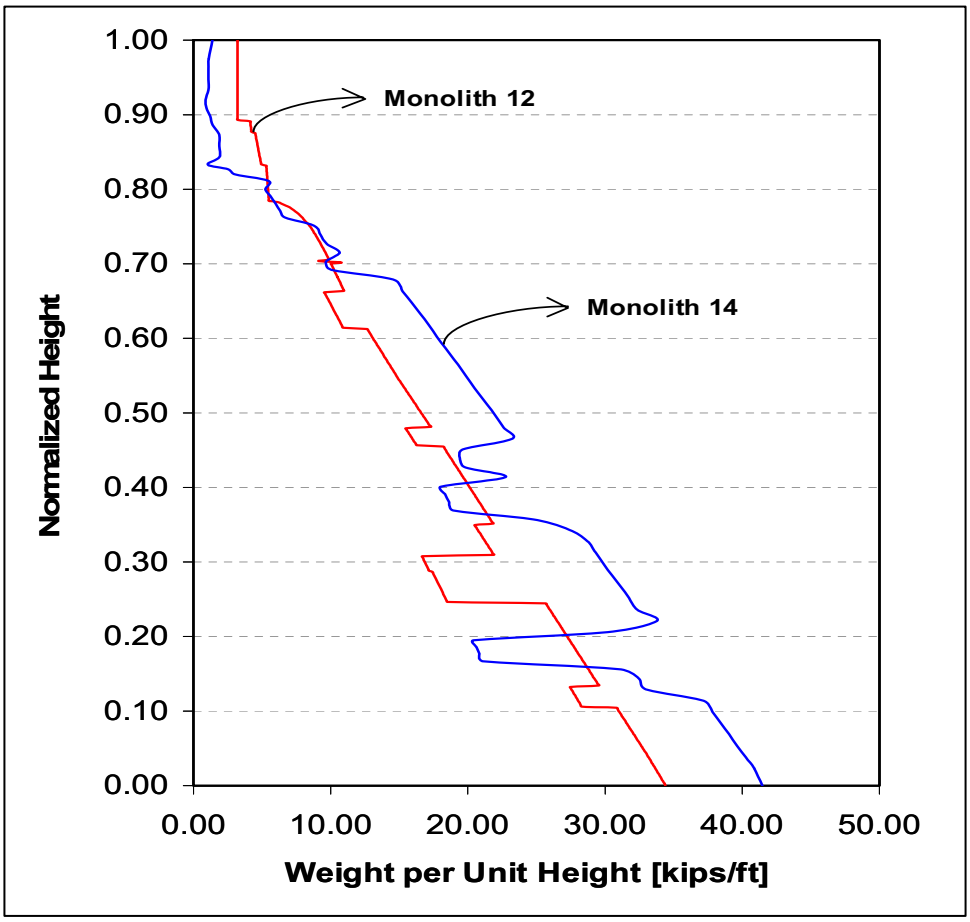

Figure 9. Weight distribution along the height of monoliths 12 and 14 (unit thickness)

$$L_1 = \frac{1}{g}\sum_{i=1}^{N_b} w_s(y_i)\phi(y_i)$$

$$M_1 = \frac{1}{g}\sum_{i=1}^{N_b} w_s(y_i)\left[\phi(y_i)\right]^2 \qquad (22)$$

Their computed values are $L_1 = 25.83$ (kips·sec^2/ft) and $M_1 = 10.36$ (kips·sec^2/ft). It is interesting to compare the values of these parameters as well as their ratio L_1 / M_1 for monoliths 12 and 14, and Table 4 shows these values.

Table 4
Generalized Earthquake Force and Mass Coefficients

Parameters	Monolith	
	12	14
L_1, kips · sec^2/ft	25.83	44.59
M_1, kips · sec^2/ft	10.36	17.40
L_1/M_1	2.49	2.56

Next, it is necessary to compute the two sets of parameters (R_r, ξ_r) and (R_f, ξ_f) associated with the hydrodynamic actions and the influence of the foundation, respectively. In the case of

monolith 14, whose computations are followed as a fundamental baseline, the parameters associated with the hydrodynamic effects were computed using monolith-specific data (Chopra and Basu 2003a) rather than the standard tables provided by Chopra and Tan (1989). The parameters in these tables, based on standard cross-sectional weight distribution and mode shape, are presented only for $E_s \leq 5 \cdot 10^6$ psi. For the purpose of these preliminary analyses of monolith 12, the value of the parameter R_r was estimated based on engineering judgment, considering the standard information provided in Tables 2 and 3 of Chopra and Tan (1989) and the value computed for monolith 14 ($R_r = 1.699$). This information is presented in Figure 10, which shows the two curves corresponding to the standard values provided for lower and higher dams. The figure indicates the value adopted for monolith 12 ($R_r = 1.642$), which was directly obtained by extrapolating the standard data. To determine the added damping ratio due to dam-water interaction and reservoir bottom absorption, a different approach was followed. Figure 11 shows the two curves corresponding to the standard values provided for lower and higher dams, and it also indicates the value specifically computed for monolith 14 ($\xi_r = 0.166$). However, this high damping value was not used in the previous study, in which a limit value was adopted for the total damping of the equivalent SDOF system. A similar approach was employed here,

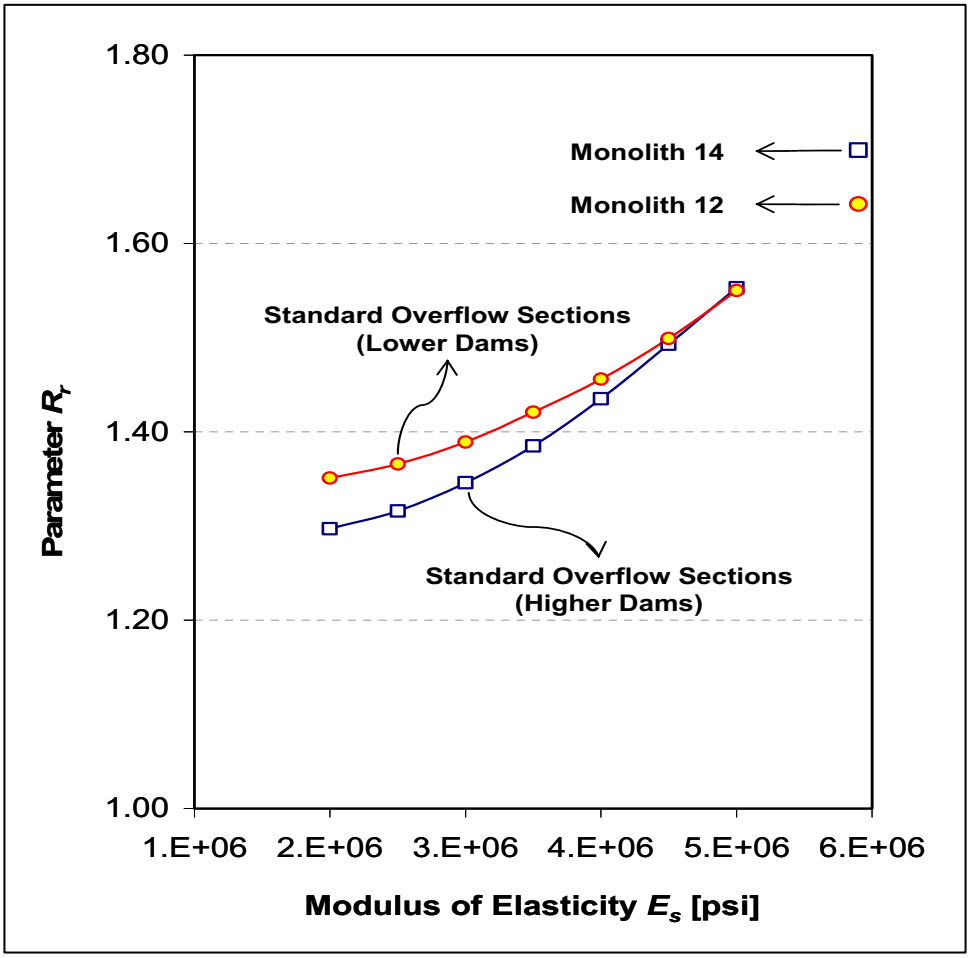

Figure 10. Coefficient R_r as a function of the elastic modulus of the dam concrete

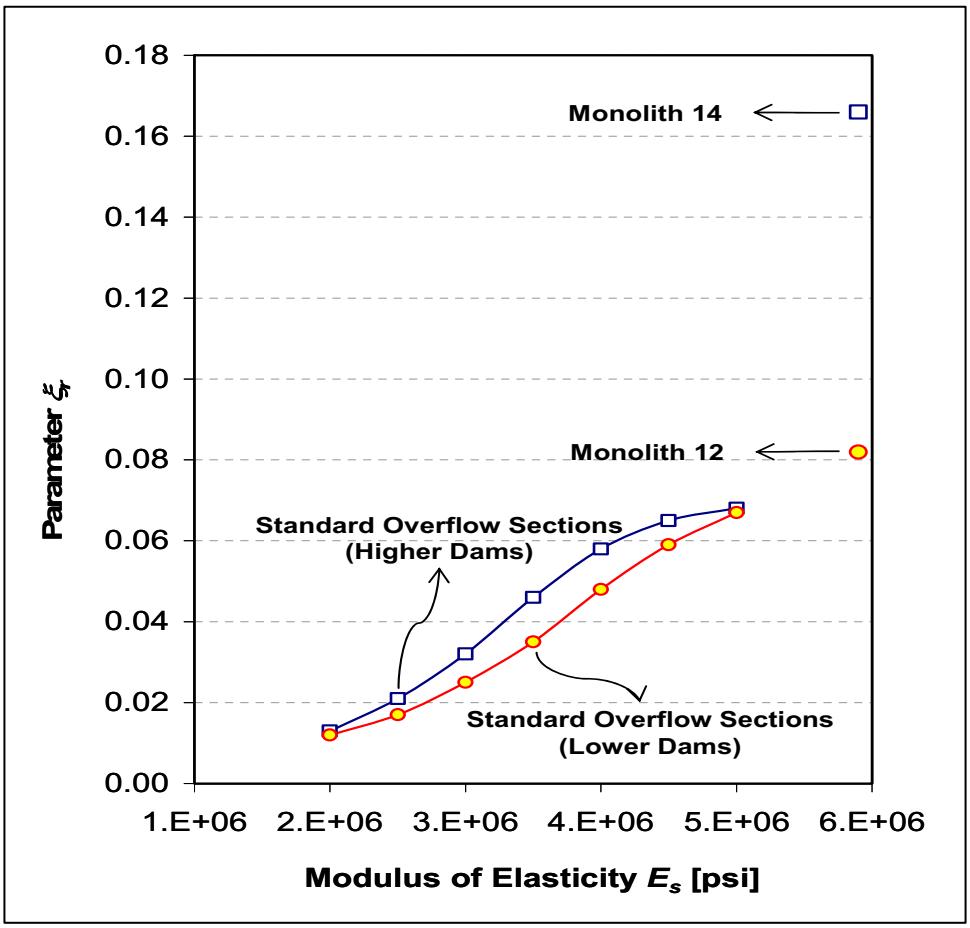

Figure 11. Coefficient ξ_r as a function of the elastic modulus of the dam concrete

and the value of the hydrodynamic added damping was determined by establishing the same limit on the final value of total damping. The resulting value (ξ_r = 0.082) is shown in Figure 11.

The parameters (R_f, ξ_f) associated with the influence of the foundation are determined based on the standard data provided in the work by Chopra and Tan (1989). Figure 12 shows the variation of R_r as a function of the ratio E_f/E_s for both lower and higher dams, and it also indicates the value determined for monolith 12 (R_r = 1.178). Similarly, Figure 13 shows the variation of the added damping ratio due to dam-foundation interaction as a function of E_f/E_s and the value determined for this monolith (ξ_f = 0.059).

Based on these parameters, the natural vibration period and the damping ratio of the equivalent SDOF representing the fundamental mode response of the dam on flexible foundation rock with impounded reservoir can be computed; these are given by $\tilde{T}_1 = 0.293$ sec and $\tilde{\xi}_1 = 0.160$, respectively. Figure 14 shows the MCE acceleration response spectra for damping levels of 5 and 16 percent and indicates the spectral acceleration corresponding to these values of $\tilde{T}_1$ and $\tilde{\xi}_1$, which is S_a = 0.504 g.

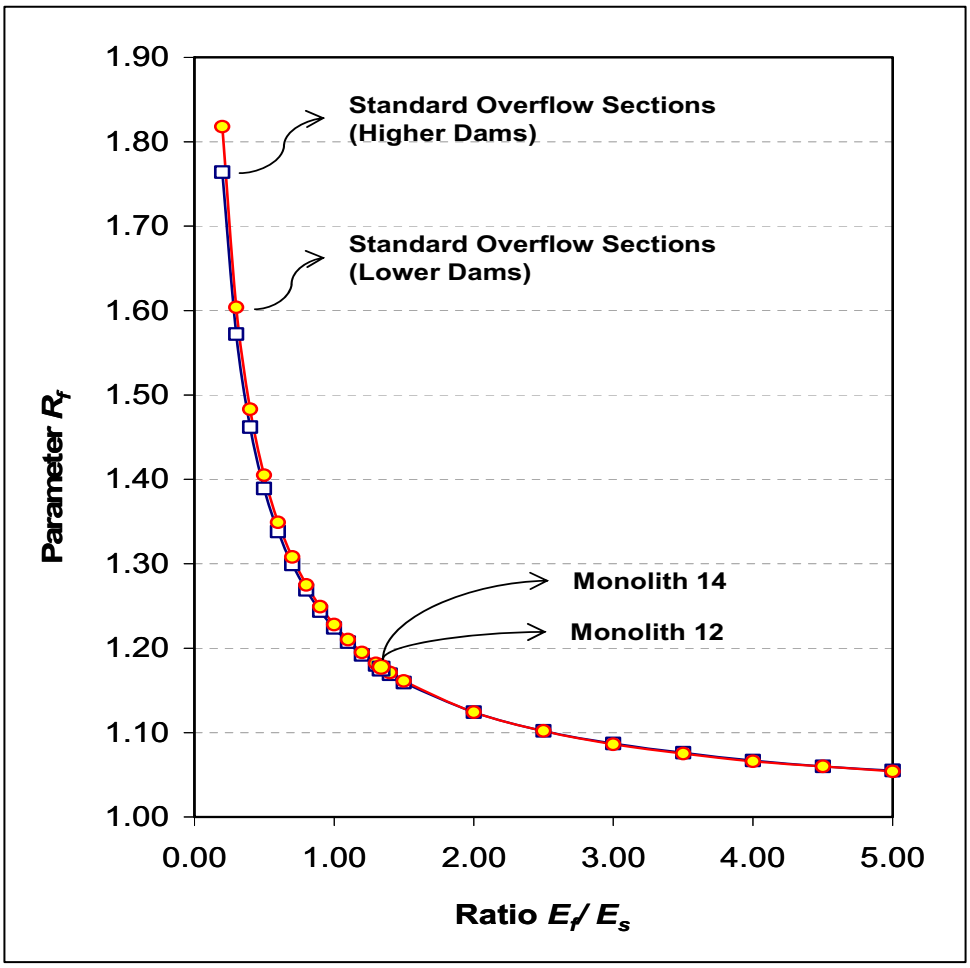

Figure 12. Coefficient R_f as a function of the elastic modulus ratio

To define the lateral loads associated with the hydrodynamic actions on the upstream face, it is necessary to determine the hydrodynamic pressure functions $gp(\hat{y})/\gamma_w H$ and $gp_0(\hat{y})/\gamma_w H$, defined in terms of the normalized height $\hat{y} = y/H$. A monolith-specific pressure function determined for previous studies of monolith 14 is shown in Figure 15. The figure also shows the hydrodynamic pressure function adopted for monolith 12. This pressure distribution was determined based on the standard data in Table 6 of Chopra and Tan (1989), which were arbitrarily increased by 20 percent to achieve levels similar to those defined for monolith 14. Figure 16 shows the hydrodynamic pressure function $gp_0(\hat{y})/\gamma_w H$, which corresponds to the case of a rigid dam with incompressible fluid.

To complete the determination of the equivalent lateral forces, it is necessary to compute the generalized coefficients $\widetilde{L}_1$ and $\widetilde{M}_1$ of the equivalent SDOF system. Based on the values for M_1 and R_r, it is straightforward to compute the coefficient $\widetilde{M}_1$ using the expression in Equation 14. The determination of the coefficient $\widetilde{L}_1$ could also be performed using the corresponding expression in

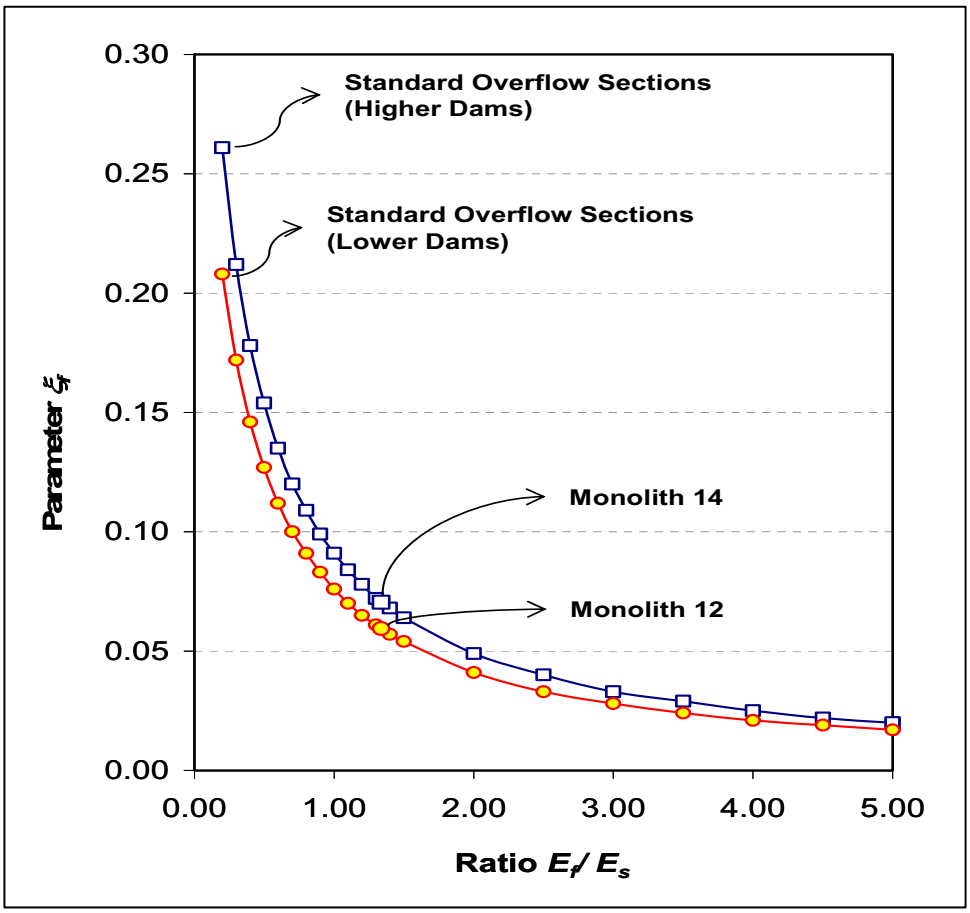

Figure 13. Coefficient ξ_f as a function of the elastic modulus ratio

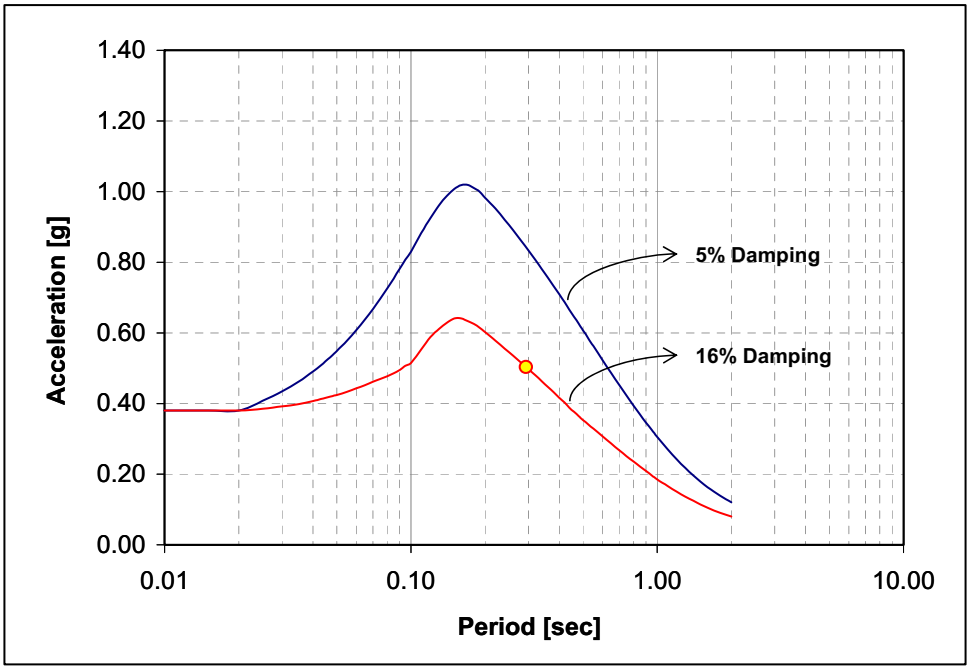

Figure 14. MCE response spectra for different damping levels

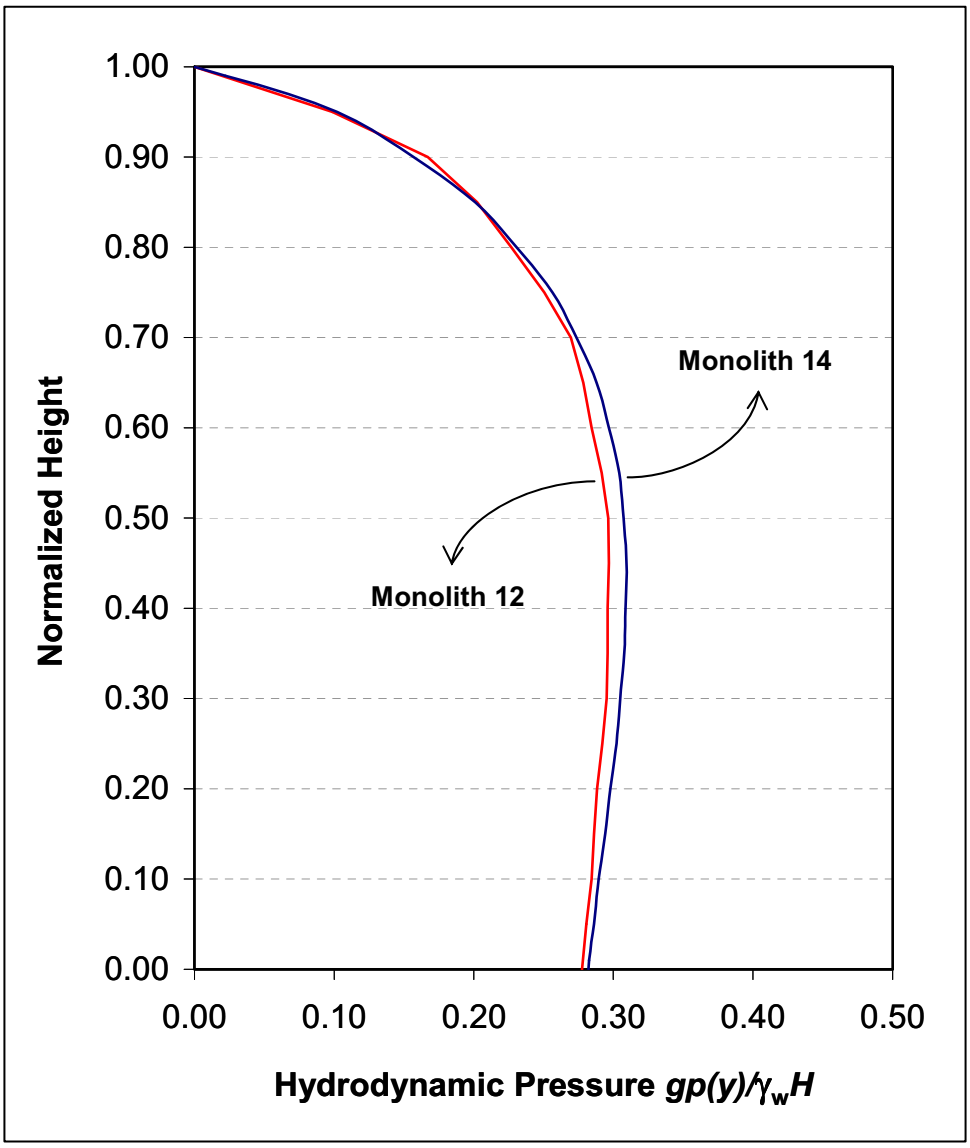

Figure 15. Hydrodynamic pressure distributions for monoliths 12 and 14

Equation 14. However, the process is a little more involved since the parameter A_p reflects the influence of the hydrodynamic pressure function, and this expression actually represents an approximation where only the real component of the hydrodynamic pressure is considered.

Considering the standard data provided in Table 7 of Chopra and Tan (1989), a value of $A_p = 0.480$ can be determined for $\alpha = 0.75$ and $R_w = 0.92$. However, a monolith-specific value of this coefficient developed by Chopra and Basu (2003a) was used in previous studies of monolith 14 instead of the standard values in Chopra and Tan (1989). This more refined calculation considered not only the real part of the hydrodynamic pressure but also the influence of its imaginary component. The value determined for monolith 14 was $A_p = 0.573$, and this higher value is preliminarily adopted for the analysis of monolith 12.

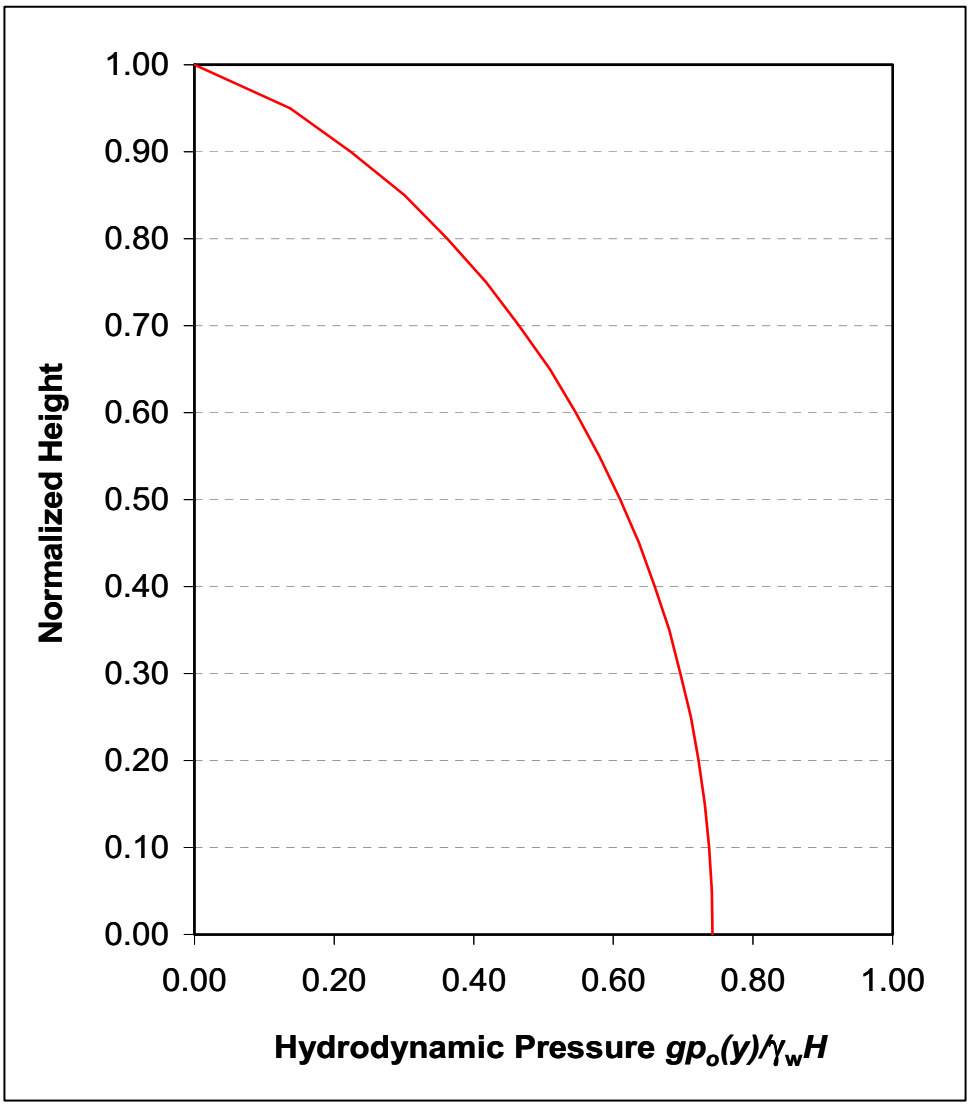

Figure 16. Hydrodynamic pressure distribution for rigid dam and incompressible fluid

Table 5 compares the values of the generalized earthquake force and generalized mass coefficients for monoliths 12 and 14, as well as their ratios.

Table 5
Generalized Earthquake Force and Mass Coefficients — Equivalent SDOF System

Parameters	Monolith	
	12	14
$\tilde{L}_1, kips \cdot sec^2/ft$	62.56	100.12
$\tilde{M}_1, kips \cdot sec^2/ft$	27.92	50.21
$\tilde{L}_1/\tilde{M}_1$	2.24	1.99

The value of the parameter β_1, which depends on the hydrodynamic pressure function $gp_0(\hat{y})/\gamma_w H$ and the mode shape, was determined based on the pressure function shown in Figure 16 and the simplified mode shape defined for monolith 12. The computed value was very close to the standard value provided in the literature ($\beta_1 = 0.249 \cong 0.25$).

Finally, Table 6 summarizes the relevant parameters associated with the simplified dynamic analysis of monolith 12.

Table 6
Parameters for Simplified Dynamic Analysis

Parameter	Value	Parameter	Value
H_S, ft	285.50	R_r	1.642
H, ft	271.00	A_p	0.573
H/H_S	0.95	β_1	0.250
F_{st}, kips	2,291.26	$\tilde{L}_1/\tilde{M}_1$	2.240
$\tilde{T}_1$, sec	0.293	B_1/M_1	1.547
$\tilde{\xi}_1$	0.160	$(a_g/g)L_1/M_1$	0.947
S_a, g	0.504	$(S_a/g)\tilde{L}_1/\tilde{M}_1$	1.129
a_g, g	0.380	$(a_g/g)B_1/M_1$	0.588

5 Analysis of Monolith 12

Loading Cases

The load cases described below were considered for the simplified dynamic analysis of monolith 12 subjected to the horizontal component of the input motion.

Case L1: Static loads

L.1.a) Self-weight effects

L.1.b) Hydrostatic effects

L.1.b.1) Hydrostatic pressure on upstream face

L.1.b.2) Hydrostatic pressure on tainter gate, computed as

$$R_{ST} = \frac{1}{2}\gamma_w (H - H_{sp}) t_g = 1{,}797.12 \text{ kips} \tag{23}$$

where $t_g = 25\,\text{m}$ (width of spillway section)

Case L2: Equivalent lateral forces associated with fundamental mode response

L.2.a) Inertial effects: These are introduced in the 3D finite-element model at the element level, as body forces (proportional to the mass of each finite element) corresponding to a horizontal acceleration variable with the height of the dam, and defined as follows:

$$a_{g1}^{H}(y) = 1.128\, g\, \phi(y) = 36.344\, \phi(y) \text{ ft/sec}^2 \tag{24}$$

where $\phi(y)$ indicates the fundamental mode of the model. A convenient representation of these body forces can be obtained by expressing them as lateral distributed forces that are only a function of the height. Figure 17 depicts the lateral distributed force corresponding to these inertial effects for the equivalent section with unit thickness of monolith 12.

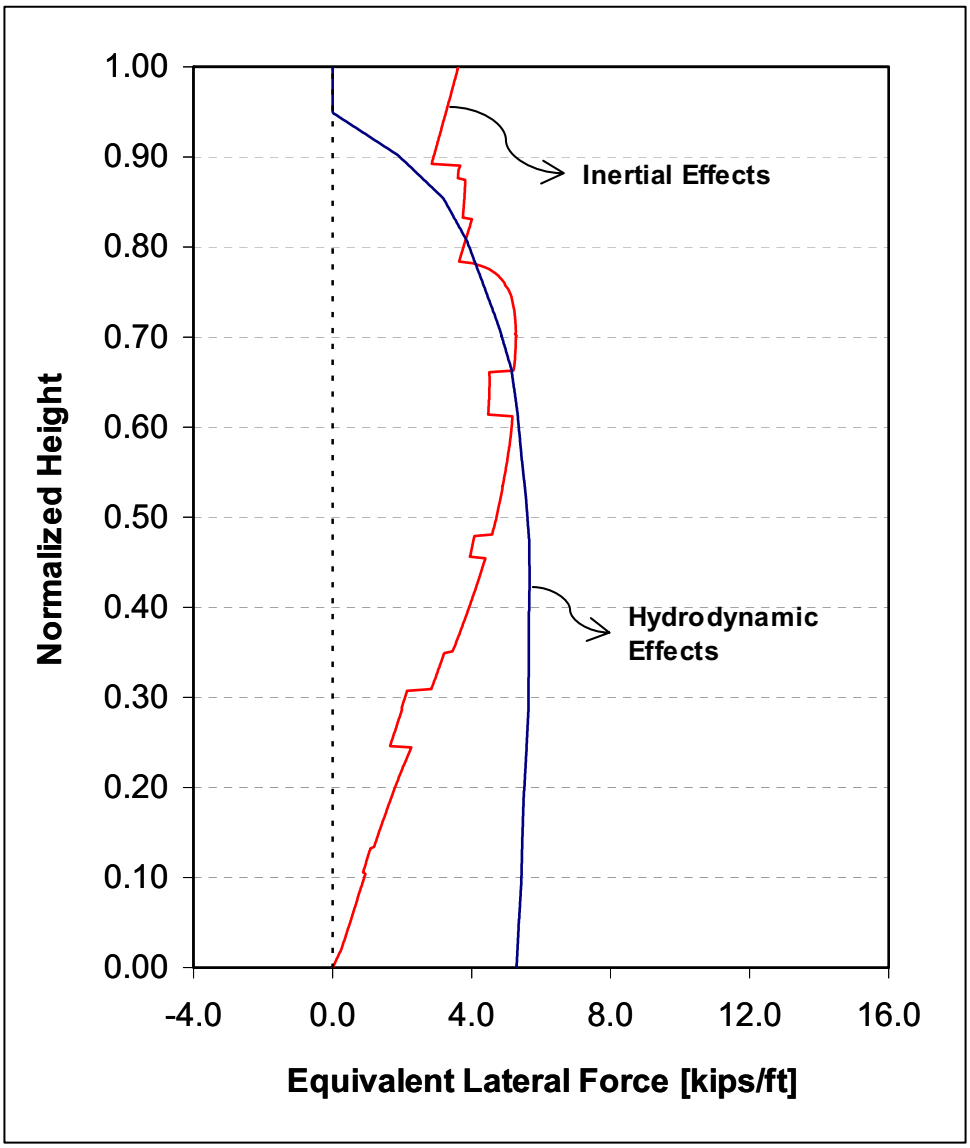

Figure 17. Lateral inertial and hydrodynamic forces per unit height of equivalent section with unit thickness (fundamental mode response)

L.2.b) Hydrodynamic effects

L.2.b.1) Lateral distributed force acting on the upstream face, according to the distribution $p_{h1}(y)$ shown in Figure 17 for the equivalent section with unit thickness.

L.2.b.2) Hydrodynamic pressure on tainter gate, computed as

$$R_{h1} = t_g \int_{H_{sp}}^{H} p_{h1}(y)\,dy = 3{,}106.90 \text{ kips} \qquad (25)$$

Case L3: Equivalent lateral forces associated with higher mode correction

L.3.a) Inertial effects: As in the previous case, these are introduced in the 3D finite-element model at the element level, as body forces (proportional to the mass of each finite element) corresponding to a horizontal acceleration variable with the height of the dam, and defined as follows:

$$a_{g2}^{H}(y) = 0.38\,g - 0.9475\,g\,\phi(y) = \left[12.236 - 30.504\,\phi(y)\right] \text{ft/sec}^2 \quad (26)$$

where again $\phi(y)$ indicates the fundamental mode of the model. As before, Figure 18 depicts the lateral distributed force corresponding to these inertial effects for the equivalent section with unit thickness of monolith 12.

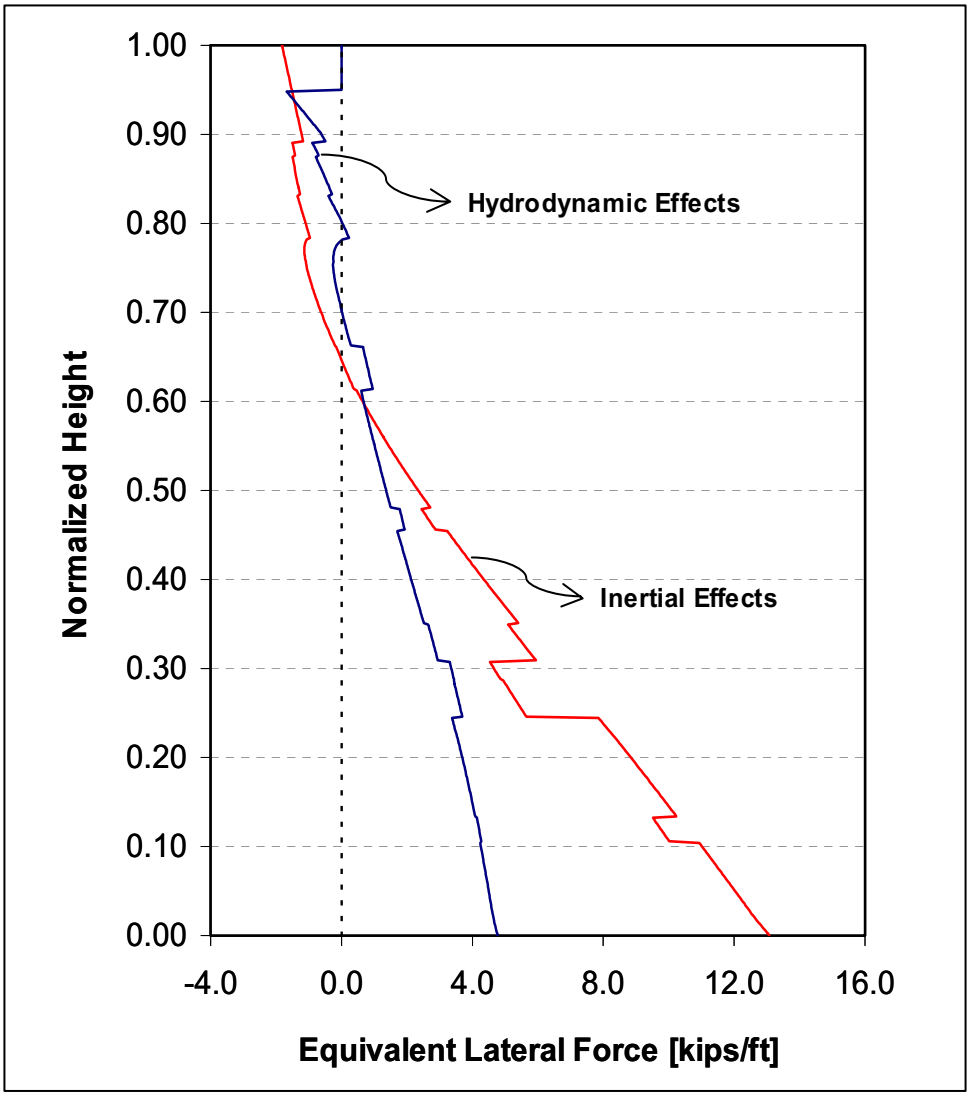

Figure 18. Lateral inertial and hydrodynamic forces per unit height of equivalent section with unit thickness (higher mode response)

L.3.b) Hydrodynamic effects

L.3.b.1) Lateral surface pressure acting on the upstream face according to the distribution $p_{h2}(y)$ shown in Figure 18 for the equivalent section with unit thickness.

L.3.b.2) Hydrodynamic pressure on tainter gate, computed as

$$R_{h2} = t_g \int_{H_{sp}}^{H} p_{h2}(y)\, dy = -72.09\ kips \tag{27}$$

Table 7
Base Resultants

Load Case	Lateral Loads	Resultant percent
L1	Hydrostatic pressure	49.9
	Gate (hydrostatic pressure)	0.8
L2	Inertial forces	20.7
	Hydrodynamic pressure	27.9
	Gate (hydrodynamic pressure)	1.4
L3	Inertial forces	21.6
	Hydrodynamic pressure	10.6
	Gate (hydrodynamic pressure)	0.03

To investigate the relative importance of the different lateral forces considered in the analysis, Table 7 compares the magnitude of their base resultants corresponding to the full section of the model (t_m = 50 ft), expressed as their percentage with respect to the weight of the monolith (226,560 kips).

Results

Figure 19 shows the distribution of normal vertical stresses (σ_{zz}) across the section under the action of the static loads (load case L1). The cross section exhibits compressive stresses at the base reaching a peak of about 360 psi, with the exception of a small region of localized tensile stresses at the heel. The spillway pier also shows an area of tensile stresses associated with the concentrated load representative of the hydrostatic loads acting on the tainter gate. The upstream and downstream views highlight the distortion in the stress contours induced by the openings along these faces. The values of the normal vertical stresses are reduced immediately above and below the openings and increased on their sides.

Figure 20 shows the distribution of normal vertical stresses across the section resulting from the equivalent lateral loads of load case L2, which is associated with the fundamental mode response of the monolith. These lateral loads induce normal stresses with the same sign along most of the upstream face of the model. The downstream face shows normal stresses with the opposite sign, and this is consistent with the fundamental in-plane response.

Figure 21 shows the contour of normal vertical stresses caused by the equivalent lateral loads of load case L3. This load case takes into account the higher mode contributions to the response of the system, and the normal stresses on the upstream and downstream surfaces exhibit a change of sign along the elevation.

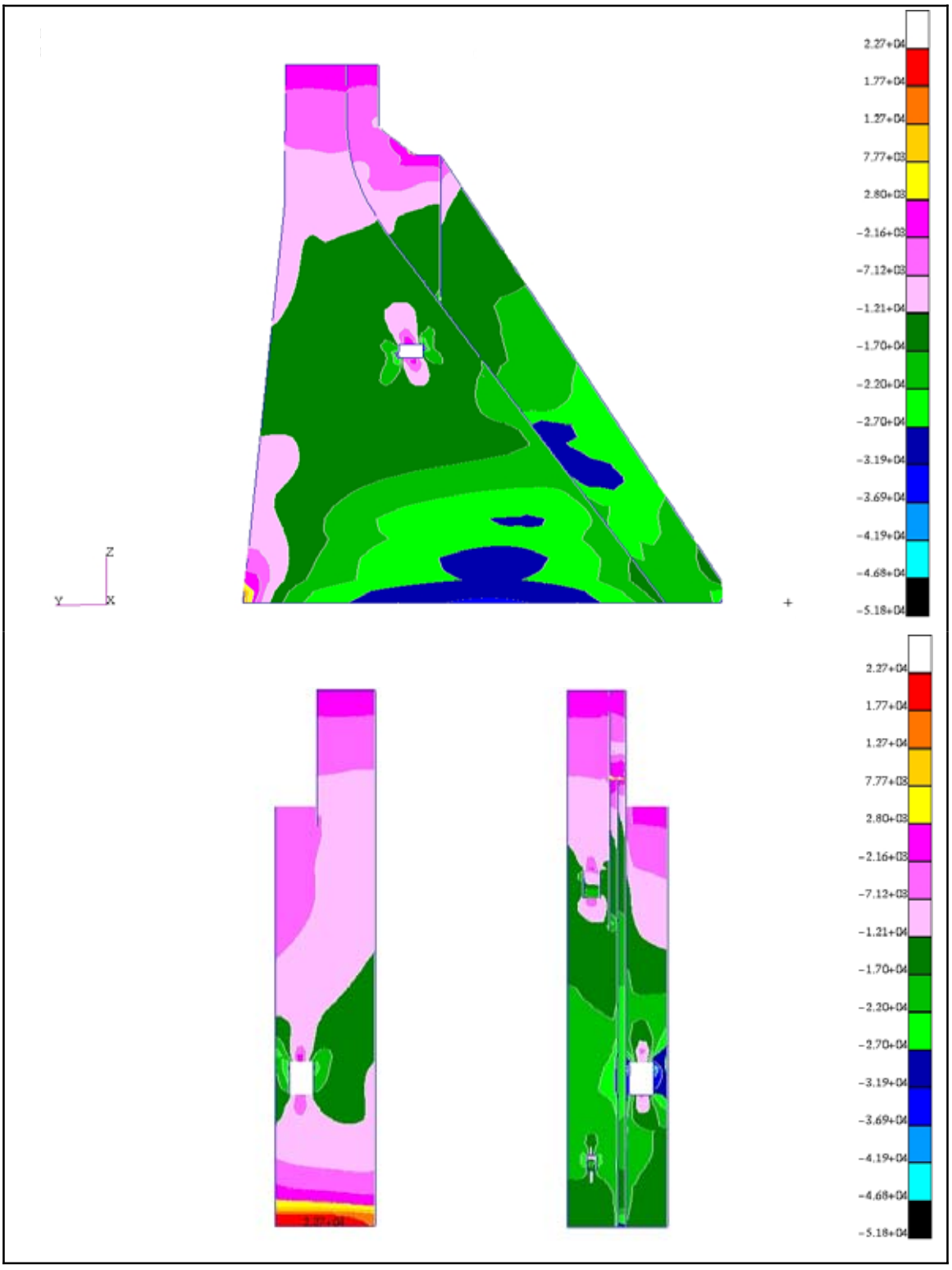

Figure 19. Load case L1 (static): Normal vertical stresses (σ_{zz})

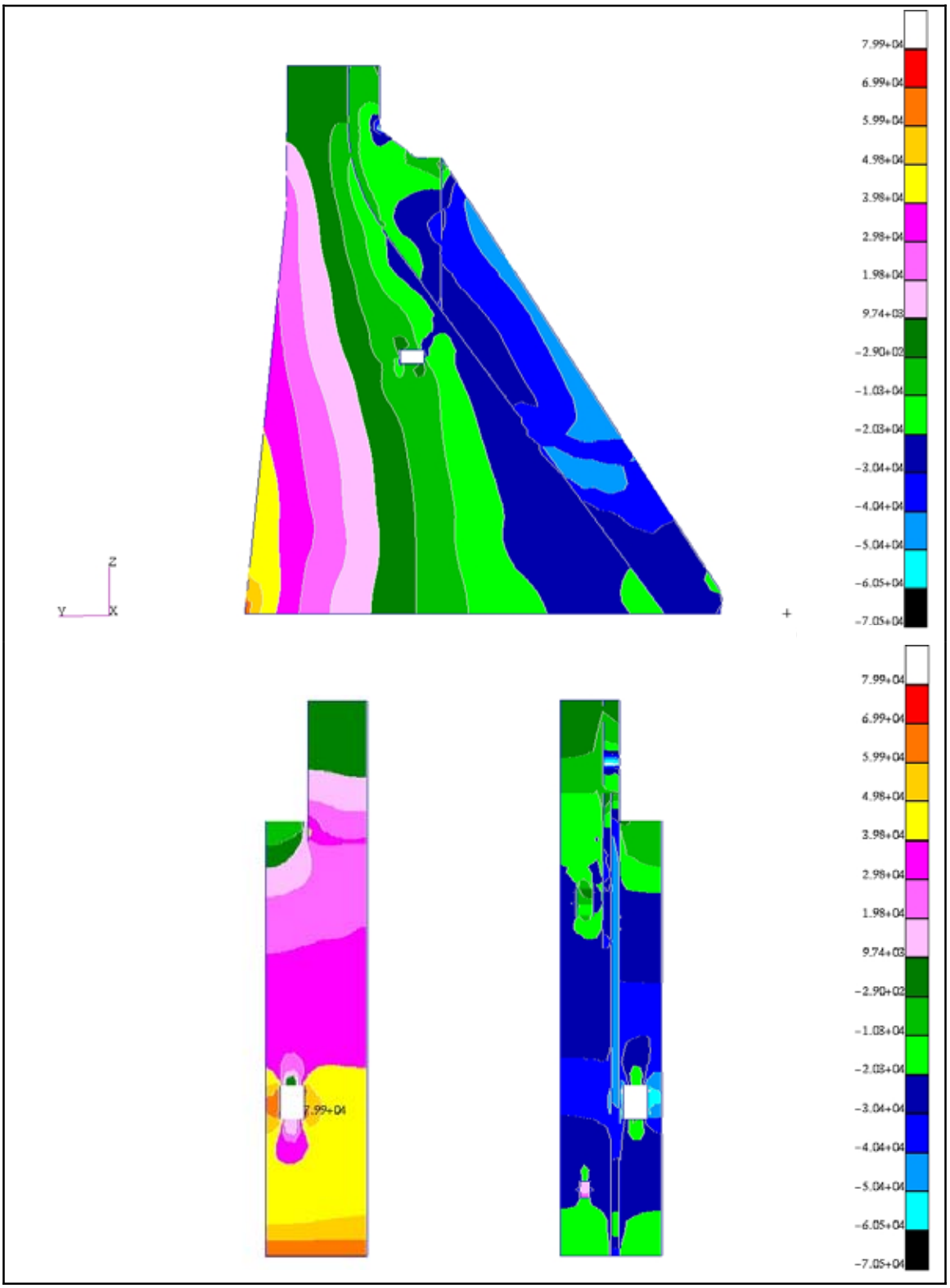

Figure 20. Load case L2 (fundamental mode response): Normal vertical stresses (σ_{zz})

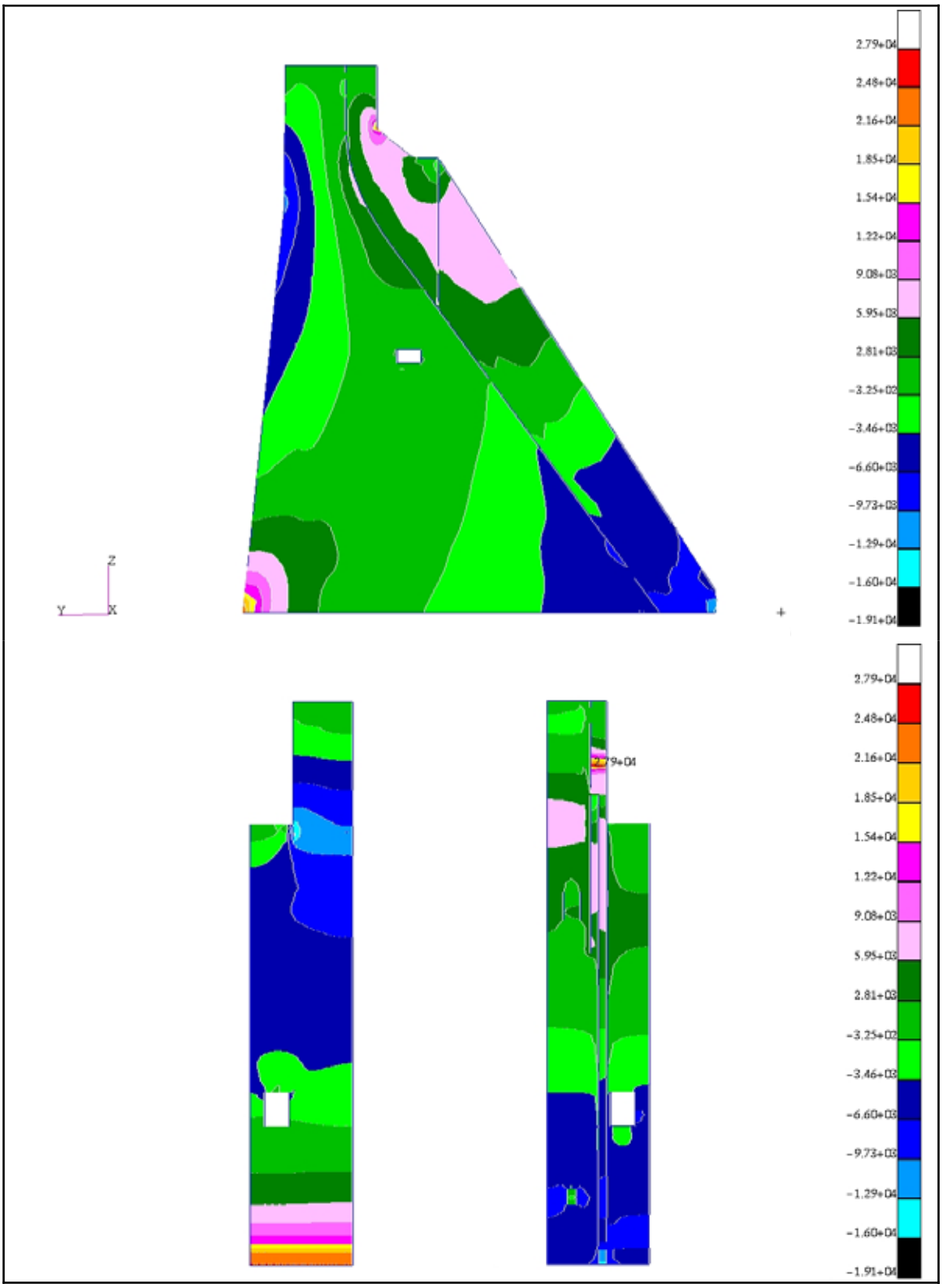

Figure 21. Load case L3 (higher mode response): Normal vertical stresses (σ_{zz})

Considering the particular geometric characteristics of monolith 12, it is interesting to compare the magnitude of the calculated stress response with those values determined for overflow and nonoverflow monoliths in previous studies. Figure 22 shows the distribution of total and dynamic normal tensile stresses (vertical component, σ_{zz}^{T}) along a vertical line on the upstream face of the nonoverflow part of monolith 12. These total tensile stresses are computed as shown in Equation 28.

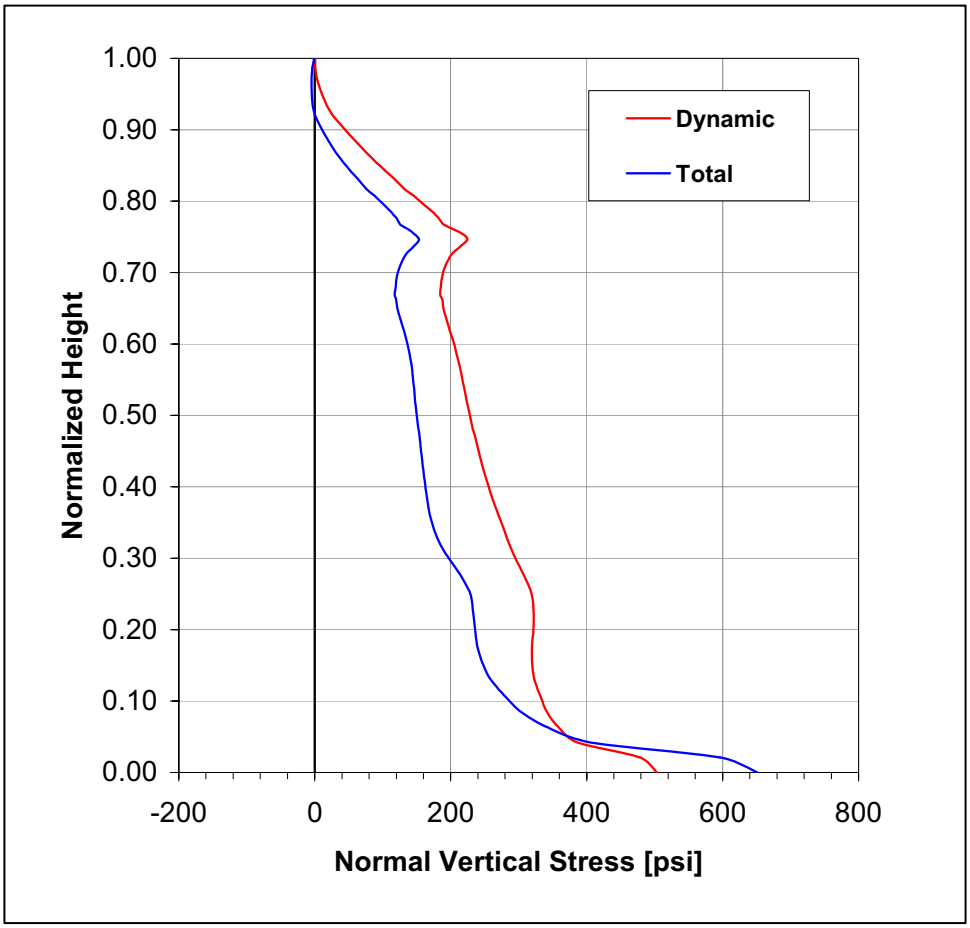

Figure 22. Variation of total normal vertical stresses (σ_{zz}) along the upstream face of monolith 12—vertical line along center of nonoverflow section

$$\sigma_{zz}^{T} = \sigma_{zz}^{(L_1)} + \sqrt{\left(\sigma_{zz}^{(L_2)}\right)^2 + \left(\sigma_{zz}^{(L_3)}\right)^2} \tag{28}$$

The stresses along this line on the upstream face show peak values of 650 psi (total vertical stress) and 500 psi (dynamic vertical stress) at the base of the section. It is interesting to notice that the stiffening presence of the spillway pier wall significantly reduces the stress peak that is typically found at about 75 percent of the height in a "true" nonoverflow monolith such as monolith 21. In the case of monolith 21, previous studies have determined large tensile stresses at that elevation with a magnitude similar to those tensile stresses at the heel. In the case of monolith 12, those tensile stresses reach about 153 psi (total vertical

stress) and 225 psi (dynamic vertical stress). In a similar fashion, Figure 23 shows the distribution of total and dynamic normal tensile stresses (vertical component, σ_{zz}^{T}) along a vertical line on the upstream face at the center line of the spillway half of monolith 12. The tensile stresses at the heel reach 658 psi (total vertical stress) and 500 psi (dynamic vertical stress). The presence of the lower conduit clearly affects the resulting stress distribution, which exhibits lower tensile stresses in the upper part of the section.

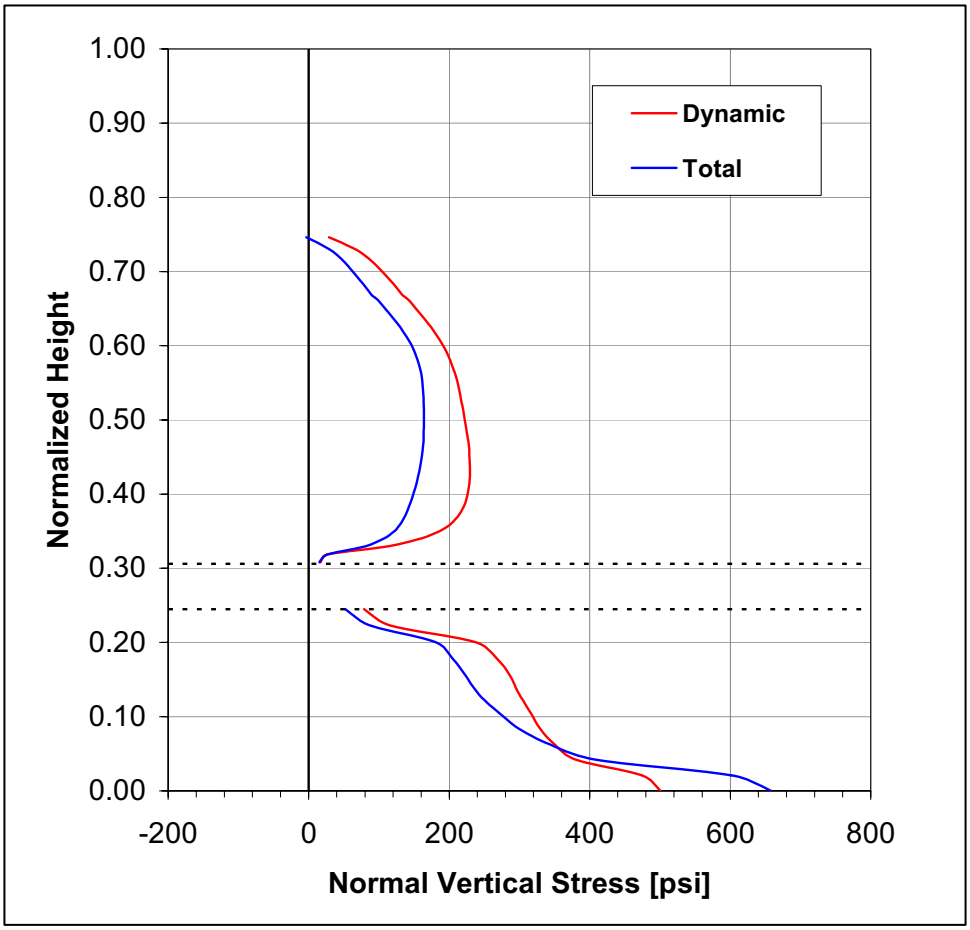

Figure 23. Variation of total normal vertical stresses (σ_{zz}) along the upstream face of monolith 12—vertical line along center of spillway section

The main purpose of this study is to evaluate the stress field in the neighborhood of the air vent in the upper part of the nonoverflow section of monolith 12. Figure 24 depicts the contour of total normal tensile stresses around the downstream exit of the air vent. The stresses shown in this figure correspond to the normal stress component that is parallel to the monolith face ($\sigma_{z'z'}^{T}$). For each load case L_i, this component is given by

$$\sigma_{z'z'}^{(L_i)} = \sigma_{zz}^{(L_i)} \cos^2(\theta) + \sigma_{yy}^{(L_i)} \sin^2(\theta) + 2\sigma_{yz}^{(L_i)} \sin(\theta)\cos(\theta) \qquad (29)$$

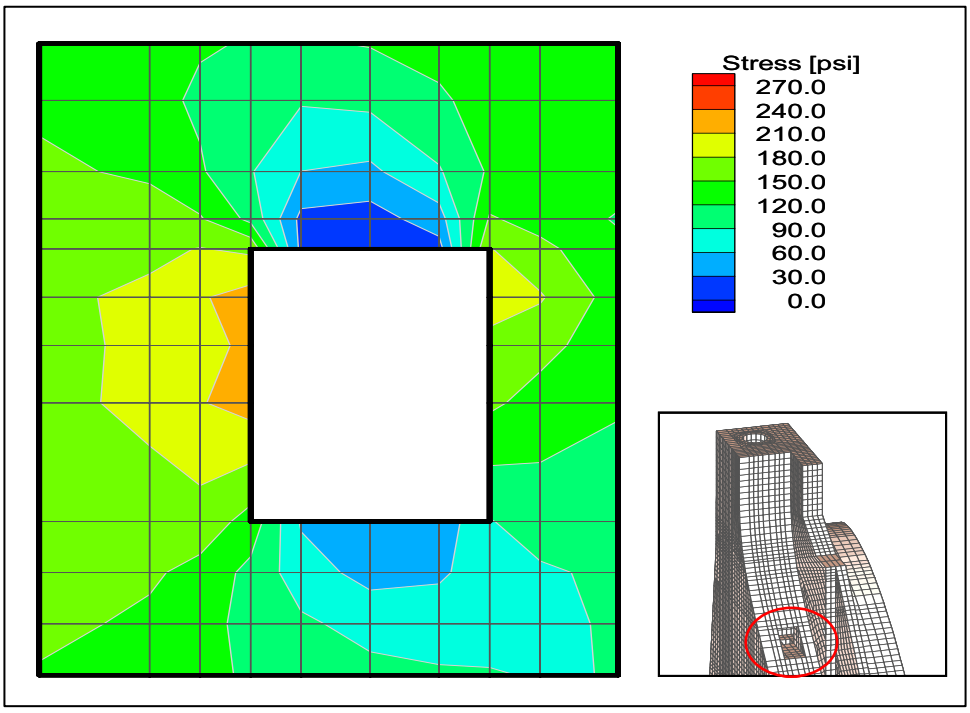

Figure 24. Total normal stresses ($\sigma_{z'z'}$) around downstream exit of air vent

By definition, these normal components are along the same direction for the three load cases. Therefore, the corresponding total response can be obtained by combining them as indicated in Equation 28 for the vertical components. The normal tensile stresses around the air vent reach a maximum value of about 225 psi. This value indicates that the presence of the air vent exit does not induce extremely severe tensile demands in its adjacent region. It must be noticed, however, that the corners of the opening might still be associated with highly localized stress concentrations that are not captured by the finite-element mesh used in these analyses.

It is important to consider, at least approximately, the effect of the vertical component of the ground motion on the resulting total tensile stresses. Previous dynamic analyses of Folsom Dam have quantified the influence of the vertical excitation for overflow and nonoverflow monoliths. Figure 25 shows the ratio between the dynamic normal stresses computed for monoliths 14 and 21 considering both input motion components and those computed considering the horizontal component only. The figure shows the variation of this ratio along the upstream face of monoliths 14 and 21 with respect to a normalized height. It can be seen that the normal stresses for the nonoverflow monolith show a very significant increase in a region close to the crest. However, below this level the stress increase is in general no more than 20 percent. In the case of the overflow section, the stress increase caused by the vertical ground motion has a similar order of magnitude without the response amplification at the top.

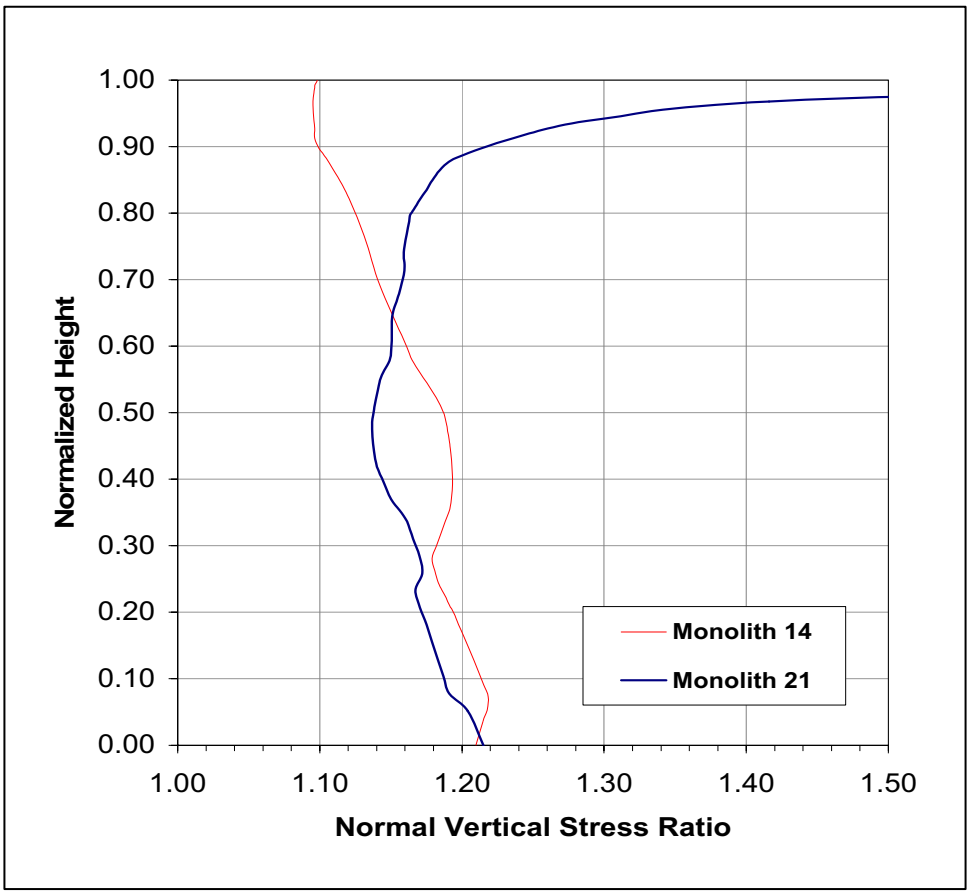

Figure 25. Effect of vertical excitation on the dynamic normal stresses (σ_{zz}) along the upstream face of overflow and nonoverflow monoliths

Based on these observations, it seems appropriate to determine the tensile stresses around the downstream exit of the air vent considering an arbitrary increase in the vertical component of the normal stresses in the region. Figure 26 shows the contour of the normal stress component ($\sigma^{T}_{z'z'}$) that results from scaling those vertical stresses up by 20 percent. The tensile stresses shown in the figure reach a maximum value of about 260 psi, and therefore they do not represent extremely severe demands for this material region.

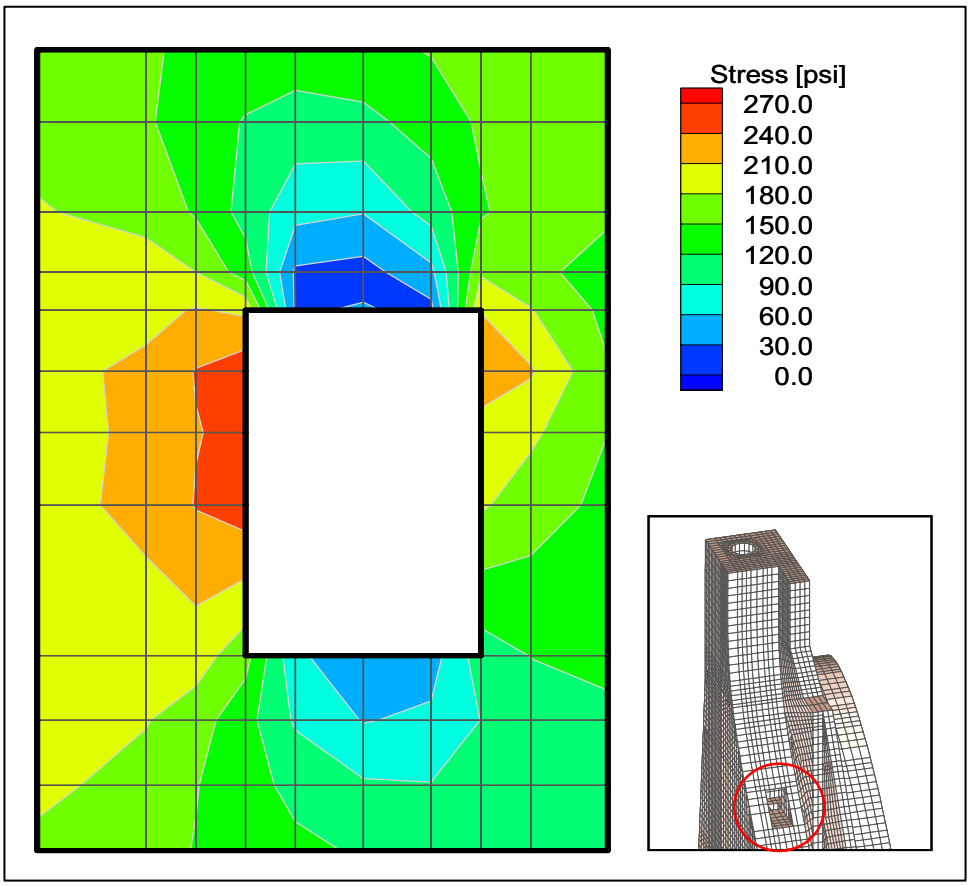

Figure 26. Total normal stresses ($\sigma_{z'z'}$) around downstream exit of air vent with 20 percent increase in normal vertical stresses ($\sigma_{z'z'}$)

6 Conclusions

The main objective of this analysis was to evaluate the severity of additional tensile demands imposed by the proposed dimensions and location of the air vent near the base of the spillway pier wall. This study has provided an estimate of the stress field in the downstream face near the air manifold exit, and therefore it provided a quantitative basis to evaluate its impact at the proposed location.

A finite element-based stress analysis of monolith 12 of Folsom Dam has been conducted. To simplify the analysis, appropriate modifications were introduced in the monolith geometry while preserving the main characteristics of the section. The analyses were conducted using a simplified dynamic analysis procedure employed in previous stress analyses of other Folsom Dam sections. Several assumptions were made to determine some of the parameters required for the simplified dynamic analysis procedure employed for this study. The selection of these parameters was conducted with conservative engineering judgment.

Based on the results presented in this report, it can be concluded that the dimensions and location of the downstream exit of the air vent will not impose unacceptable tensile demands in the structure under seismic excitations. Stress concentration effects are expected in the corner points, and appropriate steel reinforcement must be conservatively provided in these critical areas to control cracking. Additional analysis results needed to complete the preliminary design of reinforcement around the air vent are included in Appendix B of this report.

References

Chopra, A. K. (1967). "Hydrodynamic pressures on dams during earthquakes," *Journal of the Engineering Mechanics Division*, *ASCE* 93, 205-23.

_____. (1978). "Earthquake resistant design of concrete gravity dams," *Journal of the Structural Division, ASCE* 104(6), 953-71.

Chopra, A. K., and Tan, H. (1989). "Simplified earthquake analysis of gated spillway monoliths of concrete gravity dams," Technical Report SL-89-4, U.S. Army Engineer Waterways Experiment Station, Vicksburg, MS.

Chopra, A. K., and Basu, U. (2003a). "Parameters for simplified earthquake analysis of Folsom dam," Advisory Report to the U.S. Army Corps of Engineers, Washington, DC.

_____. (2003b). "Simplified analysis of concrete gravity dams subjected to vertical ground motion," Advisory Report to the U.S. Army Corps of Engineers, Washington, DC.

Fenves, G., and Chopra, A. K. (1984). "EAGD-84: A computer program for earthquake analysis of concrete gravity dams," Report No. UCB/EERC-84/11, Earthquake Engineering Research Center, University of California, Berkeley, CA.

_____. (1985a). "Simplified earthquake analysis of concrete gravity dams: Separate hydrodynamic and foundation interaction effects," *Journal of Engineering Mechanics* 111(6), 715-35.

_____. (1985b). "Simplified earthquake analysis of concrete gravity dams: Combined hydrodynamic and foundation interaction effects," *Journal of Engineering Mechanics* 111(6), 736-56.

_____. (1986). "Simplified analysis for earthquake resistant design of concrete gravity dams," Report No. UCB/EERC-85/10, Earthquake Engineering Research Center, University of California, Berkeley, CA.

_____. (1987). "Simplified earthquake analysis of concrete gravity dams," *Journal of Structural Engineering* 113(8), 1688-1708.

Hall, R. L., Woodson, S. C., and Nau, J. M. (1989). "Seismic stability evaluation of Folsom Dam and Reservoir Project; Report 3; Concrete gravity dam," Technical Report GL-87-14, U.S. Army Engineer Waterways Experiment Station, Vicksburg, MS.

URS Corporation. (2001). "Deterministic and probabilistic seismic hazard analyses–Folsom Dam–central California," Final Report (July 5), Oakland, CA.

_____. (2003). "Deterministic and probabilistic seismic hazard analyses–Folsom Dam–central California," Supplemental Report II (July 5), Oakland, CA.

Wong, C., Poeppelman, R., and Graff, S. (2002). "Preliminary earthquake response analysis of Folsom Dam spillway monoliths," *Proceedings, 3rd U.S.-Japan Workshop on Advanced Research on Earthquake Engineering for Dams.* June 22-23, San Diego, CA.

Appendix A
Relevant Equations in the Simplified Dynamic Analysis Procedure

This appendix presents a summary of the relevant equations in the simplified dynamic analysis procedure that are associated with the description of the hydrodynamic effects. The material contained in this appendix was extracted from Fenves and Chopra (1985a).

Hydrodynamic Pressure Functions

The hydrodynamic pressure function $\overline{p}_0$ (which represents the frequency response characteristics of the hydrodynamic pressure along the upstream face of a rigid dam due to horizontal ground acceleration) is defined as follows:

$$\overline{p}_0(y,\omega) = 2\rho_w H \sum_{n=1}^{\infty} \left\{ \frac{\mu_n^2(\omega)}{H\left[\mu_n^2(\omega) - (\omega q)^2\right] + i(\omega q)} \right\} \frac{I_{0n}(\omega)}{\kappa_n(\omega)} Y_n(y,\omega) \quad \text{(A1)}$$

where $\kappa_n(\omega)$ is defined as

$$\kappa_n(\omega) = \sqrt{\mu_n^2(\omega) - \frac{\omega^2}{C_w}} \quad \text{(A2)}$$

and $I_{0n}(\omega)$ is given by

$$I_{0n}(\omega) = \frac{1}{H} \int_0^H Y_n(y,\omega) dy \quad \text{(A3)}$$

The hydrodynamic pressure function $\overline{p}_1$ (which represents the frequency response characteristics of the hydrodynamic pressure along the upstream face of

the dam due to acceleration in its fundamental vibration mode) is defined as follows:

$$\overline{p}_1(y,\omega) = 2\rho_w H \sum_{n=1}^{\infty} \left\{ \frac{\mu_n^2(\omega)}{H\left[\mu_n^2(\omega) - (\omega q)^2\right] + i(\omega q)} \right\} \frac{I_{1n}(\omega)}{\kappa_n(\omega)} Y_n(y,\omega) \qquad \text{(A4)}$$

where $I_{1n}(\omega)$ is given by

$$I_{1n}(\omega) = \frac{1}{H} \int_0^H \phi(y) Y_n(y,\omega) dy \qquad \text{(A5)}$$

The parameters ρ_w and C_w in the above equations denote the density and the velocity of pressure waves in water, respectively, whereas q indicates the damping coefficient used to characterize the effects of absorption of hydrodynamic pressure waves into the reservoir bottom materials, given by

$$q = \frac{\rho_w}{\rho_r C_r} \qquad \text{(A6)}$$

where ρ_r and C_r denote the density and the velocity of pressure waves in the reservoir bottom materials, respectively. Typically, these energy-absorption effects are quantified in terms of a dimensionless wave reflection coefficient α, defined as follows:

$$\alpha = \frac{1 - qC_w}{1 + qC_w} \qquad \text{(A7)}$$

The hydrodynamic pressure functions are expressed as the summation of the contributions of an infinite number of natural vibration modes of the impounded water. The frequency-dependent parameters $\mu_n(\omega)$ denote the corresponding eigenvalues, which must satisfy the following characteristic equation:

$$e^{2i\mu_n(\omega)H} = -\frac{\mu_n(\omega) - \omega q}{\mu_n(\omega) + \omega q} \qquad \text{(A8)}$$

The corresponding eigenfunctions are given by

$$Y_n(y,\omega) = \frac{1}{2\mu_n(\omega)} \left\{ \left[\mu_n(\omega) + \omega q\right] e^{i\mu_n(\omega)y} + \left[\mu_n(\omega) - \omega q\right] e^{-i\mu_n(\omega)y} \right\} \qquad \text{(A9)}$$

Note that, in the general case, these eigenvalues and eigenfunctions are complex-valued functions. However, if the reservoir bottom is assumed perfectly rigid ($q = 0 \Rightarrow \alpha = 1$), the eigenvalues of the impounded water become real-valued and independent of the excitation frequency, with

$$\mu_n = \frac{(2n-1)}{2}\frac{\pi}{H} = \frac{\omega_n^r}{C_w} \tag{A10}$$

where ω_n^r are the natural vibration frequencies of the impounded water with rigid reservoir bottom

$$\omega_n^r = \frac{(2n-1)\pi}{2}\frac{C_w}{H} \tag{A11}$$

The fundamental natural frequency of the impounded water for this case is therefore given by

$$\omega_1^r = \frac{\pi}{2}\frac{C_w}{H} \tag{A12}$$

and the fundamental period is given by

$$T_1^r = \frac{2\pi}{\omega_1^r} = \frac{4H}{C_w} \tag{A13}$$

The eigenfunctions corresponding to this case (rigid reservoir bottom) are also real-valued and independent of the excitation frequency, and they are given by

$$Y_n(y) = \cos(\mu_n y) \tag{A14}$$

For this case (rigid reservoir bottom), the frequency response function for the hydrodynamic pressure takes the following forms:

$$\overline{p}_0(y,\omega) = 2\rho_w \sum_{n=1}^{\infty} \frac{I_{0n}}{\kappa_n(\omega)} \cos(\mu_n y) \tag{A15}$$

where

$$I_{0n} = \frac{1}{H}\int_0^H \cos(\mu_n y)dy \tag{A16}$$

and

$$\overline{p}_1(y,\omega) = 2\rho_w \sum_{n=1}^{\infty} \frac{I_{1n}}{\kappa_n(\omega)} \cos(\mu_n y) \tag{A17}$$

where

$$I_{1n} = \frac{1}{H}\int_0^H \phi(y)\cos(\mu_n y)dy \tag{A18}$$

Fundamental Mode Response of Dam-Water

The complex-valued frequency response function for the fundamental modal coordinate is given by

$$\bar{Y}_1(\omega) = \frac{-\left[L_1 + B_0(\omega)\right]}{-\omega^2\left\{M_1 + \mathrm{Re}\left[B_1(\omega)\right]\right\} + i\omega\left\{C_1 - \omega\,\mathrm{Im}\left[B_1(\omega)\right]\right\} + K_1} \tag{A19}$$

where

$$\begin{aligned} L_1 &= \frac{1}{g}\int_0^{H_s} w_s(y)\phi(y)dy \\ M_1 &= \frac{1}{g}\int_0^{H_s} w_s(y)\phi^2(y)dy \\ C_1 &= 2M_1\xi_1\omega_1 \\ K_1 &= \omega_1^2 M_1 \end{aligned} \tag{A20}$$

and

$$\begin{aligned} B_0(\omega) &= \int_0^H \bar{p}_0(y,\omega)\phi(y)dy \\ B_1(\omega) &= \int_0^H \bar{p}_1(y,\omega)\phi(y)dy \end{aligned} \tag{A21}$$

Frequency Response of Equivalent SDOF

The complex-valued frequency response function for the equivalent SDOF system representing the dam with impounded water is given by

$$\tilde{\bar{Y}}_1(\omega) = \frac{-\tilde{L}_1}{-\omega^2\tilde{M}_1 + i\omega\tilde{C}_1 + K_1} \tag{A22}$$

$$\tilde{L}_1 = L_1 + B_0(\tilde{\omega}_r)$$

$$\tilde{M}_1 = M_1 + \mathrm{Re}\left[B_1(\tilde{\omega}_r)\right] \tag{A23}$$

$$\tilde{C}_1 = C_1 - \tilde{\omega}_r \,\mathrm{Im}\left[B_1(\tilde{\omega}_r)\right]$$

The natural vibration frequency $\tilde{\omega}_r$ of the equivalent SDOF system is given by

$$\tilde{\omega}_r = \sqrt{\frac{K_1}{\tilde{M}_1}} = \sqrt{\frac{M_1}{M_1 + \mathrm{Re}\left[B_1(\tilde{\omega}_r)\right]}}\omega_1 \tag{A24}$$

Note that

$$\tilde{M}_1 = M_1 + \mathrm{Re}\left[B_1(\tilde{\omega}_r)\right] = \left(\frac{\omega_1}{\tilde{\omega}_r}\right)^2 M_1 = \left(R_r\right)^2 M_1 \tag{A25}$$

and also that

$$B_0(\tilde{\omega}_r) = \int_0^H \overline{p}_0(y, \tilde{\omega}_r)\phi(y)dy = \int_0^H \overline{p}_1(y, \tilde{\omega}_r)dy \tag{A26}$$

The added damping of the equivalent SDOF system is given by

$$\tilde{\xi}_r = \frac{1}{R_r}\xi_1 + \xi_r \tag{A27}$$

where

$$\xi_r = -\frac{1}{2}\frac{1}{\left(R_r\right)^2 M_1}\mathrm{Im}\left\{B_1(\tilde{\omega}_r)\right\} \tag{A28}$$

Appendix B
Evaluation of the Finite-Element Equivalent Nodal Forces

Introduction

As previously described, a finite-element stress analysis of monolith 12 was conducted to evaluate the stress field around the air vent near the base of the spillway wall. The analysis was based on a three-dimensional finite-element model of the monolith. The analysis included the effects of static (self-weight and hydrostatic effects) and dynamic (inertial and hydrodynamic effects) loads. The analyses account for only the effects of the horizontal component of the input ground motion. The effects of the vertical component were approximated by estimating the increase in dynamic stress response observed in previous studies for other monoliths of the dam. The corresponding results provided an estimate of the stress concentration effects induced in the downstream area near the air vent.

The objective of this appendix is to evaluate the finite-element equivalent nodal forces for selected elements around the air manifold in monolith 12 when subjected to the Maximum Credible Earthquake. The U.S. Army Engineer District, Sacramento, requested this information to implement the design of the necessary reinforcement around the conduit.

Determination of Nodal Forces

Figure B1 shows the finite-element discretization around the conduit and the global right-handed coordinate system. The element nodal forces were evaluated at three different sections. The first section was defined by a plane normal to the global Y axis, along the portion of the conduit that exits on the downstream face. The other two sections were defined by planes normal to the global X axis, and they were located after the elbow, in the spillway portion of the monolith.

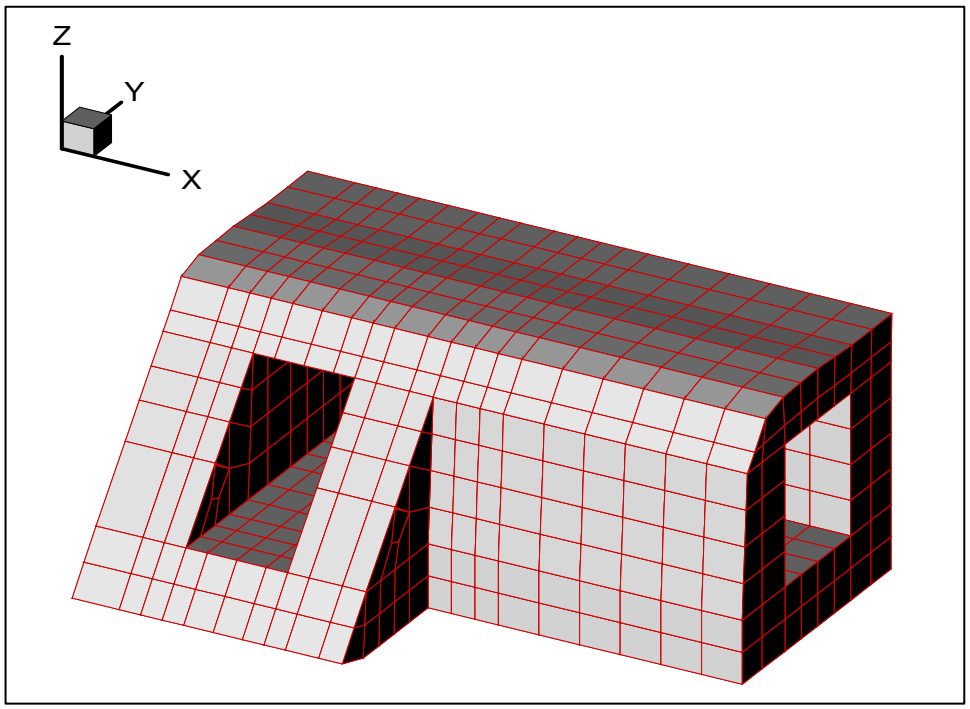

Figure B1. Air manifold

The sections are shown in Figure B2. Each section was defined such that it included no less than two layers of element around the conduit. This is necessary to define the appropriate equivalent nodal forces corresponding to two concentric sets of nodes around the opening. As shown in Figure B3, the sections correspond to vertical planes parallel to the XZ axes (Section 1, which corresponds to a plane normal to the negative Y axis) and to the YZ axes (Sections 2 and 3, which correspond to planes normal to the positive X axis).

Figures B4 through B6 indicate the nodes and elements associated with each section.

Table B1 provides the nodal coordinates for the nodes in each section. Tables B2 through B4 provide the values of the element nodal forces for each section. The element nodal forces indicated in these tables are directly obtained as standard output of the finite-element analysis conducted for each load case; therefore, they do not include any design load factor. As indicated in the main text of the report, the load cases considered for the simplified analysis of monolith 12 were these: load case 1 (static effects), load case 2 (dynamic effects associated with the fundamental mode response), and load case 3 (dynamic effects associated with higher mode contributions).

Based on the geometry of each section and considering the element nodal forces, the corresponding response quantities of interest (total shear forces and total bending moments acting on the section) can be computed for each load case.

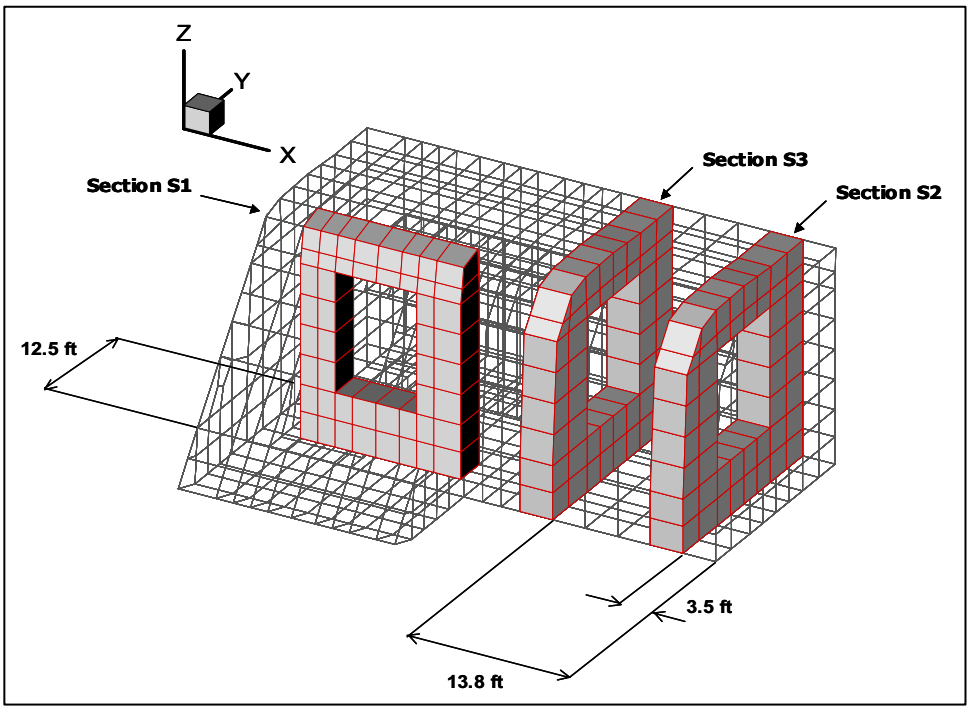

Figure B2. Location of sections around the conduit

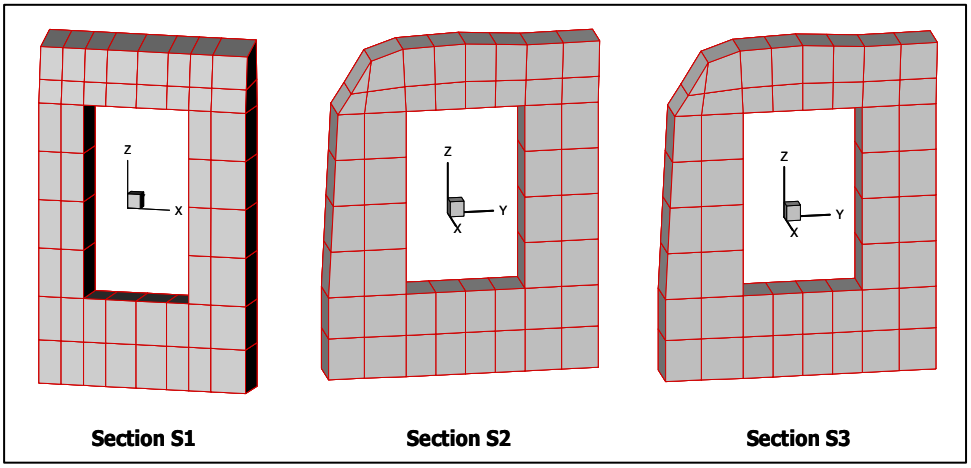

Figure B3. Sections around the conduit

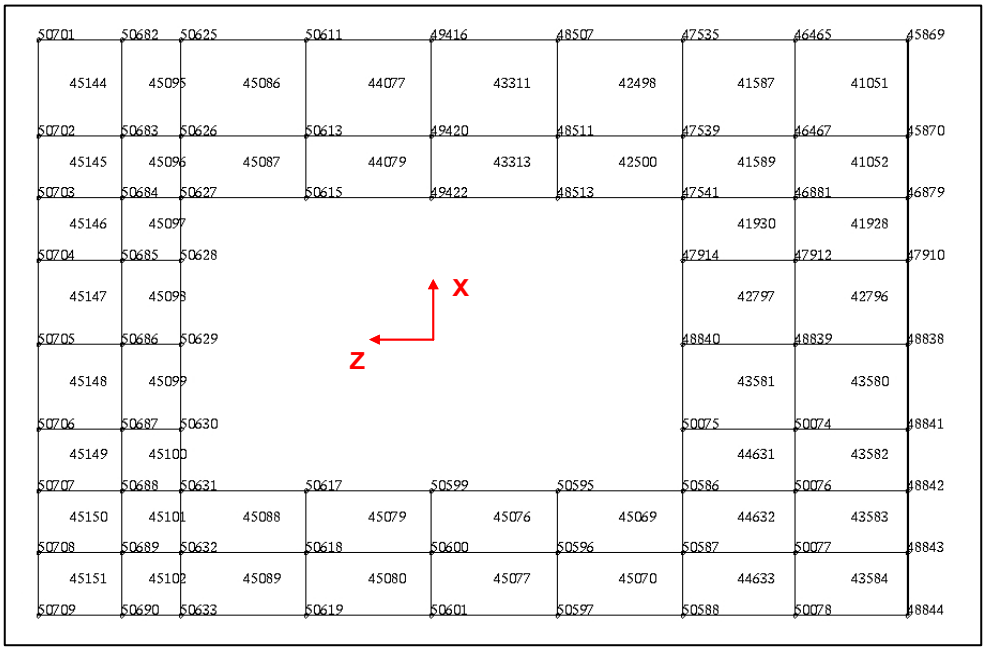

Figure B4. Node and element numbers for Section 1

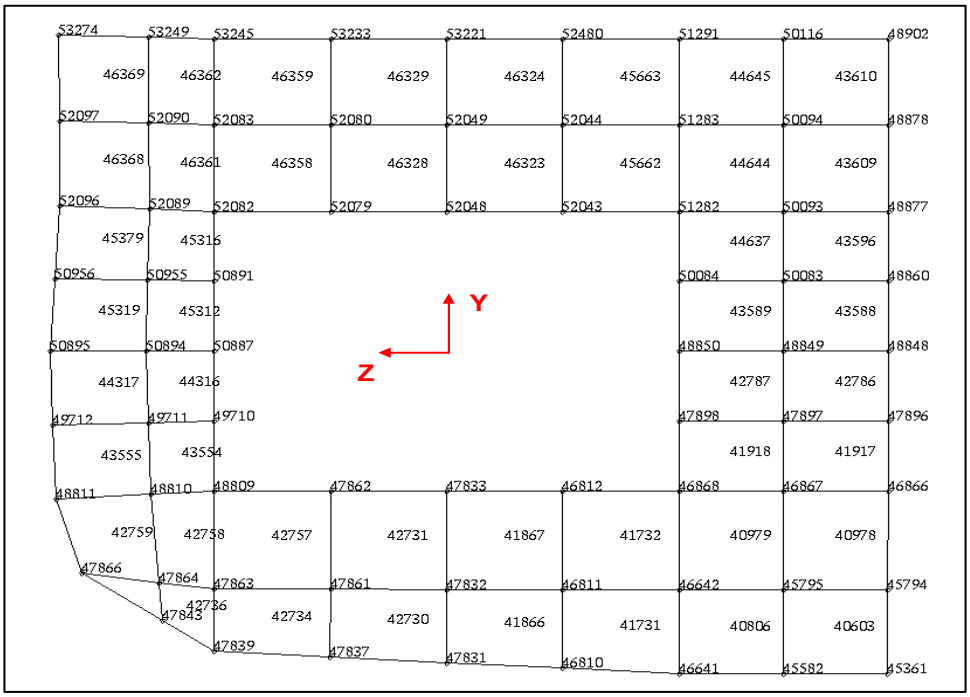

Figure B5. Node and element numbers for Section 2

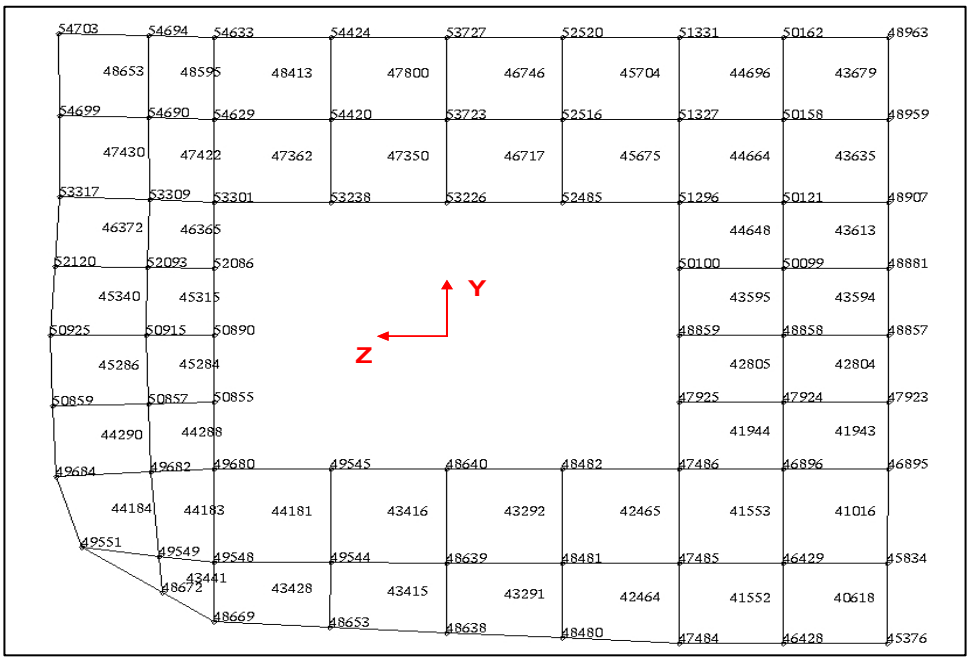

Figure B6. Node and element numbers for Section 3

For design purposes, the total response quantities should be obtained based on the appropriate combination of the responses corresponding to each load case. For example, let r_1 denote the value of a given response quantity corresponding to the static loading condition. Let r_2 and r_3 denote the values of the same response quantity that correspond to the loading conditions representative of the dynamic effects on the structure and associated with the fundamental mode and higher mode responses, respectively. These two response quantities represent maximum design values that must be appropriately combined by a statistical method, such as the square root of the sum of the squares method. Therefore, the estimate of the corresponding dynamic response r_d can be obtained as follows:

$$r_d = \sqrt{(r_2)^2 + (r_3)^2} \tag{B1}$$

and the total response can be obtained as follows:

$$r_{peak} = r_1 \pm r_d \tag{B2}$$

The analyses were performed considering only the horizontal component of the input ground motion. Since the vertical component of the excitation is likely to increase the dynamic responses, the use of a scale factor to approximately account for this effect is recommended. A scale factor of 1.50 is suggested for the results corresponding to dynamic effects (load cases 2 and 3).

$$r_{peak} = r_1 \pm 1.5\, r_d \tag{B3}$$

Table B1
Nodal Coordinates for Each Section

Section 1				Section 2				Section 3			
Node	X [ft]	Y [ft]	Z [ft]	Node	X [ft]	Y [ft]	Z [ft]	Node	X [ft]	Y [ft]	Z [ft]
45869	49.25	196.79	362.71	45361	74.54	193.79	362.71	45376	64.2	193.8	362.7
45870	46.42	196.79	362.71	45582	74.54	193.79	365.86	45834	64.2	196.8	362.7
46465	49.25	196.79	365.86	45794	74.54	196.79	362.71	46428	64.2	193.8	365.9
46467	46.42	196.79	365.86	45795	74.54	196.79	365.86	46429	64.2	196.8	365.9
46879	44.58	196.79	362.71	46641	74.54	193.79	369.00	46895	64.2	200.3	362.7
46881	44.58	196.79	365.86	46642	74.54	196.79	369.00	46896	64.2	200.3	365.8
47535	49.25	196.79	369.00	46810	74.54	193.99	372.50	47484	64.2	193.8	369.0
47539	46.42	196.79	369.00	46811	74.54	196.80	372.50	47485	64.2	196.8	369.0
47541	44.58	196.79	369.00	46812	74.54	200.29	372.50	47486	64.2	200.3	369.0
47910	42.75	196.79	362.71	46866	74.54	200.29	362.67	47923	64.2	202.8	362.7
47912	42.75	196.79	365.86	46867	74.54	200.29	365.83	47924	64.2	202.8	365.8
47914	42.75	196.79	369.00	46868	74.54	200.29	369.00	47925	64.2	202.8	369.0
48507	49.25	196.80	372.50	47831	74.54	194.19	376.00	48480	64.2	194.0	372.5
48511	46.42	196.80	372.50	47832	74.54	196.80	376.00	48481	64.2	196.8	372.5
48513	44.58	196.80	372.50	47833	74.54	200.29	376.00	48482	64.2	200.3	372.5
48838	40.25	196.79	362.71	47837	74.54	194.39	379.50	48638	64.2	194.2	376.0
48839	40.25	196.79	365.86	47839	74.54	194.58	383.00	48639	64.2	196.8	376.0
48840	40.25	196.79	369.00	47843	74.54	195.70	384.55	48640	64.2	200.3	376.0
48841	37.75	196.79	362.71	47861	74.54	196.80	379.50	48653	64.2	194.4	379.5
48842	35.92	196.79	362.71	47862	74.54	200.29	379.50	48669	64.2	194.6	383.0
48843	34.08	196.79	362.71	47863	74.54	196.80	383.00	48672	64.2	195.7	384.5
48844	32.25	196.79	362.71	47864	74.54	197.05	384.66	48857	64.2	205.3	362.7
49416	49.25	196.80	376.00	47866	74.54	197.37	386.99	48858	64.2	205.3	365.8
49420	46.42	196.80	376.00	47896	74.54	202.79	362.67	48859	64.2	205.3	369.0
49422	44.58	196.80	376.00	47897	74.54	202.79	365.83	48881	64.2	207.8	362.7
50074	37.75	196.79	365.86	47898	74.54	202.79	369.00	48907	64.2	210.3	362.7
50075	37.75	196.79	369.00	48809	74.54	200.29	383.00	48959	64.2	213.4	362.7
50076	35.92	196.79	365.86	48810	74.54	200.19	384.91	48963	64.2	216.5	362.7
50077	34.08	196.79	365.86	48811	74.54	200.03	387.78	49544	64.2	196.8	379.5
50078	32.25	196.79	365.86	48848	74.54	205.29	362.67	49545	64.2	200.3	379.5
50586	35.92	196.79	369.00	48849	74.54	205.29	365.83	49548	64.2	196.8	383.0
50587	34.08	196.79	369.00	48850	74.54	205.29	369.00	49549	64.2	197.0	384.7
50588	32.25	196.79	369.00	48860	74.54	207.79	362.67	49551	64.2	197.4	387.0
50595	35.92	196.80	372.50	48877	74.54	210.29	362.67	49680	64.2	200.3	383.0
50596	34.08	196.80	372.50	48878	74.54	213.38	362.67	49682	64.2	200.2	384.9
50597	32.25	196.80	372.50	48902	74.54	216.46	362.67	49684	64.2	200.0	387.8
50599	35.92	196.80	376.00	49710	74.54	202.79	383.00	50099	64.2	207.8	365.8
50600	34.08	196.80	376.00	49711	74.54	202.74	384.99	50100	64.2	207.8	369.0
50601	32.25	196.80	376.00	49712	74.54	202.66	387.86	50121	64.2	210.3	365.8
50611	49.25	196.80	379.50	50083	74.54	207.79	365.83	50158	64.2	213.4	365.8
50613	46.42	196.80	379.50	50084	74.54	207.79	369.00	50162	64.2	216.5	365.8
50615	44.58	196.80	379.50	50093	74.54	210.29	365.83	50855	64.2	202.8	383.0
50617	35.92	196.80	379.50	50094	74.54	213.38	365.83	50857	64.2	202.7	385.0
50618	34.08	196.80	379.50	50116	74.54	216.46	365.83	50859	64.2	202.7	387.9
50619	32.25	196.80	379.50	50887	74.54	205.29	383.00	50890	64.2	205.3	383.0

(Continued)

Table B1 (Concluded)

Section 1				Section 2				Section 3			
Node	X [ft]	Y [ft]	Z [ft]	Node	X [ft]	Y [ft]	Z [ft]	Node	X [ft]	Y [ft]	Z [ft]
50625	49.25	196.80	383.00	50891	74.54	207.79	383.00	50915	64.2	205.3	385.1
50626	46.42	196.80	383.00	50894	74.54	205.29	385.06	50925	64.2	205.3	388.0
50627	44.58	196.80	383.00	50895	74.54	205.29	387.95	51296	64.2	210.3	369.0
50628	42.75	196.80	383.00	50955	74.54	207.83	385.01	51327	64.2	213.4	369.0
50629	40.25	196.80	383.00	50956	74.54	207.88	387.80	51331	64.2	216.5	369.0
50630	37.75	196.80	383.00	51282	74.54	210.29	369.00	52086	64.2	207.8	383.0
50631	35.92	196.80	383.00	51283	74.54	213.38	369.00	52093	64.2	207.8	385.0
50632	34.08	196.80	383.00	51291	74.54	216.46	369.00	52120	64.2	207.9	387.8
50633	32.25	196.80	383.00	52043	74.54	210.29	372.50	52485	64.2	210.3	372.5
50682	49.25	197.05	384.66	52044	74.54	213.38	372.50	52516	64.2	213.4	372.5
50683	46.42	197.05	384.66	52048	74.54	210.29	376.00	52520	64.2	216.5	372.5
50684	44.58	197.05	384.66	52049	74.54	213.38	376.00	53226	64.2	210.3	376.0
50685	42.75	197.05	384.66	52079	74.54	210.29	379.50	53238	64.2	210.3	379.5
50686	40.25	197.05	384.66	52080	74.54	213.38	379.50	53301	64.2	210.3	383.0
50687	37.75	197.05	384.66	52082	74.54	210.29	383.00	53309	64.2	210.4	385.0
50688	35.92	197.05	384.66	52083	74.54	213.38	383.00	53317	64.2	210.5	387.6
50689	34.08	197.05	384.66	52089	74.54	210.37	384.96	53723	64.2	213.4	376.0
50690	32.25	197.05	384.66	52090	74.54	213.44	384.96	53727	64.2	216.5	376.0
50701	49.25	197.37	386.99	52096	74.54	210.47	387.65	54420	64.2	213.4	379.5
50702	46.42	197.37	386.99	52097	74.54	213.53	387.66	54424	64.2	216.5	379.5
50703	44.58	197.37	386.99	52480	74.54	216.46	372.50	54629	64.2	213.4	383.0
50704	42.75	197.37	386.99	53221	74.54	216.46	376.00	54633	64.2	216.5	383.0
50705	40.25	197.37	386.99	53233	74.54	216.46	379.50	54690	64.2	213.4	385.0
50706	37.75	197.37	386.99	53245	74.54	216.46	383.00	54694	64.2	216.5	385.0
50707	35.92	197.37	386.99	53249	74.54	216.51	384.97	54699	64.2	213.5	387.7
50708	34.08	197.37	386.99	53274	74.54	216.58	387.68	54703	64.2	216.6	387.7
50709	32.25	197.37	386.99								

Table B2
Element Nodal Forces for Section 1

Element	Node	Load Case 1			Load Case 2			Load Case 3		
		Fx [lb]	Fy [lb]	Fz [lb]	Fx [lb]	Fy [lb]	Fz [lb]	Fx [lb]	Fy [lb]	Fz [lb]
41051	46467	-3,230.0	-10,365.0	5,659.0	7,646.0	7,569.0	19,675.0	-588.4	450.8	1,818.0
	45870	-5,316.0	-22,895.0	-18,409.0	3,322.0	48,132.0	10,689.0	-473.3	-492.7	-2,548.0
	46465	4,651.0	-8,971.0	8,347.0	269.2	924.1	24,797.0	-436.4	1,945.0	1,889.0
	45869	2,214.0	-21,698.0	-15,861.0	-3,664.0	43,128.0	15,464.0	-371.8	779.5	-2,716.0
41052	46881	-3,365.0	-7,345.0	1,227.0	7,255.0	9,629.0	9,016.0	-15.0	-175.9	781.8
	46879	-7,193.0	-14,724.0	-13,061.0	6,287.0	31,091.0	6,756.0	-426.1	-572.0	-1,666.0
	46467	4,078.0	-3,723.0	7,011.0	-85.9	-38.0	13,816.0	-74.7	855.7	1,448.0
	45870	1,094.0	-11,362.0	-7,670.0	-1,919.0	23,223.0	9,222.0	-167.7	252.2	-1,449.0
41587	47539	-2,833.0	-7,016.0	10,567.0	2,074.0	-5,172.0	15,360.0	-633.5	1,555.0	2,324.0
	46467	-2,822.0	-13,313.0	-14,789.0	-6,572.0	25,047.0	-2,754.0	-173.2	-26.6	-3,144.0
	47535	2,852.0	-4,645.0	12,120.0	9,048.0	-14,879.0	21,720.0	-902.0	3,570.0	2,134.0
	46465	-192.0	-11,397.0	-12,744.0	6,343.0	17,859.0	3,798.0	-918.1	1,751.0	-3,388.0
41589	47541	-2,552.0	-6,139.0	4,287.0	-705.7	4,828.0	7,582.0	-6.9	-163.3	935.2
	46881	-4,084.0	-9,903.0	-11,470.0	-5,487.0	19,203.0	-2,581.0	-53.0	-813.0	-2,268.0
	47539	2,922.0	-1,302.0	9,977.0	10,186.0	-9,961.0	12,514.0	-536.0	2,238.0	1,968.0
	46467	-1,583.0	-5,724.0	-6,432.0	8,919.0	8,502.0	2,434.0	-1,068.0	948.9	-1,829.0
41928	47912	-6,108.0	-2,840.0	869.8	12,463.0	4,129.0	2,076.0	-370.8	-141.7	773.7
	47910	-9,857.0	-8,580.0	-10,660.0	8,045.0	19,642.0	1,792.0	-595.4	-571.7	-1,258.0
	46881	6,276.0	-1,412.0	5,438.0	-250.8	-1,864.0	14,754.0	143.8	377.3	1,019.0
	46879	3,626.0	-7,080.0	-5,795.0	-5,279.0	13,947.0	9,357.0	233.4	36.7	-1,363.0
41930	47914	-1,176.0	-5,893.0	-3,485.0	-3,888.0	11,702.0	483.8	416.5	-1,999.0	-419.7
	47912	-6,652.0	-6,315.0	-8,100.0	-7,031.0	13,512.0	-5,368.0	-247.7	-1,314.0	-1,374.0
	47541	2,016.0	2,362.0	9,558.0	23,797.0	-13,085.0	14,809.0	-1,727.0	2,742.0	1,865.0
	46881	-2,660.0	-2,251.0	-1,585.0	10,515.0	1,537.0	3,322.0	-1,796.0	1,159.0	-866.4
42498	48511	91.1	759.8	12,166.0	-5,267.0	-20,272.0	20,628.0	-112.9	2,357.0	2,182.0
	47539	-3,240.0	-6,998.0	-21,818.0	-11,607.0	14,134.0	6,001.0	-924.9	-1,389.0	-6,709.0
	48507	1,632.0	2,182.0	15,390.0	17,680.0	-27,155.0	30,746.0	-731.3	3,608.0	2,196.0
	47535	-1,702.0	-4,663.0	-17,106.0	10,511.0	5,466.0	14,857.0	-611.4	447.9	-6,245.0
42500	48513	1,647.0	101.7	9,243.0	-8,740.0	-11,208.0	12,854.0	729.8	1,361.0	1,829.0
	47541	-3,112.0	-6,965.0	-20,912.0	-13,324.0	15,952.0	2,724.0	-548.2	-2,116.0	-6,195.0
	48511	788.8	1,664.0	13,131.0	16,487.0	-18,020.0	20,387.0	-643.7	2,278.0	2,289.0
	47539	-2,485.0	-2,798.0	-10,816.0	14,579.0	2,179.0	11,774.0	-1,018.0	153.0	-4,135.0
42796	48839	-7,624.0	2,693.0	4,029.0	13,417.0	-8,779.0	-3,811.0	-1,560.0	641.3	1,303.0
	48838	-2,579.0	-10,163.0	-9,355.0	-10,901.0	22,812.0	-182.9	-60.3	-928.7	-982.9
	47912	13,166.0	-8,400.0	1,224.0	-1,518.0	7,208.0	25,073.0	-191.8	693.2	-266.0
	47910	17,688.0	-17,839.0	-15,894.0	-27,788.0	30,473.0	29,009.0	1,335.0	-425.4	-2,706.0
42797	48840	2,095.0	-1,614.0	145.6	-1,629.0	2,645.0	-1,072.0	659.8	-784.3	263.8
	48839	1,283.0	-4,626.0	-2,336.0	-12,423.0	13,371.0	-3,367.0	671.9	-699.8	-78.4
	47914	2,611.0	-7,116.0	-59.8	7,881.0	7,730.0	12,194.0	-3,104.0	1,505.0	-463.6
	47912	8,983.0	-11,229.0	-5,248.0	-11,490.0	19,701.0	13,439.0	-1,060.0	807.9	-828.8
43311	49420	4,080.0	4,053.0	16,088.0	-2,390.0	-10,684.0	-1,953.0	177.5	1,231.0	5,531.0
	48511	-1,336.0	-6,125.0	-31,147.0	-2,850.0	18,384.0	26,949.0	-918.1	-2,511.0	-9,852.0
	49416	-514.5	3,963.0	20,403.0	7,772.0	-14,289.0	1,856.0	90.6	1,585.0	6,072.0
	48507	-2,766.0	-5,430.0	-26,244.0	3,019.0	14,406.0	30,511.0	-164.3	-1,880.0	-8,857.0
43313	49422	834.1	2,479.0	11,232.0	465.5	-4,983.0	-3,401.0	-119.3	760.4	3,951.0
	48513	804.4	-4,520.0	-19,567.0	1,230.0	12,599.0	21,869.0	-252.4	-1,513.0	-6,547.0
	49420	-217.4	2,706.0	12,432.0	-18.2	-7,175.0	-1,666.0	250.5	895.5	4,115.0
	48511	-1,360.0	-4,284.0	-18,595.0	-346.9	11,296.0	19,418.0	23.9	-1,498.0	-6,131.0

(Sheet 1 of 4)

Table B2 (Continued)

Element	Node	Load Case 1			Load Case 2			Load Case 3		
		Fx [lb]	Fy [lb]	Fz [lb]	Fx [lb]	Fy [lb]	Fz [lb]	Fx [lb]	Fy [lb]	Fz [lb]
43580	50074	-12,020.0	2,222.0	11,365.0	18,137.0	-9,271.0	-12,727.0	-2,326.0	1,694.0	3,219.0
	48841	1,547.0	-18,896.0	-13,186.0	-12,853.0	38,966.0	15,852.0	1,088.0	-1,193.0	-1,677.0
	48839	9,346.0	-12,818.0	-6,031.0	-3,767.0	14,012.0	27,773.0	-405.9	661.4	-1,521.0
	48838	20,316.0	-30,401.0	-25,844.0	-30,879.0	55,001.0	48,175.0	2,560.0	-1,714.0	-4,906.0
43581	50075	-1,775.0	791.1	3,834.0	4,083.0	-5,880.0	-3,885.0	289.0	1,111.0	1,036.0
	50074	2,717.0	-9,231.0	-3,586.0	-9,075.0	19,778.0	4,647.0	1,230.0	-179.2	-201.6
	48840	6,588.0	-16,181.0	-4,339.0	-12,235.0	27,435.0	14,405.0	-1,265.0	-30.1	-1,149.0
	48839	15,771.0	-23,920.0	-11,589.0	-27,643.0	46,333.0	23,020.0	1,271.0	-1,016.0	-2,184.0
43582	50076	-8,338.0	2,421.0	13,403.0	10,584.0	-7,144.0	-16,031.0	-893.0	1,418.0	4,057.0
	48842	311.0	-15,056.0	-12,091.0	-5,781.0	30,968.0	17,864.0	1,389.0	-953.1	-1,845.0
	50074	3,802.0	-8,233.0	-4,845.0	-126.2	9,190.0	18,075.0	-1,173.0	373.1	-904.4
	48841	13,608.0	-24,179.0	-26,097.0	-18,514.0	44,220.0	45,531.0	1,562.0	-1,762.0	-5,602.0
43583	50077	-6,786.0	3,541.0	13,663.0	8,784.0	-9,877.0	-14,593.0	-317.5	1,639.0	4,354.0
	48843	-258.9	-16,157.0	-17,361.0	-2,563.0	32,015.0	27,449.0	1,395.0	-1,157.0	-3,291.0
	50076	4,467.0	-7,232.0	-524.0	-4,844.0	8,839.0	9,395.0	-1,059.0	204.7	414.7
	48842	11,739.0	-24,079.0	-28,119.0	-16,599.0	44,385.0	46,657.0	1,088.0	-2,049.0	-6,231.0
43584	50078	-6,662.0	2,907.0	11,277.0	9,150.0	-9,051.0	-9,516.0	-232.2	1,571.0	3,810.0
	48844	-2,659.0	-17,931.0	-21,896.0	2,486.0	34,562.0	34,889.0	793.4	-1,492.0	-4,563.0
	50077	6,225.0	-4,747.0	3,905.0	-9,001.0	4,687.0	2,259.0	-378.7	490.8	1,789.0
	48843	9,866.0	-23,788.0	-28,462.0	-14,329.0	44,111.0	46,064.0	699.4	-2,192.0	-6,334.0
44077	50613	-685.5	9,921.0	29,768.0	8,777.0	-21,791.0	-42,606.0	-1,818.0	2,820.0	10,922.0
	49420	2,727.0	-10,003.0	-43,574.0	-5,972.0	25,012.0	66,263.0	169.4	-3,354.0	-14,270.0
	50611	219.8	6,108.0	25,228.0	2,757.0	-17,150.0	-20,742.0	406.2	2,152.0	8,078.0
	49416	1,695.0	-11,527.0	-45,352.0	-8,738.0	25,558.0	78,439.0	1,675.0	-3,527.0	-15,567.0
44079	50615	7,129.0	4,895.0	12,434.0	-14,386.0	-9,143.0	-14,493.0	1,563.0	1,422.0	5,476.0
	49422	2,097.0	-6,897.0	-28,161.0	-5,472.0	16,855.0	45,002.0	426.2	-2,041.0	-9,413.0
	50613	-5,496.0	6,665.0	19,563.0	13,970.0	-15,553.0	-24,561.0	-1,404.0	1,888.0	6,716.0
	49420	-4,623.0	-5,794.0	-26,851.0	9,867.0	12,573.0	45,473.0	-836.4	-1,790.0	-9,592.0
44631	50586	-14,283.0	14,855.0	21,373.0	22,682.0	-34,928.0	-31,068.0	-2,572.0	3,779.0	6,123.0
	50076	2,276.0	-7,766.0	-9,144.0	-5,713.0	15,003.0	16,454.0	1,616.0	-254.0	-1,784.0
	50075	16,321.0	-21,901.0	-11,737.0	-34,084.0	43,221.0	24,170.0	1,592.0	-2,657.0	-2,681.0
	50074	24,617.0	-29,601.0	-25,442.0	-43,999.0	58,670.0	44,604.0	4,149.0	-3,646.0	-6,004.0
44632	50587	-10,246.0	9,124.0	15,655.0	15,484.0	-22,432.0	-18,300.0	-1,674.0	2,742.0	5,012.0
	50077	-1,213.0	-14,565.0	-21,384.0	973.3	27,975.0	36,934.0	654.2	-1,644.0	-5,123.0
	50586	12,177.0	-10,372.0	1,948.0	-23,472.0	18,559.0	2,932.0	1,421.0	-781.0	1,432.0
	50076	17,131.0	-29,866.0	-33,766.0	-30,023.0	58,704.0	57,805.0	2,644.0	-4,116.0	-8,170.0
44633	50588	-9,219.0	5,361.0	11,098.0	14,564.0	-14,429.0	-10,159.0	-1,335.0	2,059.0	3,806.0
	50078	-4,485.0	-17,799.0	-24,836.0	6,846.0	34,243.0	41,796.0	-215.0	-2,262.0	-6,145.0
	50587	10,559.0	-4,502.0	5,086.0	-19,059.0	6,303.0	-415.9	1,361.0	357.6	2,483.0
	50077	13,059.0	-27,056.0	-31,634.0	-22,819.0	52,901.0	53,363.0	1,838.0	-3,734.0	-7,695.0
45069	50596	-9,554.0	4,891.0	16,615.0	15,096.0	-14,496.0	-19,406.0	-2,134.0	1,984.0	5,644.0
	50587	-1,793.0	-20,302.0	-28,215.0	1,270.0	39,252.0	51,589.0	-301.0	-3,622.0	-7,698.0
	50595	3,365.0	131.9	3,422.0	-5,958.0	-3,433.0	4,359.0	379.0	1,160.0	2,681.0
	50586	19,805.0	-36,503.0	-55,009.0	-36,446.0	75,166.0	98,802.0	4,282.0	-6,593.0	-14,499.0
45070	50597	-9,696.0	4,206.0	12,216.0	15,641.0	-12,039.0	-12,849.0	-2,103.0	1,997.0	4,243.0
	50588	-4,660.0	-20,381.0	-26,752.0	6,844.0	40,128.0	47,785.0	-929.2	-3,567.0	-7,448.0
	50596	6,810.0	-1,405.0	1,241.0	-11,733.0	293.1	6,974.0	1,229.0	1,006.0	1,704.0
	50587	15,336.0	-29,515.0	-39,804.0	-27,832.0	60,181.0	71,472.0	3,202.0	-5,200.0	-10,570.0

(Sheet 2 of 4)

Table B2 (Continued)

Element	Node	Load Case 1			Load Case 2			Load Case 3		
		Fx [lb]	Fy [lb]	Fz [lb]	Fx [lb]	Fy [lb]	Fz [lb]	Fx [lb]	Fy [lb]	Fz [lb]
45076	50600	-89.4	3,434.0	7,679.0	-697.5	-8,717.0	-6,053.0	-103.8	1,833.0	3,485.0
	50596	1,491.0	-24,380.0	-34,450.0	-3,263.0	50,781.0	63,758.0	258.1	-5,303.0	-10,369.0
	50599	-258.4	3,624.0	5,878.0	1,643.0	-9,399.0	-2,650.0	-136.6	1,989.0	2,922.0
	50595	-2,028.0	-23,272.0	-32,741.0	4,368.0	48,229.0	60,706.0	-271.4	-5,026.0	-10,259.0
45077	50601	-3,078.0	3,126.0	10,577.0	4,533.0	-8,243.0	-11,554.0	-738.6	1,731.0	4,138.0
	50597	-624.4	-22,812.0	-30,855.0	53.2	47,360.0	57,352.0	-227.3	-5,009.0	-9,398.0
	50600	454.4	2,141.0	5,106.0	368.4	-6,670.0	-1,269.0	-139.4	1,691.0	2,584.0
	50596	5,134.0	-25,196.0	-38,227.0	-8,612.0	52,394.0	70,787.0	1,351.0	-5,362.0	-11,486.0
45079	50618	1,410.0	4,652.0	7,283.0	-2,628.0	-10,766.0	-6,895.0	743.1	2,225.0	3,523.0
	50600	40.4	-22,447.0	-34,264.0	-337.5	48,390.0	65,165.0	48.9	-5,982.0	-11,778.0
	50617	-597.8	2,849.0	5,751.0	1,090.0	-6,858.0	-3,373.0	-523.1	1,613.0	2,852.0
	50599	334.1	-23,457.0	-32,453.0	-707.2	50,448.0	62,406.0	63.0	-6,236.0	-11,196.0
45080	50619	-1,569.0	2,627.0	4,688.0	2,117.0	-6,132.0	-3,787.0	-536.6	1,457.0	2,354.0
	50601	-2,874.0	-23,773.0	-36,496.0	3,923.0	50,870.0	68,827.0	-1,257.0	-6,471.0	-12,488.0
	50618	3,630.0	4,360.0	10,643.0	-4,239.0	-10,204.0	-11,816.0	1,281.0	2,178.0	4,725.0
	50600	-301.1	-23,159.0	-31,911.0	1,244.0	49,002.0	62,059.0	4.2	-6,092.0	-10,916.0
45086	50626	-16,715.0	7,390.0	28,611.0	44,075.0	-17,023.0	-50,107.0	-6,602.0	2,545.0	11,569.0
	50613	-9,120.0	-35,993.0	-65,728.0	17,967.0	79,538.0	119,880.0	-3,184.0	-9,779.0	-20,507.0
	50625	17,572.0	-10,159.0	15,237.0	-33,502.0	17,139.0	-6,033.0	4,717.0	-720.8	6,199.0
	50611	27,437.0	-44,938.0	-76,285.0	-64,675.0	96,432.0	152,780.0	8,427.0	-11,469.0	-24,380.0
45087	50627	-21,274.0	16,996.0	33,780.0	49,549.0	-34,763.0	-69,840.0	-7,884.0	4,080.0	14,459.0
	50615	-7,777.0	-26,621.0	-49,933.0	16,772.0	59,337.0	97,493.0	-2,365.0	-7,060.0	-15,825.0
	50626	19,415.0	-9,477.0	1,277.0	-40,693.0	19,248.0	9,243.0	5,361.0	-1,572.0	1,968.0
	50613	26,762.0	-36,708.0	-65,535.0	-59,849.0	78,890.0	135,570.0	8,316.0	-9,416.0	-21,267.0
45088	50632	-8,358.0	-1,947.0	-1,925.0	14,040.0	3,145.0	8,063.0	-3,105.0	-269.9	-200.2
	50618	-10,926.0	-29,353.0	-44,864.0	16,826.0	63,374.0	85,173.0	-4,537.0	-9,851.0	-17,463.0
	50631	9,946.0	13,983.0	19,318.0	-11,346.0	-32,665.0	-22,959.0	4,278.0	5,393.0	8,829.0
	50617	-698.0	-24,027.0	-35,613.0	3,279.0	52,378.0	71,404.0	-84.3	-8,018.0	-13,676.0
45089	50633	-7,573.0	443.1	800.4	13,128.0	-1,507.0	1,102.0	-2,818.0	616.2	844.3
	50619	-10,673.0	-25,271.0	-37,378.0	17,474.0	54,935.0	72,982.0	-4,318.0	-8,290.0	-14,270.0
	50632	9,671.0	7,339.0	11,626.0	-14,474.0	-16,220.0	-15,126.0	3,889.0	2,950.0	5,265.0
	50618	2,968.0	-21,189.0	-28,249.0	-3,851.0	46,329.0	58,206.0	1,368.0	-6,876.0	-10,653.0
45095	50683	-7,511.0	8,800.0	33,210.0	22,630.0	-20,098.0	-63,741.0	-2,696.0	3,774.0	11,946.0
	50626	-2,696.0	-27,457.0	-46,203.0	2,411.0	59,594.0	86,454.0	-835.0	-7,695.0	-15,744.0
	50682	11,070.0	-4,761.0	29,157.0	-17,414.0	5,496.0	-46,246.0	1,870.0	1,694.0	10,242.0
	50625	16,362.0	-37,173.0	-48,154.0	-40,456.0	79,688.0	95,765.0	4,355.0	-9,366.0	-16,606.0
45096	50684	-12,274.0	11,000.0	27,737.0	28,150.0	-22,822.0	-59,698.0	-3,740.0	3,151.0	10,413.0
	50627	-1,258.0	-12,995.0	-27,563.0	2,238.0	28,430.0	56,352.0	-124.6	-3,728.0	-9,572.0
	50683	7,687.0	-2,089.0	15,161.0	-14,241.0	3,862.0	-28,568.0	860.6	755.0	5,941.0
	50626	20,660.0	-28,523.0	-37,972.0	-45,924.0	60,332.0	80,112.0	5,791.0	-6,936.0	-13,299.0
45097	50685	-17,006.0	7,193.0	19,379.0	39,467.0	-14,842.0	-43,348.0	-5,907.0	1,887.0	6,985.0
	50628	5,001.0	89.8	-244.2	-8,281.0	569.6	138.2	1,825.0	-630.5	56.1
	50684	-31.2	-3,380.0	1,941.0	129.1	7,073.0	-3,681.0	-1,609.0	385.0	1,193.0
	50627	30,713.0	-24,714.0	-34,167.0	-69,902.0	52,674.0	74,899.0	8,901.0	-5,184.0	-12,077.0
45098	50686	-4,757.0	2,899.0	2,114.0	13,234.0	-5,456.0	-5,933.0	-1,649.0	1,169.0	735.1
	50629	5,967.0	-2,094.0	524.2	-11,782.0	6,006.0	-1,863.0	2,528.0	-789.1	91.6
	50685	1,164.0	-724.0	-4,545.0	-448.6	135.9	10,515.0	-515.0	1,189.0	-1,455.0
	50628	1,514.0	-5,857.0	-2,151.0	-5,600.0	11,300.0	6,428.0	-977.7	-371.1	-939.5

(Sheet 3 of 4)

Table B2 (Concluded)

Element	Node	Load Case 1			Load Case 2			Load Case 3		
		Fx [lb]	Fy [lb]	Fz [lb]	Fx [lb]	Fy [lb]	Fz [lb]	Fx [lb]	Fy [lb]	Fz [lb]
45099	50687	-3,060.0	-1,959.0	-2,230.0	9,208.0	6,058.0	2,550.0	-949.6	-255.7	-1,012.0
	50630	262.8	-6,353.0	-957.7	-1,949.0	16,224.0	1,148.0	413.2	-2,051.0	-570.8
	50686	308.2	3,975.0	900.9	3,824.0	-10,145.0	-911.7	116.7	2,110.0	485.9
	50629	-6,734.0	853.6	-1,023.0	14,588.0	-3,802.0	4,239.0	-3,169.0	786.9	-414.8
45100	50688	-162.7	-2,191.0	741.8	2,763.0	5,245.0	713.7	426.6	-354.6	415.8
	50631	-18,536.0	-19,243.0	-23,170.0	29,870.0	44,907.0	40,097.0	-7,387.0	-6,896.0	-9,864.0
	50687	7,905.0	7,971.0	11,315.0	-8,280.0	-20,367.0	-16,841.0	3,540.0	3,182.0	4,929.0
	50630	-6,910.0	2,604.0	-793.7	18,709.0	-7,899.0	3,089.0	-2,746.0	800.4	-309.7
45101	50689	-2,648.0	2,517.0	8,403.0	5,635.0	-6,147.0	-12,913.0	-793.4	1,341.0	3,796.0
	50632	-11,172.0	-19,927.0	-26,726.0	19,778.0	44,422.0	51,212.0	-4,546.0	-7,487.0	-11,313.0
	50688	5,172.0	10,733.0	16,129.0	-7,842.0	-25,042.0	-25,928.0	2,275.0	4,236.0	7,127.0
	50631	-977.1	-9,736.0	-19,856.0	4,731.0	21,475.0	37,530.0	-293.2	-3,846.0	-8,355.0
45102	50690	-3,674.0	4,872.0	9,167.0	7,445.0	-11,171.0	-16,465.0	-1,342.0	2,219.0	4,132.0
	50633	-7,320.0	-17,509.0	-23,862.0	13,702.0	38,667.0	48,261.0	-2,951.0	-6,667.0	-10,066.0
	50689	4,665.0	8,985.0	12,499.0	-8,801.0	-19,974.0	-22,591.0	1,944.0	3,645.0	5,546.0
	50632	1,995.0	-13,529.0	-21,034.0	-2,862.0	30,206.0	42,483.0	898.1	-5,321.0	-8,895.0
45144	50702	-2,105.0	7,268.0	15,665.0	7,531.0	-19,420.0	-31,524.0	-841.4	3,113.0	5,704.0
	50683	1,034.0	-18,031.0	-34,285.0	-9,552.0	38,401.0	62,744.0	500.4	-6,144.0	-12,848.0
	50701	13,269.0	-10,899.0	10,584.0	-15,198.0	14,546.0	-4,807.0	781.7	1,323.0	3,445.0
	50682	15,669.0	-33,566.0	-37,879.0	-36,217.0	70,489.0	80,427.0	3,315.0	-8,332.0	-14,735.0
45145	50703	-4,835.0	8,399.0	14,682.0	9,870.0	-18,960.0	-33,330.0	-1,584.0	2,620.0	5,882.0
	50684	4,984.0	-6,388.0	-12,752.0	-13,341.0	13,282.0	24,838.0	1,936.0	-2,640.0	-5,252.0
	50702	1,255.0	-1,652.0	-1,418.0	-184.6	4,412.0	5,327.0	-463.5	-236.3	237.2
	50683	13,294.0	-20,247.0	-30,862.0	-28,119.0	42,523.0	67,235.0	3,682.0	-5,706.0	-11,860.0
45146	50704	-9,105.0	6,557.0	14,126.0	19,112.0	-15,579.0	-32,957.0	-3,634.0	2,166.0	5,545.0
	50685	6,022.0	-3,953.0	-2,271.0	-15,412.0	8,143.0	3,419.0	1,921.0	-1,820.0	-1,300.0
	50703	715.5	-2,849.0	-5,311.0	841.5	6,593.0	13,321.0	-64.4	-619.5	-1,507.0
	50684	15,536.0	-15,746.0	-29,400.0	-33,980.0	33,647.0	65,779.0	5,433.0	-4,763.0	-11,441.0
45147	50705	-12,325.0	3,107.0	6,259.0	27,632.0	-8,226.0	-17,680.0	-5,284.0	1,095.0	2,419.0
	50686	-269.2	-5,250.0	-1,360.0	-3,081.0	11,328.0	963.6	-718.8	-2,557.0	-1,304.0
	50704	5,107.0	-2,120.0	-5,762.0	-7,558.0	5,074.0	14,667.0	2,069.0	-313.9	-1,767.0
	50685	18,349.0	-12,282.0	-19,594.0	-42,133.0	26,415.0	47,294.0	6,669.0	-4,044.0	-7,956.0
45148	50706	-7,406.0	-136.0	-1,735.0	20,346.0	-1,094.0	-96.1	-3,258.0	-47.7	-744.1
	50687	-11,943.0	-10,478.0	-12,425.0	20,706.0	23,456.0	21,136.0	-5,539.0	-4,639.0	-6,215.0
	50705	9,958.0	709.4	1,071.0	-18,089.0	-1,095.0	2,344.0	4,474.0	659.7	966.6
	50686	4,644.0	-5,790.0	-5,370.0	-13,819.0	12,354.0	17,207.0	1,853.0	-2,404.0	-2,664.0
45149	50707	-3,151.0	-1,589.0	-2,139.0	12,488.0	2,463.0	2,939.0	-1,329.0	-603.1	-854.8
	50688	-11,407.0	-13,761.0	-20,695.0	23,795.0	30,918.0	37,800.0	-5,136.0	-5,823.0	-9,680.0
	50706	7,469.0	3,750.0	8,194.0	-16,358.0	-7,529.0	-11,691.0	3,487.0	1,703.0	3,905.0
	50687	-2,002.0	-3,930.0	-4,871.0	-608.1	8,503.0	13,853.0	-729.4	-1,925.0	-2,424.0
45150	50708	-2,311.0	-681.7	793.4	10,011.0	608.4	-985.4	-832.7	-207.5	531.4
	50689	-8,218.0	-16,315.0	-23,474.0	19,006.0	36,168.0	46,482.0	-3,613.0	-6,821.0	-10,852.0
	50707	3,944.0	5,059.0	9,051.0	-11,484.0	-10,538.0	-14,624.0	1,863.0	2,145.0	4,328.0
	50688	-2,359.0	-7,310.0	-12,830.0	1,178.0	16,606.0	27,373.0	-896.1	-3,405.0	-5,970.0
45151	50690	-6,282.0	-15,872.0	-21,985.0	15,494.0	34,951.0	46,261.0	-2,710.0	-6,694.0	-10,116.0
	50709	-3,379.0	714.5	2,712.0	10,818.0	-2,132.0	-4,596.0	-1,255.0	353.5	1,437.0
	50708	3,038.0	4,719.0	6,856.0	-10,321.0	-9,774.0	-12,375.0	1,303.0	1,970.0	3,357.0
	50689	1,146.0	-10,889.0	-18,134.0	-4,970.0	24,760.0	37,933.0	557.3	-4,824.0	-8,327.0

(Sheet 4 of 4)

Table B3
Element Nodal Forces for Section 2

Element	Node	Load Case 1			Load Case 2			Load Case 3		
		Fx [lb]	Fy [lb]	Fz [lb]	Fx [lb]	Fy [lb]	Fz [lb]	Fx [lb]	Fy [lb]	Fz [lb]
40603	45795	4,927.0	18,856.0	18,852.0	-2,233.0	-31,463.0	-14,641.0	576.2	-1,508.0	3,285.0
	45582	4,268.0	-5,063.0	6,449.0	-763.2	-7,368.0	20,081.0	247.6	3,511.0	1,908.0
	45361	4,601.0	-20,511.0	-21,496.0	-1,353.0	36,033.0	22,292.0	510.8	1,396.0	-4,158.0
	45794	5,281.0	6,975.0	-5,212.0	-2,881.0	3,088.0	-24,834.0	847.5	-3,074.0	-1,645.0
40806	46642	3,971.0	12,268.0	20,145.0	39.7	-15,999.0	-19,569.0	510.5	-820.1	5,095.0
	46641	3,555.0	375.4	8,520.0	972.9	-21,340.0	14,269.0	320.7	4,564.0	1,650.0
	45582	4,004.0	-14,315.0	-22,705.0	351.9	21,524.0	27,163.0	725.8	866.5	-5,900.0
	45795	4,486.0	1,616.0	-7,716.0	-683.1	16,952.0	-18,661.0	942.3	-4,460.0	-1,610.0
40978	46867	5,553.0	23,554.0	14,384.0	-1,467.0	-48,311.0	-3,683.0	353.4	-1,598.0	1,112.0
	45795	4,573.0	-7,652.0	2,821.0	129.9	-7,194.0	41,486.0	-130.6	3,510.0	332.3
	45794	4,965.0	-24,882.0	-17,276.0	-762.0	51,151.0	9,285.0	93.6	1,478.0	-2,168.0
	46866	5,877.0	9,585.0	-1,318.0	-2,282.0	3,753.0	-44,357.0	548.6	-2,861.0	155.0
40979	46868	3,832.0	8,419.0	6,838.0	3,657.0	-8,003.0	20,413.0	50.7	-2,856.0	546.8
	46642	2,247.0	-1,439.0	5,313.0	7,436.0	-27,637.0	39,836.0	-598.2	5,453.0	-100.5
	45795	2,142.0	-12,591.0	-12,271.0	8,965.0	20,733.0	-6,211.0	-342.6	2,468.0	-2,474.0
	46867	3,657.0	6,127.0	-1,701.0	5,351.0	14,822.0	-51,263.0	288.4	-4,635.0	1,285.0
41731	46811	3,509.0	10,751.0	25,198.0	1,562.0	-17,756.0	-39,799.0	632.2	1,256.0	7,274.0
	46810	3,354.0	5,761.0	7,581.0	1,378.0	-33,643.0	18,467.0	570.2	4,916.0	474.0
	46641	4,345.0	-11,826.0	-27,739.0	-737.1	18,774.0	46,096.0	1,216.0	-813.0	-8,224.0
	46642	4,574.0	-5,180.0	-7,271.0	-703.6	35,010.0	-20,924.0	1,316.0	-5,472.0	-516.2
41732	46812	2,230.0	5,072.0	9,023.0	10,071.0	-15,040.0	26,569.0	64.4	1,145.0	2,466.0
	46811	430.8	5,388.0	4,801.0	17,689.0	-38,067.0	52,656.0	-565.0	4,773.0	-1,367.0
	46642	1,627.0	-5,635.0	-16,730.0	13,532.0	8,138.0	2,940.0	406.1	503.1	-5,097.0
	46868	3,594.0	-4,762.0	-35.5	5,940.0	45,822.0	-78,583.0	1,100.0	-6,301.0	2,881.0
41866	47832	2,985.0	12,630.0	30,452.0	1,281.0	-29,381.0	-50,293.0	780.9	3,297.0	8,230.0
	47831	3,176.0	8,845.0	4,684.0	725.1	-31,718.0	23,143.0	909.0	3,433.0	80.6
	46810	4,525.0	-13,055.0	-32,940.0	-2,211.0	28,487.0	58,999.0	1,601.0	-3,104.0	-9,314.0
	46811	4,437.0	-9,362.0	-4,655.0	-1,833.0	36,101.0	-27,724.0	1,519.0	-4,052.0	-114.5
41867	47833	3,161.0	6,924.0	18,833.0	3,072.0	-17,763.0	-6,600.0	1,227.0	1,833.0	5,578.0
	47832	2,225.0	4,814.0	10,532.0	4,795.0	-14,996.0	18,434.0	1,193.0	1,297.0	2,679.0
	46811	3,858.0	-7,130.0	-24,124.0	2,813.0	19,918.0	17,499.0	1,731.0	-2,174.0	-6,537.0
	46812	4,803.0	-5,112.0	-8,372.0	1,268.0	14,736.0	-25,444.0	1,723.0	-1,193.0	-2,828.0
41917	47897	4,046.0	28,610.0	13,448.0	-1,395.0	-59,303.0	-22,724.0	113.4	-212.3	1,139.0
	46867	3,600.0	-12,986.0	-5,697.0	-1,333.0	2,561.0	51,078.0	-196.0	2,990.0	-2,007.0
	46866	3,938.0	-28,760.0	-14,135.0	-2,390.0	58,293.0	21,045.0	-6.2	520.6	-1,391.0
	47896	4,327.0	13,652.0	5,677.0	-2,436.0	-2,346.0	-47,998.0	284.8	-2,875.0	1,981.0
41918	47898	2,265.0	11,953.0	5,099.0	3,918.0	-12,007.0	-17,702.0	-411.6	-5,286.0	1,239.0
	46868	1,757.0	-3,378.0	-5,598.0	1,635.0	-38,699.0	59,307.0	-631.4	8,968.0	-3,787.0
	46867	1,122.0	-16,297.0	-5,181.0	5,259.0	29,572.0	5,131.0	-985.6	3,287.0	-704.0
	47897	1,417.0	8,444.0	5,004.0	7,663.0	20,548.0	-45,793.0	-852.4	-6,463.0	2,984.0
42730	47861	3,058.0	26,920.0	42,507.0	-1,234.0	-61,328.0	-79,969.0	925.7	6,882.0	11,303.0
	47837	4,669.0	3,387.0	-2,477.0	-5,602.0	-11,286.0	28,253.0	1,631.0	931.4	-593.2
	47831	7,059.0	-24,046.0	-40,737.0	-10,024.0	56,109.0	76,889.0	2,505.0	-6,457.0	-11,132.0
	47832	5,672.0	-7,834.0	-2,019.0	-6,081.0	21,385.0	-20,422.0	1,896.0	-2,159.0	-877.6
42731	47862	4,951.0	7,867.0	33,415.0	-2,099.0	-18,064.0	-45,816.0	1,640.0	2,188.0	9,820.0
	47861	4,463.0	8,652.0	19,156.0	-1,511.0	-20,771.0	-12,161.0	1,752.0	2,087.0	5,594.0
	47832	5,866.0	-10,273.0	-38,098.0	-3,260.0	23,886.0	55,429.0	2,436.0	-2,789.0	-10,909.0
	47833	6,371.0	-7,100.0	-18,307.0	-3,690.0	17,722.0	8,031.0	2,281.0	-1,938.0	-5,988.0

(Sheet 1 of 4)

Table B3 (Continued)

Element	Node	Load Case 1			Load Case 2			Load Case 3		
		Fx [lb]	Fy [lb]	Fz [lb]	Fx [lb]	Fy [lb]	Fz [lb]	Fx [lb]	Fy [lb]	Fz [lb]
42734	47863	3,432.0	39,309.0	37,797.0	-3,590.0	-89,504.0	-75,688.0	928.8	9,406.0	10,549.0
	47839	4,986.0	-9,759.0	-7,276.0	-8,130.0	20,024.0	31,772.0	1,789.0	-1,930.0	-1,245.0
	47837	7,328.0	-37,115.0	-39,125.0	-12,704.0	85,272.0	78,673.0	2,678.0	-9,389.0	-11,274.0
	47861	6,007.0	5,253.0	5,873.0	-8,618.0	-9,328.0	-29,610.0	1,917.0	708.6	552.9
42736	47843	1,623.0	-1,261.0	7,666.0	-3,115.0	1,339.0	-5,166.0	486.2	571.1	3,102.0
	47839	2,973.0	-19,060.0	-15,365.0	-5,638.0	44,157.0	30,972.0	1,161.0	-4,730.0	-4,942.0
	47863	2,535.0	1,253.0	-8,748.0	-3,998.0	-981.3	6,912.0	899.0	-626.2	-3,586.0
	47864	1,112.0	18,049.0	15,451.0	-1,369.0	-41,778.0	-30,752.0	206.4	4,251.0	4,878.0
42757	48809	7,549.0	53,852.0	79,715.0	-9,507.0	-118,300.0	-152,420.0	2,089.0	12,273.0	21,323.0
	47863	13,504.0	-6,228.0	15,176.0	-22,838.0	13,227.0	-11,805.0	4,087.0	-964.1	5,207.0
	47861	19,681.0	-42,051.0	-67,152.0	-35,043.0	93,548.0	125,950.0	5,927.0	-10,295.0	-18,585.0
	47862	14,562.0	-8,344.0	-33,391.0	-23,452.0	18,684.0	48,519.0	4,290.0	-2,423.0	-10,518.0
42758	48810	5,358.0	31,854.0	48,706.0	-9,267.0	-71,026.0	-95,262.0	1,167.0	7,231.0	13,802.0
	47864	7,210.0	-3,647.0	27,211.0	-14,261.0	8,408.0	-46,053.0	1,880.0	571.8	8,205.0
	47863	9,252.0	-35,897.0	-44,126.0	-17,851.0	80,323.0	84,126.0	2,912.0	-8,785.0	-13,121.0
	48809	7,538.0	5,426.0	-34,090.0	-13,212.0	-11,923.0	61,677.0	2,241.0	-167.9	-10,053.0
42759	48811	5,203.0	26,214.0	36,124.0	-9,158.0	-58,256.0	-74,173.0	1,116.0	6,668.0	11,139.0
	47866	6,816.0	-8,778.0	11,728.0	-14,312.0	19,564.0	-17,238.0	1,931.0	252.4	3,140.0
	47864	7,975.0	-31,355.0	-35,331.0	-15,644.0	71,353.0	70,582.0	2,760.0	-7,968.0	-11,558.0
	48810	6,374.0	10,803.0	-15,052.0	-10,472.0	-24,328.0	25,686.0	1,948.0	-595.1	-4,147.0
42786	48849	4,501.0	35,311.0	19,553.0	-3,056.0	-63,351.0	-40,536.0	84.8	68.2	2,578.0
	47897	4,373.0	-13,074.0	-9,218.0	-3,598.0	-4,155.0	49,704.0	-117.1	4,242.0	-2,971.0
	47896	4,718.0	-34,930.0	-18,924.0	-3,907.0	64,410.0	35,842.0	-67.3	-125.9	-2,326.0
	48848	4,806.0	13,115.0	8,127.0	-3,392.0	2,292.0	-44,004.0	118.8	-3,777.0	2,540.0
42787	48850	3,297.0	20,910.0	7,284.0	-3,305.0	-40,792.0	-18,075.0	-94.7	-2,965.0	1,198.0
	47898	3,128.0	-11,779.0	-4,132.0	-2,985.0	11,483.0	17,890.0	-327.4	5,128.0	-1,285.0
	47897	2,559.0	-23,646.0	-7,390.0	-3,077.0	41,677.0	19,385.0	-440.6	2,481.0	-1,274.0
	48849	2,772.0	14,791.0	4,063.0	-3,541.0	-12,569.0	-18,842.0	-193.8	-4,283.0	1,295.0
43554	49711	8,397.0	46,470.0	32,913.0	-16,452.0	-100,120.0	-68,861.0	1,650.0	9,464.0	8,605.0
	48810	7,200.0	-5,543.0	10,202.0	-15,085.0	14,600.0	-19,384.0	1,675.0	1,043.0	2,616.0
	48809	6,597.0	-60,695.0	-45,732.0	-12,937.0	132,990.0	93,909.0	1,969.0	-12,812.0	-12,074.0
	49710	7,085.0	17,097.0	1,398.0	-12,878.0	-40,886.0	-3,382.0	1,615.0	996.0	245.5
43555	49712	5,472.0	36,065.0	37,323.0	-9,425.0	-76,631.0	-80,206.0	924.2	7,675.0	11,043.0
	48811	6,071.0	-3,534.0	1,535.0	-12,323.0	5,932.0	-311.9	1,592.0	2,479.0	-387.1
	48810	7,183.0	-38,971.0	-43,513.0	-13,665.0	84,722.0	91,726.0	2,312.0	-8,607.0	-13,049.0
	49711	6,515.0	3,547.0	2,408.0	-10,596.0	-5,966.0	-7,409.0	1,625.0	-3,071.0	1,171.0
43588	50083	5,397.0	44,870.0	34,445.0	-5,836.0	-76,467.0	-60,673.0	222.6	1,326.0	4,693.0
	48849	6,208.0	-13,530.0	-9,552.0	-6,962.0	5,666.0	35,823.0	145.4	3,861.0	-2,344.0
	48848	7,251.0	-41,406.0	-30,245.0	-9,063.0	69,721.0	53,948.0	320.7	-754.4	-4,081.0
	48860	6,496.0	10,236.0	4,960.0	-8,070.0	485.1	-28,243.0	408.0	-4,092.0	1,600.0
43589	50084	4,767.0	35,267.0	11,075.0	-6,930.0	-73,429.0	-22,307.0	145.1	-425.7	1,404.0
	48850	4,598.0	-20,890.0	-6,251.0	-6,715.0	40,404.0	18,182.0	-70.1	2,762.0	-1,215.0
	48849	4,426.0	-36,431.0	-12,080.0	-8,043.0	69,172.0	23,948.0	-86.1	351.1	-1,593.0
	50083	4,645.0	22,008.0	7,112.0	-8,418.0	-36,034.0	-19,513.0	142.0	-2,404.0	1,361.0
43596	50093	6,644.0	35,948.0	40,890.0	-7,924.0	-57,896.0	-60,655.0	386.0	68.6	5,485.0
	50083	7,283.0	-6,515.0	562.9	-8,197.0	749.9	14,118.0	301.6	4,414.0	-493.9
	48860	7,350.0	-36,673.0	-38,096.0	-8,575.0	58,172.0	58,457.0	373.6	64.6	-5,073.0
	48877	6,783.0	7,249.0	-3,856.0	-8,439.0	-1,491.0	-11,014.0	476.2	-4,254.0	-60.7

(Sheet 2 of 4)

Table B3 (Continued)

Element	Node	Load Case 1			Load Case 2			Load Case 3		
		Fx [lb]	Fy [lb]	Fz [lb]	Fx [lb]	Fy [lb]	Fz [lb]	Fx [lb]	Fy [lb]	Fz [lb]
43609	50094	9,454.0	36,181.0	43,160.0	-10,919.0	-60,747.0	-47,677.0	599.4	-414.2	4,910.0
	50093	9,507.0	-11,725.0	18,026.0	-9,557.0	16,951.0	-7,337.0	387.0	3,213.0	2,356.0
	48877	10,294.0	-34,731.0	-43,608.0	-11,519.0	55,517.0	52,727.0	559.3	831.0	-5,160.0
	48878	10,318.0	10,172.0	-18,394.0	-13,005.0	-12,177.0	3,518.0	787.1	-3,286.0	-2,312.0
43610	50116	9,454.0	33,708.0	35,974.0	-9,000.0	-58,198.0	-25,912.0	498.5	-851.1	2,313.0
	50094	9,048.0	-16,606.0	20,117.0	-7,171.0	24,626.0	2,259.0	136.1	1,416.0	2,596.0
	48878	9,990.0	-31,986.0	-38,219.0	-9,097.0	53,112.0	32,617.0	377.6	1,517.0	-3,102.0
	48902	10,417.0	14,771.0	-18,819.0	-10,952.0	-20,004.0	-7,750.0	741.9	-1,722.0	-2,020.0
44316	50894	1,692.0	20,191.0	3,251.0	-2,256.0	-44,092.0	-8,148.0	-21.7	2,063.0	927.0
	49711	3,008.0	-12,180.0	-6,687.0	-5,838.0	25,034.0	14,444.0	579.5	278.2	-1,932.0
	49710	4,137.0	-17,821.0	-937.8	-7,182.0	42,424.0	3,730.0	1,045.0	-1,334.0	-357.0
	50887	2,890.0	8,418.0	3,950.0	-3,743.0	-19,171.0	-9,526.0	481.8	-1,713.0	1,139.0
44317	50895	4,706.0	35,108.0	22,885.0	-7,385.0	-73,421.0	-53,915.0	571.2	6,469.0	6,805.0
	49712	5,191.0	-6,187.0	-8,283.0	-9,944.0	4,709.0	21,752.0	1,139.0	2,462.0	-3,038.0
	49711	5,773.0	-39,364.0	-27,843.0	-9,881.0	84,463.0	63,266.0	1,710.0	-7,412.0	-8,333.0
	50894	5,300.0	8,196.0	11,291.0	-7,295.0	-8,919.0	-28,434.0	1,156.0	-2,739.0	3,555.0
44637	51282	7,198.0	74,608.0	53,312.0	-11,455.0	-142,740.0	-85,529.0	546.5	5,427.0	7,719.0
	50084	10,389.0	-35,398.0	-10,087.0	-16,072.0	73,214.0	22,470.0	877.2	193.9	-1,424.0
	50083	14,119.0	-60,427.0	-40,200.0	-24,311.0	110,860.0	66,518.0	1,404.0	-3,387.0	-5,625.0
	50093	11,200.0	20,705.0	-3,560.0	-20,175.0	-40,648.0	-2,640.0	1,116.0	-2,036.0	-769.8
44644	51283	12,594.0	49,067.0	48,291.0	-18,003.0	-89,982.0	-56,451.0	1,339.0	2,735.0	6,086.0
	51282	11,627.0	-23,252.0	26,133.0	-14,524.0	45,485.0	-24,708.0	981.1	-572.6	4,957.0
	50093	13,319.0	-45,091.0	-53,479.0	-17,866.0	80,641.0	71,435.0	1,439.0	-1,329.0	-7,190.0
	50094	14,380.0	18,897.0	-22,207.0	-21,495.0	-35,877.0	11,446.0	1,841.0	-603.1	-4,106.0
44645	51291	9,911.0	39,121.0	36,907.0	-10,142.0	-72,589.0	-29,383.0	819.4	1,260.0	2,609.0
	51283	9,562.0	-17,073.0	15,738.0	-8,757.0	26,549.0	13,074.0	436.9	-295.6	2,594.0
	50094	10,426.0	-38,610.0	-39,167.0	-10,083.0	70,822.0	34,971.0	756.5	-474.4	-3,570.0
	50116	10,762.0	16,403.0	-14,857.0	-11,430.0	-24,982.0	-17,021.0	1,136.0	-162.9	-1,926.0
45312	50955	1,591.0	10,817.0	3,036.0	-1,257.0	-19,712.0	-11,447.0	-81.8	-915.7	1,210.0
	50894	1,921.0	-4,873.0	-1,704.0	-3,460.0	3,611.0	4,404.0	167.1	2,944.0	-717.8
	50887	2,960.0	-8,740.0	-3,386.0	-4,370.0	19,970.0	9,657.0	580.9	1,565.0	-1,202.0
	50891	2,663.0	2,277.0	1,616.0	-2,250.0	-1,229.0	-2,163.0	353.6	-3,892.0	501.4
45316	52089	426.0	6,307.0	163.7	4,387.0	-15,819.0	9,964.0	-762.7	-1,334.0	-461.8
	50955	302.9	106.7	-4,194.0	5,663.0	-27,948.0	34,199.0	-891.0	6,107.0	-3,475.0
	50891	1,635.0	-2,245.0	-1,122.0	2,496.0	1,503.0	2,295.0	-204.8	3,901.0	-576.4
	52082	2,275.0	-3,624.0	4,240.0	801.1	43,402.0	-45,790.0	130.3	-8,508.0	4,155.0
45319	50956	2,171.0	24,686.0	10,698.0	-568.1	-52,661.0	-28,343.0	-214.3	3,279.0	3,369.0
	50895	3,041.0	-6,176.0	-9,093.0	-3,130.0	-4,873.0	32,760.0	279.2	3,158.0	-3,908.0
	50894	4,527.0	-24,461.0	-11,907.0	-5,435.0	51,727.0	33,115.0	1,073.0	-2,767.0	-4,158.0
	50955	3,812.0	4,592.0	8,478.0	-3,095.0	10,809.0	-35,592.0	649.4	-4,462.0	3,839.0
45379	52096	1,640.0	16,788.0	5,624.0	1,667.0	-39,455.0	-7,755.0	-363.3	1,380.0	1,335.0
	50956	2,244.0	-5,691.0	-5,916.0	251.9	-8,586.0	40,469.0	-39.9	3,207.0	-3,808.0
	50955	3,785.0	-15,896.0	-6,466.0	-1,686.0	38,133.0	13,595.0	626.1	-923.4	-1,932.0
	52089	3,403.0	4,083.0	4,845.0	-568.0	13,447.0	-44,703.0	389.1	-4,125.0	3,630.0
45662	52044	17,349.0	38,052.0	62,667.0	-24,472.0	-71,090.0	-81,958.0	2,769.0	4,098.0	9,233.0
	52043	13,685.0	2,955.0	30,289.0	-17,304.0	-6,805.0	-20,958.0	1,824.0	769.5	7,094.0
	51282	11,091.0	-51,626.0	-78,250.0	-11,835.0	96,793.0	111,300.0	1,776.0	-5,136.0	-12,831.0
	51283	14,581.0	10,328.0	-17,178.0	-18,685.0	-18,581.0	-4,932.0	2,718.0	409.8	-4,056.0

(Sheet 3 of 4)

Table B3 (Concluded)

Element	Node	Load Case 1			Load Case 2			Load Case 3		
		Fx [lb]	Fy [lb]	Fz [lb]	Fx [lb]	Fy [lb]	Fz [lb]	Fx [lb]	Fy [lb]	Fz [lb]
45663	52480	10,315.0	37,962.0	43,402.0	-10,184.0	-72,355.0	-44,831.0	1,093.0	3,156.0	3,976.0
	52044	10,141.0	-5,077.0	6,797.0	-9,054.0	1,693.0	31,544.0	738.2	448.8	743.4
	51283	9,834.0	-42,515.0	-45,251.0	-7,770.0	80,967.0	49,846.0	931.2	-3,100.0	-4,894.0
	51291	9,974.0	9,488.0	-7,003.0	-8,792.0	-10,426.0	-34,181.0	1,274.0	-177.9	-288.2
46323	52049	4,710.0	5,519.0	31,555.0	-462.5	-10,938.0	-24,120.0	1,350.0	1,011.0	5,968.0
	52048	5,534.0	4,108.0	17,359.0	-1,342.0	-11,475.0	5,152.0	1,023.0	1,065.0	4,603.0
	52043	7,563.0	-3,022.0	-29,741.0	-4,477.0	6,228.0	22,244.0	1,487.0	-773.1	-7,343.0
	52044	6,712.0	-6,613.0	-22,031.0	-3,472.0	16,114.0	552.8	1,784.0	-1,185.0	-4,095.0
46324	53221	8,694.0	22,698.0	41,623.0	-6,473.0	-45,327.0	-43,482.0	1,125.0	3,064.0	4,873.0
	52049	7,862.0	6,348.0	11,827.0	-4,511.0	-22,045.0	25,953.0	666.1	2,075.0	309.0
	52044	8,049.0	-26,432.0	-46,161.0	-3,987.0	52,008.0	51,926.0	878.4	-3,277.0	-6,311.0
	52480	8,826.0	-2,677.0	-9,901.0	-5,781.0	15,211.0	-31,590.0	1,306.0	-1,551.0	478.6
46328	52080	3,448.0	4,155.0	18,135.0	2,771.0	-12,207.0	2,441.0	954.0	1,458.0	3,545.0
	52079	4,183.0	1,914.0	8,324.0	1,941.0	-7,659.0	28,511.0	662.3	649.4	2,022.0
	52048	5,819.0	-4,147.0	-16,967.0	-480.1	10,848.0	-3,751.0	1,321.0	-1,054.0	-4,962.0
	52049	5,045.0	-1,921.0	-12,963.0	541.5	8,990.0	-23,018.0	1,567.0	-935.5	-1,780.0
46329	53233	4,994.0	10,029.0	29,199.0	1,591.0	-20,175.0	-26,246.0	509.8	1,739.0	4,606.0
	52080	5,245.0	6,327.0	9,403.0	531.0	-32,584.0	37,959.0	315.9	4,283.0	-2,005.0
	52049	6,764.0	-9,953.0	-29,518.0	-157.2	22,636.0	23,441.0	597.9	-2,030.0	-5,090.0
	53221	6,421.0	-6,335.0	-12,205.0	1,040.0	30,068.0	-32,356.0	735.6	-3,672.0	1,667.0
46358	52083	1,615.0	1,935.0	10,894.0	11,872.0	1,420.0	8,627.0	-167.9	-1,039.0	3,128.0
	52082	2,475.0	4,586.0	-1,068.0	6,366.0	-42,268.0	75,821.0	9.7	7,039.0	-4,957.0
	52079	4,583.0	-1,908.0	-8,197.0	6,759.0	7,067.0	-27,094.0	282.8	-606.8	-2,504.0
	52080	3,376.0	-4,110.0	-5,875.0	12,426.0	34,082.0	-53,480.0	-60.9	-5,131.0	2,831.0
46359	53245	4,033.0	6,746.0	20,824.0	3,479.0	-7,868.0	-16,445.0	181.1	-43.0	4,587.0
	52083	4,389.0	3,292.0	7,998.0	2,356.0	-33,879.0	33,930.0	65.6	6,397.0	-2,469.0
	52080	6,143.0	-6,282.0	-21,094.0	1,592.0	9,489.0	15,196.0	318.7	-438.6	-5,087.0
	53233	5,765.0	-3,701.0	-11,089.0	2,678.0	32,931.0	-30,411.0	410.6	-5,675.0	2,109.0
46361	52090	449.4	3,261.0	4,931.0	6,834.0	-6,004.0	21,993.0	-663.6	-975.5	405.4
	52089	1,031.0	-1,365.0	1,025.0	4,454.0	-17,302.0	46,395.0	-439.0	4,561.0	-2,981.0
	52082	3,010.0	-709.1	-2,943.0	2,142.0	-1,421.0	-29,041.0	188.5	1,595.0	350.8
	52083	2,578.0	-926.5	-4,869.0	4,315.0	25,681.0	-38,115.0	-14.8	-5,095.0	1,613.0
46362	53249	1,651.0	5,148.0	13,690.0	2,859.0	-8,603.0	1,416.0	-151.7	211.0	2,539.0
	52090	1,920.0	448.0	9,483.0	1,805.0	-18,008.0	21,418.0	-176.1	4,521.0	-388.9
	52083	3,785.0	-4,146.0	-13,648.0	398.3	6,233.0	-3,095.0	275.0	-111.0	-2,841.0
	53245	3,514.0	-1,573.0	-11,452.0	1,520.0	21,390.0	-18,754.0	262.2	-4,596.0	215.7
46368	52097	1,716.0	10,687.0	6,139.0	4,316.0	-23,875.0	8,827.0	-540.9	-126.4	804.7
	52096	2,570.0	-5,596.0	-436.4	1,746.0	-6,345.0	41,346.0	-162.3	3,248.0	-2,759.0
	52089	4,599.0	-9,137.0	-5,455.0	-494.0	20,319.0	-10,811.0	568.0	842.9	-627.3
	52090	3,951.0	3,490.0	-2,783.0	1,844.0	13,019.0	-37,747.0	242.2	-4,292.0	1,751.0
46369	53274	2,372.0	8,597.0	11,343.0	3,427.0	-14,658.0	1,971.0	-286.5	-316.8	2,067.0
	52097	3,083.0	-4,039.0	5,928.0	1,058.0	-7,569.0	27,077.0	-90.7	3,745.0	-1,246.0
	52090	5,139.0	-7,367.0	-11,197.0	-714.9	11,338.0	-4,853.0	450.5	731.4	-2,198.0
	53249	4,525.0	2,201.0	-8,774.0	1,553.0	13,424.0	-23,112.0	259.3	-4,368.0	725.8
42740	47866	1,396.0	3,269.0	11,562.0	-2,630.0	-8,101.0	-20,985.0	342.4	1,297.0	3,721.0
	47843	2,434.0	-19,628.0	-4,950.0	-5,246.0	45,180.0	13,813.0	921.0	-4,026.0	-1,937.0
	47864	1,548.0	15,733.0	-7,155.0	-2,307.0	-35,422.0	8,290.0	431.9	2,398.0	-2,098.0

(Sheet 4 of 4)

Table B4
Element Nodal Forces for Section 3

Element	Node	Load Case 1			Load Case 2			Load Case 3		
		Fx [lb]	Fy [lb]	Fz [lb]	Fx [lb]	Fy [lb]	Fz [lb]	Fx [lb]	Fy [lb]	Fz [lb]
40618	46429	4,554.0	19,157.0	19,803.0	-2,038.0	-31,522.0	-15,351.0	658.3	-1,194.0	3,657.0
	46428	3,635.0	-5,614.0	7,925.0	-284.1	-7,485.0	19,266.0	-196.6	3,568.0	2,406.0
	45376	4,744.0	-20,603.0	-23,217.0	-3,644.0	35,945.0	25,808.0	382.0	1,510.0	-4,889.0
	45834	5,723.0	7,765.0	-7,395.0	-5,670.0	2,829.0	-21,399.0	1,285.0	-2,650.0	-2,419.0
41016	46896	5,309.0	23,765.0	15,101.0	-2,036.0	-48,623.0	-3,746.0	494.0	-1,254.0	1,307.0
	46429	3,723.0	-8,172.0	4,406.0	1,145.0	-7,518.0	40,559.0	-659.7	3,589.0	786.6
	45834	5,014.0	-24,634.0	-18,945.0	-2,885.0	50,175.0	12,532.0	-40.3	1,726.0	-2,813.0
	46895	6,439.0	10,642.0	-3,568.0	-5,832.0	2,443.0	-40,698.0	1,056.0	-2,274.0	-600.2
41552	47485	3,446.0	12,568.0	21,233.0	553.6	-15,900.0	-20,693.0	504.1	-560.9	5,603.0
	47484	2,941.0	-296.2	10,126.0	937.5	-21,353.0	13,535.0	-64.7	4,621.0	2,208.0
	46428	4,439.0	-14,505.0	-24,818.0	-2,696.0	21,911.0	31,363.0	727.5	928.6	-6,847.0
	46429	5,120.0	2,412.0	-10,317.0	-3,575.0	17,359.0	-15,022.0	1,411.0	-4,158.0	-2,527.0
41553	47486	3,554.0	8,899.0	7,899.0	2,856.0	-8,397.0	19,968.0	146.9	-2,547.0	816.2
	47485	1,346.0	-2,224.0	7,194.0	8,017.0	-27,983.0	38,861.0	-1,102.0	5,520.0	430.9
	46429	2,578.0	-12,458.0	-14,606.0	5,982.0	20,008.0	-2,102.0	-309.1	2,712.0	-3,377.0
	46896	4,662.0	7,366.0	-4,693.0	1,121.0	13,909.0	-47,172.0	968.8	-4,107.0	306.7
41943	47924	4,064.0	28,838.0	13,411.0	-2,398.0	-59,841.0	-22,064.0	344.4	101.3	1,089.0
	46896	2,899.0	-13,518.0	-4,617.0	-127.9	2,517.0	50,373.0	-664.3	2,958.0	-1,749.0
	46895	3,755.0	-28,588.0	-14,714.0	-3,019.0	57,375.0	22,285.0	-225.8	661.0	-1,624.0
	47923	4,756.0	14,678.0	4,311.0	-5,107.0	-3,960.0	-45,793.0	721.5	-2,342.0	1,556.0
41944	47925	2,713.0	12,622.0	4,710.0	1,990.0	-12,775.0	-17,046.0	36.3	-4,910.0	1,113.0
	47486	834.5	-4,391.0	-4,132.0	2,899.0	-39,115.0	58,521.0	-1,231.0	9,023.0	-3,491.0
	46896	966.7	-16,063.0	-5,804.0	4,633.0	28,372.0	6,348.0	-1,220.0	3,547.0	-966.1
	47924	2,179.0	9,994.0	3,580.0	4,770.0	18,881.0	-44,045.0	-283.3	-5,864.0	2,587.0
42464	48481	2,843.0	10,837.0	26,052.0	2,397.0	-17,240.0	-40,814.0	519.1	1,414.0	7,832.0
	48480	2,710.0	5,021.0	9,372.0	633.2	-33,268.0	17,948.0	254.2	4,931.0	1,099.0
	47484	5,040.0	-12,043.0	-30,092.0	-4,741.0	19,794.0	50,873.0	1,351.0	-838.3	-9,363.0
	47485	5,323.0	-4,381.0	-10,416.0	-3,560.0	36,084.0	-17,098.0	1,759.0	-5,307.0	-1,581.0
42465	48482	1,469.0	5,031.0	10,460.0	9,157.0	-14,989.0	25,906.0	11.0	1,258.0	2,931.0
	48481	-343.7	4,525.0	7,130.0	16,772.0	-37,794.0	51,781.0	-840.5	4,737.0	-705.9
	47485	2,663.0	-5,594.0	-19,972.0	8,591.0	8,255.0	8,487.0	767.1	607.3	-6,407.0
	47486	5,104.0	-3,309.0	-4,867.0	194.3	45,274.0	-72,818.0	1,963.0	-5,900.0	1,389.0
42804	48858	4,509.0	35,850.0	19,357.0	-4,048.0	-64,312.0	-39,756.0	325.1	463.1	2,497.0
	47924	3,728.0	-13,768.0	-8,545.0	-2,310.0	-3,980.0	49,331.0	-552.6	4,175.0	-2,840.0
	47923	4,461.0	-34,981.0	-19,180.0	-3,987.0	63,713.0	36,415.0	-308.0	-55.0	-2,445.0
	48857	5,109.0	14,169.0	7,277.0	-5,603.0	441.9	-42,512.0	498.1	-3,249.0	2,284.0
42805	48859	3,390.0	21,134.0	7,165.0	-4,379.0	-41,212.0	-17,780.0	216.1	-2,694.0	1,165.0
	47925	2,704.0	-11,849.0	-4,007.0	-2,486.0	10,945.0	17,945.0	-685.5	5,303.0	-1,282.0
	47924	2,143.0	-23,680.0	-7,351.0	-2,896.0	40,999.0	19,492.0	-763.1	2,620.0	-1,296.0
	48858	2,913.0	15,490.0	3,780.0	-5,150.0	-13,628.0	-18,343.0	149.8	-3,889.0	1,219.0
43291	48639	2,034.0	12,392.0	31,499.0	2,975.0	-28,347.0	-51,488.0	442.7	3,302.0	8,962.0
	48638	2,566.0	8,365.0	6,417.0	-581.1	-30,938.0	22,761.0	716.9	3,403.0	729.8
	48480	5,618.0	-13,193.0	-35,772.0	-7,071.0	30,062.0	64,169.0	1,942.0	-3,263.0	-10,681.0
	48481	5,317.0	-8,991.0	-8,283.0	-4,184.0	37,806.0	-23,683.0	1,839.0	-4,125.0	-1,318.0
43292	48640	2,118.0	6,846.0	20,228.0	1,622.0	-17,359.0	-7,835.0	1,248.0	1,862.0	6,388.0
	48639	1,145.0	4,613.0	12,322.0	2,886.0	-14,499.0	17,484.0	1,105.0	1,285.0	3,470.0
	48481	5,177.0	-7,092.0	-28,144.0	-3,449.0	20,923.0	23,587.0	2,303.0	-2,282.0	-8,130.0
	48482	6,229.0	-4,943.0	-12,505.0	-4,369.0	15,486.0	-20,479.0	2,366.0	-1,229.0	-4,149.0

(Sheet 1 of 4)

Table B4 (Continued)

Element	Node	Load Case 1			Load Case 2			Load Case 3		
		Fx [lb]	Fy [lb]	Fz [lb]	Fx [lb]	Fy [lb]	Fz [lb]	Fx [lb]	Fy [lb]	Fz [lb]
43415	49544	1,555.0	26,682.0	43,564.0	2,090.0	-59,770.0	-81,032.0	209.3	6,816.0	12,145.0
	48653	4,186.0	2,958.0	-1,350.0	-7,464.0	-9,847.0	28,311.0	1,565.0	747.3	-27.0
	48638	8,743.0	-24,430.0	-44,135.0	-15,906.0	58,317.0	82,479.0	3,124.0	-6,833.0	-12,759.0
	48639	6,678.0	-8,087.0	-5,563.0	-7,672.0	23,863.0	-16,239.0	2,052.0	-2,477.0	-2,165.0
	49544	3,164.0	8,548.0	20,481.0	-3,267.0	-19,947.0	-12,843.0	1,664.0	2,019.0	6,503.0
	48639	7,859.0	-10,526.0	-42,983.0	-10,654.0	25,453.0	62,769.0	3,245.0	-3,085.0	-12,992.0
	48640	8,300.0	-7,146.0	-22,921.0	-9,688.0	19,030.0	13,901.0	2,966.0	-2,120.0	-7,659.0
43428	49548	1,462.0	38,805.0	38,442.0	1,579.0	-86,666.0	-76,126.0	-213.4	9,012.0	11,223.0
	48669	4,830.0	-10,312.0	-6,659.0	-10,524.0	21,741.0	32,066.0	1,843.0	-2,198.0	-709.5
	48653	9,650.0	-37,853.0	-42,556.0	-19,468.0	87,736.0	84,088.0	3,562.0	-9,860.0	-12,950.0
	49544	6,824.0	4,706.0	2,608.0	-8,642.0	-5,998.0	-25,456.0	1,773.0	206.7	-805.5
43441	48672	742.9	-1,306.0	9,295.0	-2,828.0	1,244.0	-6,996.0	247.6	643.0	4,184.0
	48669	4,331.0	-19,404.0	-17,004.0	-9,103.0	45,050.0	33,513.0	1,715.0	-4,892.0	-5,800.0
	49548	3,698.0	792.3	-11,497.0	-4,866.0	1,157.0	10,555.0	1,050.0	-1,024.0	-5,072.0
	49549	-36.6	17,796.0	16,088.0	1,671.0	-40,352.0	-31,561.0	-446.8	3,985.0	5,385.0
43594	50099	5,159.0	45,483.0	34,533.0	-6,354.0	-77,464.0	-60,099.0	400.1	1,724.0	4,706.0
	48858	5,686.0	-13,983.0	-9,401.0	-5,778.0	5,856.0	35,810.0	-212.4	3,838.0	-2,329.0
	48857	6,986.0	-41,733.0	-30,547.0	-8,783.0	69,375.0	54,255.0	87.9	-762.8	-4,196.0
	48881	6,585.0	10,932.0	4,478.0	-9,636.0	-1,140.0	-27,259.0	704.5	-3,677.0	1,450.0
43595	50100	4,586.0	35,414.0	11,056.0	-7,327.0	-73,739.0	-22,086.0	369.8	-162.1	1,399.0
	48859	4,255.0	-20,892.0	-6,238.0	-6,275.0	40,155.0	18,230.0	-368.3	2,891.0	-1,225.0
	48858	4,079.0	-36,601.0	-12,168.0	-7,742.0	68,845.0	24,033.0	-368.3	415.1	-1,635.0
	50099	4,521.0	22,382.0	7,005.0	-9,272.0	-36,834.0	-19,189.0	390.0	-2,085.0	1,333.0
43613	50121	6,175.0	36,430.0	41,191.0	-7,961.0	-58,799.0	-60,234.0	502.0	387.4	5,556.0
	50099	6,733.0	-6,764.0	649.3	-6,974.0	1,005.0	14,161.0	-14.3	4,433.0	-465.9
	48881	7,118.0	-37,041.0	-38,659.0	-8,144.0	58,046.0	58,805.0	167.6	55.6	-5,236.0
	48907	6,739.0	7,667.0	-4,376.0	-9,486.0	-2,889.0	-10,144.0	718.5	-3,934.0	-224.1
43635	50158	8,605.0	36,541.0	43,584.0	-10,304.0	-61,472.0	-47,272.0	648.3	-142.2	4,994.0
	50121	8,720.0	-11,961.0	18,299.0	-8,108.0	17,287.0	-7,329.0	63.0	3,250.0	2,460.0
	48907	10,067.0	-35,058.0	-44,517.0	-11,076.0	55,365.0	53,279.0	388.4	891.8	-5,383.0
	48959	10,153.0	10,493.0	-19,312.0	-13,631.0	-13,533.0	4,634.0	1,006.0	-2,969.0	-2,577.0
43679	50162	8,476.0	33,979.0	36,333.0	-8,169.0	-58,696.0	-25,444.0	539.3	-652.1	2,339.0
	50158	8,108.0	-16,966.0	20,553.0	-5,647.0	25,169.0	2,072.0	-178.8	1,412.0	2,748.0
	48959	9,760.0	-32,251.0	-39,214.0	-8,607.0	52,995.0	33,136.0	224.8	1,627.0	-3,289.0
	48963	10,186.0	15,145.0	-19,923.0	-11,230.0	-21,292.0	-6,558.0	950.6	-1,404.0	-2,307.0
44181	49680	4,283.0	53,739.0	81,179.0	-4,606.0	-115,790.0	-153,250.0	847.5	12,113.0	22,824.0
	49548	12,625.0	-7,138.0	15,661.0	-24,968.0	15,980.0	-11,348.0	4,082.0	-1,403.0	6,018.0
	49544	23,192.0	-43,343.0	-73,364.0	-44,864.0	96,723.0	135,530.0	7,307.0	-11,068.0	-21,476.0
	49545	17,193.0	-9,087.0	-39,424.0	-29,852.0	21,679.0	57,770.0	5,061.0	-2,983.0	-13,163.0
44183	49682	2,765.0	31,605.0	50,585.0	-4,151.0	-68,763.0	-97,338.0	-4.7	6,912.0	15,169.0
	49549	5,953.0	-3,809.0	28,806.0	-13,812.0	9,099.0	-47,841.0	1,516.0	607.8	9,455.0
	49548	12,167.0	-37,141.0	-48,251.0	-24,651.0	83,005.0	90,332.0	3,973.0	-9,408.0	-15,314.0
	49680	9,129.0	4,425.0	-37,884.0	-15,948.0	-8,422.0	67,243.0	2,558.0	-866.8	-12,025.0
44184	49684	2,863.0	25,900.0	37,216.0	-3,878.0	-55,236.0	-75,742.0	-257.4	6,169.0	12,209.0
	49551	6,404.0	-8,788.0	12,002.0	-16,261.0	19,377.0	-16,805.0	1,885.0	576.6	3,695.0
	49549	10,813.0	-32,742.0	-39,324.0	-22,214.0	74,650.0	76,862.0	3,813.0	-8,636.0	-13,783.0
	49682	7,147.0	8,997.0	-17,869.0	-9,695.0	-17,481.0	29,231.0	1,672.0	-2,118.0	-5,586.0

(Sheet 2 of 4)

Table B4 (Continued)

Element	Node	Load Case 1			Load Case 2			Load Case 3		
		Fx [lb]	Fy [lb]	Fz [lb]	Fx [lb]	Fy [lb]	Fz [lb]	Fx [lb]	Fy [lb]	Fz [lb]
44288	50857	6,406.0	46,525.0	33,768.0	-12,758.0	-97,949.0	-69,948.0	732.1	9,272.0	9,211.0
	49682	6,857.0	-5,583.0	10,130.0	-16,811.0	14,797.0	-18,923.0	1,668.0	1,307.0	2,756.0
	49680	8,925.0	-62,506.0	-48,267.0	-19,791.0	135,920.0	97,831.0	2,924.0	-13,557.0	-13,421.0
	50855	6,359.0	15,561.0	827.3	-11,415.0	-36,028.0	-2,634.0	1,124.0	-89.6	23.4
44290	50859	2,949.0	36,089.0	38,101.0	-4,109.0	-73,535.0	-81,637.0	-443.0	7,209.0	11,866.0
	49684	5,713.0	-3,508.0	631.4	-14,821.0	5,408.0	1,755.0	1,604.0	2,905.0	-573.4
	49682	9,661.0	-40,624.0	-46,987.0	-20,576.0	87,606.0	97,263.0	3,346.0	-9,232.0	-14,970.0
	50857	6,632.0	2,000.0	1,172.0	-9,411.0	556.3	-6,397.0	1,271.0	-4,525.0	692.8
44648	51296	6,383.0	75,057.0	53,852.0	-10,712.0	-142,940.0	-85,441.0	655.2	5,805.0	7,927.0
	50100	10,176.0	-35,687.0	-10,277.0	-15,743.0	73,454.0	22,681.0	642.0	232.0	-1,463.0
	50099	14,082.0	-61,039.0	-40,826.0	-24,216.0	111,010.0	66,881.0	1,214.0	-3,463.0	-5,811.0
	50121	10,994.0	20,800.0	-4,006.0	-20,557.0	-41,163.0	-2,015.0	1,316.0	-1,797.0	-878.2
44664	51327	11,428.0	49,414.0	48,844.0	-16,706.0	-90,203.0	-56,213.0	1,315.0	2,983.0	6,270.0
	51296	10,790.0	-23,585.0	26,457.0	-13,303.0	45,837.0	-24,640.0	727.2	-575.9	5,137.0
	50121	13,372.0	-45,566.0	-54,840.0	-17,921.0	80,728.0	72,464.0	1,317.0	-1,323.0	-7,528.0
	50158	14,292.0	19,070.0	-23,480.0	-21,917.0	-36,546.0	12,869.0	2,045.0	-346.5	-4,453.0
44696	51331	8,725.0	39,394.0	37,268.0	-8,989.0	-72,792.0	-28,881.0	809.1	1,440.0	2,659.0
	51327	8,413.0	-17,470.0	16,205.0	-7,132.0	27,084.0	12,843.0	102.8	-322.9	2,791.0
	50158	10,393.0	-38,907.0	-40,534.0	-10,031.0	70,690.0	35,976.0	650.5	-376.4	-3,854.0
	50162	10,672.0	16,772.0	-16,308.0	-11,827.0	-25,993.0	-15,375.0	1,361.0	146.2	-2,306.0
45284	50915	213.7	19,782.0	3,074.0	-417.7	-41,472.0	-7,993.0	-697.5	1,488.0	871.4
	50857	2,551.0	-12,283.0	-7,128.0	-7,885.0	24,617.0	15,176.0	521.8	534.0	-2,132.0
	50855	4,402.0	-17,716.0	-1,084.0	-10,220.0	42,039.0	3,973.0	1,227.0	-1,030.0	-407.4
	50890	2,286.0	7,612.0	3,720.0	-3,240.0	-15,584.0	-9,518.0	114.5	-2,545.0	1,101.0
45286	50925	2,397.0	35,245.0	22,760.0	-3,384.0	-70,660.0	-54,196.0	-544.1	6,016.0	7,044.0
	50859	4,456.0	-6,663.0	-9,276.0	-12,131.0	4,251.0	23,999.0	1,058.0	2,734.0	-3,402.0
	50857	7,403.0	-40,688.0	-29,948.0	-15,437.0	86,302.0	66,691.0	2,475.0	-7,775.0	-9,457.0
	50915	5,320.0	7,609.0	10,315.0	-6,724.0	-3,707.0	-28,119.0	939.2	-3,768.0	3,272.0
45315	52093	570.4	10,732.0	2,688.0	-615.3	-17,768.0	-11,226.0	-444.5	-1,382.0	1,102.0
	50915	874.7	-4,870.0	-1,898.0	-4,299.0	2,439.0	4,861.0	-114.1	3,334.0	-789.6
	50890	2,610.0	-8,325.0	-3,627.0	-6,267.0	18,614.0	10,099.0	548.0	2,089.0	-1,328.0
	52086	2,430.0	2,035.0	1,476.0	-2,906.0	1,337.0	-2,200.0	288.5	-4,475.0	478.5
45340	52120	153.7	24,563.0	10,161.0	2,269.0	-49,948.0	-28,006.0	-1,051.0	2,678.0	3,286.0
	50925	1,937.0	-7,059.0	-9,402.0	-4,445.0	-5,425.0	34,416.0	48.1	3,307.0	-4,077.0
	50915	5,458.0	-24,969.0	-13,040.0	-9,577.0	51,792.0	35,121.0	1,601.0	-2,593.0	-4,744.0
	52093	4,079.0	5,025.0	6,742.0	-3,729.0	14,304.0	-34,808.0	731.1	-5,013.0	3,295.0
45675	52516	15,885.0	38,391.0	63,328.0	-22,582.0	-71,127.0	-81,501.0	2,612.0	4,261.0	9,498.0
	52485	12,197.0	2,853.0	30,737.0	-15,178.0	-6,587.0	-20,780.0	1,502.0	786.2	7,380.0
	51296	11,484.0	-52,198.0	-80,836.0	-12,786.0	96,932.0	113,850.0	1,808.0	-5,203.0	-13,556.0
	51327	14,730.0	10,423.0	-19,189.0	-19,442.0	-18,862.0	-2,343.0	2,952.0	582.6	-4,638.0
45704	52520	8,874.0	38,262.0	43,728.0	-8,836.0	-72,405.0	-44,001.0	1,018.0	3,314.0	4,013.0
	52516	8,652.0	-5,422.0	7,207.0	-7,095.0	2,207.0	31,348.0	333.2	427.0	956.6
	51327	9,903.0	-42,834.0	-47,125.0	-8,159.0	80,708.0	51,476.0	883.0	-3,003.0	-5,329.0
	51331	10,016.0	9,884.0	-8,925.0	-9,575.0	-11,407.0	-31,763.0	1,549.0	131.0	-823.5
46365	53309	-409.4	6,197.0	371.4	4,723.0	-14,645.0	10,026.0	-990.4	-1,693.0	-432.1
	52093	-1,073.0	-633.6	-3,194.0	6,112.0	-29,106.0	34,107.0	-1,368.0	6,323.0	-3,224.0
	52086	1,003.0	-1,519.0	-1,582.0	1,822.0	-652.9	2,911.0	-381.9	4,618.0	-764.6
	53301	3,307.0	-1,810.0	1,852.0	-1,707.0	43,824.0	-44,114.0	690.4	-8,352.0	3,397.0

(Sheet 3 of 4)

Table B4 (Concluded)

Element	Node	Load Case 1			Load Case 2			Load Case 3		
		Fx [lb]	Fy [lb]	Fz [lb]	Fx [lb]	Fy [lb]	Fz [lb]	Fx [lb]	Fy [lb]	Fz [lb]
46372	53317	-81.5	16,412.0	5,484.0	3,415.0	-37,129.0	-7,457.0	-914.7	762.5	1,288.0
	52120	917.9	-6,582.0	-5,218.0	-346.0	-9,315.0	41,254.0	-364.2	3,349.0	-3,635.0
	52093	4,394.0	-15,700.0	-7,773.0	-4,740.0	37,267.0	15,335.0	1,018.0	-439.3	-2,471.0
	53309	3,999.0	4,864.0	2,093.0	-2,087.0	15,619.0	-43,102.0	749.2	-4,370.0	2,724.0
46717	53723	2,962.0	5,605.0	32,065.0	1,478.0	-10,897.0	-23,587.0	1,009.0	1,035.0	6,129.0
	53226	3,664.0	4,011.0	17,970.0	1,174.0	-11,319.0	4,980.0	523.7	1,052.0	4,892.0
	52485	7,829.0	-3,021.0	-32,374.0	-5,579.0	5,994.0	25,563.0	1,683.0	-702.0	-8,223.0
	52516	7,059.0	-6,473.0	-24,724.0	-4,953.0	15,646.0	4,132.0	2,093.0	-1,075.0	-5,012.0
46746	53727	7,125.0	22,904.0	41,970.0	-5,320.0	-45,379.0	-42,392.0	992.0	3,161.0	4,872.0
	53723	6,063.0	6,078.0	12,485.0	-2,304.0	-21,579.0	25,669.0	162.7	2,048.0	594.1
	52516	8,262.0	-26,562.0	-48,586.0	-4,897.0	51,508.0	54,162.0	946.1	-3,125.0	-6,946.0
	52520	9,146.0	-2,236.0	-12,424.0	-7,325.0	14,053.0	-28,504.0	1,685.0	-1,240.0	-281.8
47350	54420	1,487.0	4,135.0	18,689.0	4,470.0	-12,229.0	3,068.0	533.5	1,475.0	3,659.0
	53238	2,023.0	1,779.0	9,230.0	4,594.0	-7,410.0	28,028.0	10.6	589.7	2,411.0
	53226	6,281.0	-4,083.0	-20,207.0	-2,260.0	10,573.0	610.7	1,666.0	-964.4	-6,167.0
	53723	5,654.0	-1,626.0	-16,422.0	-1,877.0	8,273.0	-18,548.0	2,078.0	-745.0	-3,041.0
47362	54629	21.4	2,596.0	11,178.0	12,370.0	1,051.0	9,406.0	-407.5	-891.5	3,158.0
	53301	-555.9	3,714.0	848.3	9,264.0	-42,819.0	75,699.0	-1,011.0	7,094.0	-4,465.0
	53238	5,455.0	-1,634.0	-12,532.0	3,986.0	6,554.0	-21,599.0	825.6	-399.3	-4,212.0
	54420	4,815.0	-2,816.0	-10,569.0	8,634.0	33,146.0	-48,702.0	820.5	-4,768.0	1,229.0
47422	54690	-941.0	3,403.0	6,224.0	7,538.0	-5,648.0	21,458.0	-965.0	-1,097.0	793.0
	53309	-902.6	-1,817.0	2,971.0	5,795.0	-18,254.0	45,833.0	-1,082.0	4,770.0	-2,422.0
	53301	3,592.0	-547.9	-5,837.0	163.4	-2,048.0	-26,348.0	526.3	1,875.0	-680.6
	54629	3,904.0	176.5	-8,250.0	1,452.0	25,709.0	-35,582.0	695.1	-4,925.0	514.9
47430	54699	-129.7	10,443.0	6,840.0	5,364.0	-22,196.0	8,845.0	-937.5	-592.1	964.4
	53317	867.6	-6,209.0	917.2	1,668.0	-7,272.0	41,679.0	-594.7	3,469.0	-2,367.0
	53309	5,342.0	-8,977.0	-8,153.0	-3,324.0	19,533.0	-8,403.0	1,006.0	1,327.0	-1,540.0
	54690	4,884.0	4,124.0	-6,323.0	-431.7	14,657.0	-35,621.0	841.0	-4,442.0	611.4
47800	54424	3,385.0	10,324.0	29,383.0	2,159.0	-20,480.0	-24,970.0	387.9	1,854.0	4,506.0
	54420	3,111.0	5,757.0	10,412.0	2,737.0	-32,238.0	37,786.0	-318.5	4,225.0	-1,700.0
	53723	7,128.0	-9,856.0	-32,263.0	-1,536.0	21,968.0	26,033.0	782.8	-1,799.0	-5,864.0
	53727	7,081.0	-5,545.0	-15,397.0	-1,389.0	28,619.0	-29,019.0	1,288.0	-3,276.0	701.2
48413	54633	2,376.0	7,258.0	21,056.0	3,456.0	-8,124.0	-15,471.0	110.8	56.5	4,512.0
	54629	2,197.0	2,595.0	8,882.0	3,830.0	-34,143.0	34,271.0	-559.3	6,487.0	-2,275.0
	54420	6,529.0	-6,375.0	-23,943.0	-101.3	8,881.0	17,797.0	542.6	-188.8	-5,938.0
	54424	6,578.0	-2,637.0	-14,444.0	-215.7	31,847.0	-27,690.0	1,083.0	-5,305.0	1,147.0
48595	54694	153.8	5,371.0	14,848.0	3,264.0	-8,479.0	1,282.0	-339.4	163.0	2,783.0
	54690	179.8	88.0	10,922.0	2,794.0	-18,553.0	21,257.0	-667.6	4,655.0	-11.9
	54629	4,602.0	-4,301.0	-16,334.0	-1,420.0	5,977.0	-1,149.0	617.3	77.2	-3,629.0
	54633	4,534.0	-1,011.0	-14,272.0	-646.7	21,412.0	-17,190.0	833.7	-4,476.0	-553.8
48653	54703	568.2	8,667.0	12,306.0	3,787.0	-13,680.0	1,980.0	-470.7	-575.8	2,225.0
	54699	1,402.0	-4,445.0	7,157.0	965.6	-8,446.0	27,438.0	-462.6	3,984.0	-917.7
	54690	5,986.0	-7,647.0	-14,274.0	-3,054.0	11,009.0	-2,733.0	847.7	1,051.0	-3,067.0
	54694	5,367.0	2,567.0	-12,006.0	-466.4	14,528.0	-21,749.0	848.6	-4,431.0	-151.1
43444	49551	668.1	3,221.0	12,331.0	-1,425.0	-7,721.0	-21,983.0	-13.2	1,261.0	4,336.0
	48672	3,247.0	-19,588.0	-5,363.0	-8,395.0	44,733.0	14,831.0	1,412.0	-3,853.0	-2,092.0
	49549	1,757.0	15,036.0	-8,677.0	-771.6	-32,706.0	10,225.0	173.1	1,781.0	-3,010.0

(Sheet 4 of 4)

REPORT DOCUMENTATION PAGE

Form Approved
OMB No. 0704-0188

1. REPORT DATE *(DD-MM-YYYY)*	2. REPORT TYPE	3. DATES COVERED *(From - To)*
June 2005	Final report	

4. TITLE AND SUBTITLE

Folsom Dam Outlet Works Modification Project; Simplified Three-Dimensional Stress Analysis of Monolith 12

5a. CONTRACT NUMBER

5b. GRANT NUMBER

5c. PROGRAM ELEMENT NUMBER

6. AUTHOR(S)

Enrique E. Matheu, Sharon B. Garner

5d. PROJECT NUMBER

5e. TASK NUMBER

5f. WORK UNIT NUMBER

7. PERFORMING ORGANIZATION NAME(S) AND ADDRESS(ES)

U.S. Army Engineer Research and Development Center
Geotechnical and Structures Laboratory
3909 Halls Ferry Road
Vicksburg, MS 39180-6199

8. PERFORMING ORGANIZATION REPORT NUMBER

ERDC/GSL TR-05-14

9. SPONSORING / MONITORING AGENCY NAME(S) AND ADDRESS(ES)

U.S. Army Engineer District, Sacramento
Sacramento, CA 95814-2922

10. SPONSOR/MONITOR'S ACRONYM(S)

11. SPONSOR/MONITOR'S REPORT NUMBER(S)

12. DISTRIBUTION / AVAILABILITY STATEMENT

Approved for public release; distribution is unlimited.

13. SUPPLEMENTARY NOTES

14. ABSTRACT

This report presents a finite-element stress analysis of monolith 12 conducted to assess any potential adverse effects caused by the proposed dimensions of the air vent near the base of the spillway pier wall. A simplified three-dimensional finite-element model was developed to simplify the analysis while preserving the main characteristics of the section. The numerical model included fixed boundary conditions along the base and appropriate boundary conditions along the two lateral planes representative of the vertical contraction joints. The analyses included static (self-weight and hydrostatic) and dynamic (inertial and hydrodynamic) effects. The dynamic effects were accounted for using equivalent lateral loads and following Chopra's simplified procedure for seismic analysis of concrete gravity sections. The results provide an estimate of the stress field around the air manifold opening along the downstream face, and they provide a quantitative basis to evaluate its impact at the proposed location and to complete the design of any necessary reinforcement to be placed around the conduit.

15. SUBJECT TERMS

Concrete dams	Dynamic stresses	Nonoverflow monolith
Dynamic stress analysis	Ground motions	Overflow monolith

16. SECURITY CLASSIFICATION OF:			17. LIMITATION OF ABSTRACT	18. NUMBER OF PAGES	19a. NAME OF RESPONSIBLE PERSON
a. REPORT	b. ABSTRACT	c. THIS PAGE			19b. TELEPHONE NUMBER *(include area code)*
UNCLASSIFIED	UNCLASSIFIED	UNCLASSIFIED		76	